Thesis

Theory of Nonadiabatic Transitions at Level-Crossing in Condensed Matter

Hiroyuki NAKAYAMA

Division of Materials Physics
Department of Physical Science
Graduate School of Engineering Science
OSAKA UNIVERSITY

January, 1999

Thesis

Theory of Nonadiabatic Transitions at Level-Crossing in Condensed Matter

Hiroyuki NAKAYAMA

Division of Materials Physics
Department of Physical Science
Graduate School of Engineering Science
OSAKA UNIVERSITY

January, 1999

Preface

The nonadiabatic transitions at level crossing play an essential role in various dynamical aspects of quantum systems. In condensed matter, a typical example is the nonradiative transitions of the strongly-coupled localized centers in solids. The dynamical processes in condensed systems are, in many cases, subject to the perturbation by the elementary excitations in surrounding media, which will generally modurate the transition rate at the crossing. This effect is known as the effect of quantum dissipation. In this work, a comprehensive investigation of the dynamics of the nonadiabatic transitions of a level-crossing system with quantum dissipation has been carried out for the two-level system coupled with a system of phonons. Calculations based upon the Landau-Zener model tell us that the transition dynamics is characterized by the competition between the energy fluctuation and the energy dissipation. Calculations for the potential crossing system have made clear the transition dynamics after the electronic excitation, which is governed by the motion of wave packet of phonons.

A part of the numerical calculations was performed by using NEC SX-4 supercomputer at the Computation Center, Osaka University. Workstations in Yoshida laboratory were also used for numerical calculations. I am very grateful to the administrators for the continuous and devotional support of the computer system.

The preliminary study of this work was started in the autumn of 1994, as my master thesis at Tohoku University. Since this very early stage of the study, Professor Yosuke Kayanuma of Osaka Prefecture University has continuously supported me with helpfull discussions, advice, and encouragement. I would like to express sincere gratitude for his kindness.

Also, I would like to express sincere gratitude to Professor Hiroshi Katayama-Yoshida, for his continuous encouragement, advice, and fruitful discussions throughout this study. I thank gratefully all the staffs and the colleagues on Yoshida laboratory.

A part of this work, the result of the calculations for the Landau-Zener model coupled with the system of phonons, has already been published in Phys. Rev. B **57**, 13099(1998).

January 19, 1999

Hiroyuki NAKAYAMA
e-mail : nakayama@cmp.sanken.osaka-u.ac.jp

Contents

Chapter 1

Introduction

1.1 What is level-crossing?

The nonadiabatic transition at a level crossing is a fundamental process that plays a crucial role in various aspects of the dynamical evolution of quantum systems in various fields. We can refer to a number of examples both in physics and in chemistry, but the best known may be the atomic inelastic collisions with charge transfer [1] (for example, $A + B \rightarrow A^+ + B^-$, where A denotes alkali atom and B halogen) . The potential energy surface of the ionized state and that of the neutral-charged covalent state, as a function of the separation R cross at a certain internuclear separation R_c (see Figure 1.1). In case of the scattering problem, the separation R is time-dependent. If the two atoms have enough kinetic energy to approach each other within the crossing separation R_c, transition to the ionized state is induced dynamically and nonadiabatically. The Born-Oppenheimer approximation breaks down around the avoided crossing of the potential curves associated with each charge state, and the nonadiabatic transition around the potential-crossing region through the off-diagonal matrix element is primarily important in determining the branching ratio to respective scattering channels.

In general, we can define level-crossing as the dynamical phenomena in which more than two electronic energy levels approach and cross in accordance to the motion of a heavy degree of freedom and then the transition to another level is induced nonadiabatically. Landau and Zener derived a useful formula for the nonadiabatic transition rate [2], under the condition that the transition is induced only within the neighborhood of the potential-crossings where one can regard the crossing velocity of the energy levels v and off-diagonal matrix element J as constant, that is,

$$P_{LZ} = 1 - \exp[-2\pi J^2/\hbar|v|]\,. \tag{1.1}$$

Since the discovery of the celebrated Landau-Zener formula in 1932, continuous effort has been devoted to elaborating the theoretical treatment [3].

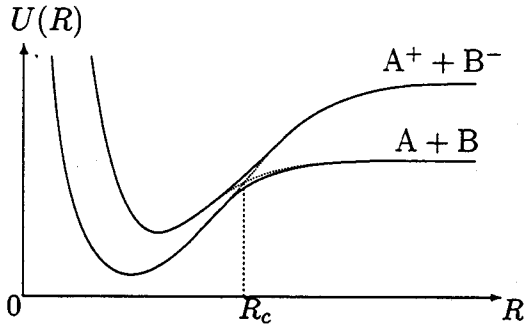

Figure 1.1: Potential surfaces of a diatomic molecule as a function of separation R.

1.2 Examples of the level-crossing system

The femtosecond transition-state spectroscopy using laser-induced fluorescence technique has made clear the dynamical motion of $R(t)$ as a wave packet motion on the potential surface. An elegant experiment for NaI molecule indicates the successive nonadiabatic transitions around the crossing region of the adiabatic potentials induced by the motion of the wave packet in excited state [4].

Also, in astrophysics, problem of the sun neutrino loss generated by the nuclear fusion reactions can be explained as a kind of the nonadiabatic transition induced by level-crossings between the neutrinos with different flavor $(\nu_e, \nu_\mu, \nu_\tau)$. Definite experimental evidence for this so-called Mikheyev-Smirnov-Wolfenstein (MSW) mechanism was discovered very recently [5].

In condensed matter, a typical example would be the nonradiative transitions in the strongly coupled localized electron-phonon system in solids. The radiationless transitions of color centers in ionic crystals [6, 7], or the nonradiative capture of deep impurities in semiconductor [8] are included in this category. In this case, the level crossing is defined in the configuration coordinate space instead of in the real space, and the nonradiative transition occurs during the lattice relaxation as the wave packet passes the crossing point of the adiabatic potentials. The analysis of the transition dynamics by referring to the Landau-Zener formula has been done by several authors [8, 9, 10, 11]. Inelastic scattering of atoms on metal surfaces [12] is another example which is well-understood according to Landau-Zener formula. A sort of chemical reaction at the surface of crystals [13] and in the solvent [14] can be classified in this category, in which the nonadiabaticity of the process must be taken into account. It is pointed out that an analogous nonadiabatic level crossing is relevant in some nuclear reactions [15]. A slightly different version of the same problem can be found in the area of magnetic resonance [16] and in nonlinear optics [17]. By changing the applied magnetic fields or the electric fields, one can attain a level crossing between the two discrete levels. The so-called adiabatic rapid passage or its optical analogue has been

analyzed in the framework equivalent to the Landau-Zener formula [18]. With relation to adiabatic demagnetization, the quantum dynamics of a coupled spin system under a time-dependent magnetic field has been studied as a kind of nonadiabatic level-crossing system [19].

1.3 Level-crossing system in condensed matter

1.3.1 What are the problems?

In contrast to the case of atomic collisions, the dynamical processes in condensed systems are, in many cases, subject to the perturbation by the elementary excitations in surrounding media that have infinite degrees of freedom. The coupling with the surrounding media will generally modulate the transition rate at level crossings. This effect is known as the effect of quantum dissipation. Moreover, in some systems, the electronic levels that cross is continuous and make band, which can also modulate the transition rate. Although this effect might take a crucial role in dynamical processes in semiconductor defect systems [8], it is not discussed in this study. Attention is focused on the effect of quantum dissipation, because the effect of quantum dissipation is an essential nature in condensed matter physics which appears in most of the systems and I am much interested in investigating the transition process under the influence of quantum dissipation.

It should be emphasized here that the concept of quantum dissipation should be understood from two distinct viewpoints. One is the dissipation of energy and the other is the fluctuation of energy, or in other words, the dissipation of the phase memory. The relative magnitudes of the effects of these are connected to each other through the fluctuation-dissipation theorem.

1.3.2 Analytical works

One of the standpoints to investigate the effects of quantum dissipation, the dissipation and fluctuation of the energy, is to take the time-dependent model of Zener coupled with a bath of many mode phonons. Although it may seem artificial to assume an explicit time dependence for diabatic energies at the crossing event, this model is useful to get insight into the essential dynamics of the nonadiabatic transitions at a single crossing event, and it is called a standard model. The effect of the environmental perturbation in the level-crossing problem has been investigated by several authors within the standard model [20, 21, 22, 23]. From the theoretical point of view, this problem gives an interesting time-dependent version of the quantum tunneling with dissipation [24, 25].

Kayanuma [21] investigated the effect of the phase relaxation on the transition probability by reducing the standard model to a stochastic model at high temperature. He has shown that the existence of the phase relaxation generally increases the apparent nonadiabaticity, and obtained a closed formula of the transition rate in the limit of strong

dephasing, that is,

$$P_{SD} = \frac{1}{2}\left(1 - \exp[-4\pi J^2/\hbar|v|]\right), \tag{1.2}$$

which shows an incoherent or a diffusionlike transfer. Also he calculated the probability of the dynamical nonradiative transition in strongly-coupled electron-phonon system [11]. He has shown that in the case that the semiclassical condition is satisfied, the dynamical transition rate at the potential-curve crossing is given by the Landau-Zener formula, because the associated energy levels cross so rapidly that the quantum dissipation does not affect the transition rate. Sumi [10] has also derived the same result for the transition rate between two localized electronic states.

Leggett and his coworkers [25] have established the formalism by use of influence-functional method based on path-integral approach in their study on quantum tunneling problem with dissipation. They started from the "spin-boson" Hamiltonian

$$H = -\frac{1}{2}\hbar\Delta\sigma_x + \frac{1}{2}\epsilon\sigma_z + \frac{1}{2}q_0\sigma_z\sum_k C_k x_k + \sum_k\left(\frac{1}{2}m_k\omega_k {x_k}^2 + \frac{{p_k}^2}{2m_k}\right), \tag{1.3}$$

where σ_x and σ_z denote Pauli spin matrices. They obtained analytical expression of the decay rate from metastable state for various cases. Above all, non-biased case of $\epsilon = 0$ is fully examined. They showed that even the qualitative behavior of the dissipative system is sensitive to the low-frequency behavior of the spectral function $J(\omega)$ defined as

$$J(\omega) = \frac{\pi}{2}\sum_k \frac{{C_k}^2}{m_k\omega_k}\delta(\omega - \omega_k) \tag{1.4}$$

and tunneling processes shows exponential relaxations or damped oscillations, which are determined also by the dimensionless dissipation constant or temperature.

Ao and Rammer [23] developed an extensive analysis for the original standard model and obtained analytical expressions of the transition rate for some extreme cases of the parameter value, by using Leggett's method for the time-dependent model. A remarkable conclusion is that the effect of the environmental perturbation on the transition rate disappears at low temperatures and transition rate is given by the Landau-Zener formula, in the case that the system starts from the lower branch in the initial state. This assertion is not consistent with the previous result of the analytical study in the same model [22], and it was required to settle the inconsistency in a clear form.

1.3.3 Numerical works

The standard model based on Landau-Zener theory is the most suitable way to analyze the transion dynamics as a single crossing event, if the degree of freedom, which modulates the electronic levels, is *heavy* enough and the levels can be assumed to be an explicit function of time. In actual situations, however, the energy levels aren't an explicit function of time,

because the degree of freedom itself is fluctuating and is not a well-defined parameter. It can not be allowed to treat the degree of freedom as a semi-classical variable, so one have to treat the motion of the degree of freedom on the potential surfaces quantum-mechanically as the motion of a wave packet. Furthermore, in some systems, the electronic system is so strongly coupled with the surrounding media that the modulation of the energy itself is caused by this coupling. The strongly coupled localized electron-phonon system in solids mentioned above is such example. In order to analyze the dynamical phenomena of such systems, the whole process must be treated as an autonomous evolution.

Since analysis based upon Landau-Zener formula have been done mostly in the literature, it has been awaited to develop an efficient and reliable technique of numerical calculation for the dynamical processes of the realistic system. Several researchers tried to tackle the problem [20, 26, 27, 28] with various methods, however, useful calculational method has not been yet established.

Tsukada [20] did a numerical calculation of the transition dynamics of absorbates for a semiclassical version of the standard model by utilizing the stochastic-trajectory method. It has been clearly shown in this work that, because the back-transfer effect, the energy relaxation dramatically modifies the transition rate in the case that the system initially occupies the upper level. The validity of the approximation adopted to derive the force term in the stochastic equation is, however, not always justified since the environmental oscillators are assumed as being driven by a common force irrespective of the electronic subspace.

Tully [26] developed a numerical calculation method based on stochastic-trajectory method, by considering stochastic jump process to another electronic levels. In this method, the system can jump to another levels by a finite probability. At each calculational step, the transition probabilities to another levels are calculated, and stochastically decided whether the system makes a transition or not. The force term in the stochastic equation of motion is calculated consistently from the electronic state the system is in. Photodissociation dynamics of Ar clusters has been simulated by using this method [27] and obtained good agreement with the experiment. In order to calculate physical quantity with high accuracy, however, we need the averaging over many stochastic paths, and this method would not be suitable for calculations of the dynamics in solid systems where it takes too much computational costs to calculate excited states.

Tanimura *et al.* [28] deduced the quantum Fokker-Plank equation for the system with a bath of Gaussian-Markovian noise, and calculated the motion of the wave packet in Wigner representation for the system of molecules with Morse potentials. The optical absorption spectrum and the femtosecond pump-probe spectrum are calculated as well. However, care must be taken when one treat the dynamics of the system at low temperature in this approach.

Finally, damping hyperoperator technique is widely utilized to describe the quantum

damping of photon fields [29]. It was also applied to the calculation of the second-order optical spectrum of a localized electron-phonon system [30]. Murao and coworkers [31] developed an elegant formalism to solve the equation of motion for the density matrix with a damping term and carried out numerical calculations of transition dynamics of a level-crossing system. This calculation method is the best way to investigate qualitative behavior of the dynamics of the quantum system, which shows a wide variety, although this technique has a difficulty in application to the transition dynamics of actual systems, because the potential curvature of actual systems are, strictly speaking, not harmonic. The state-vector Monte Carlo, and the quantum-state diffusion method are classified into stochastic versions of this method and gave the same results as that of usual damping hyperoperator method [32].

1.4 Aim of the thesis

The aim of the thesis is:

1. to make a comprehensive investigation of the level-crossing problem in condensed matter as an elementary process within the framework of the standard model,
2. to get the complete knowledge about the role of the quantum dissipation in nonadiabatic transition processes at level-crossings,
3. to clarify whole transition dynamics of the potential-crossing system, and finally,
4. to get complete understandings about the mechanism of the nonadiabatic process.

Both analytical and numerical calculation are performed from the standard Hamiltonian. In next chapter 2, the model is presented with some remarks about the physical parameters. Analytical method using the formal perturbation expansion series, and numerical method utilizing damping hyperoperator technique are briefly presented in chapter 3.

Chapter 4 is devoted to the analytical investigations of the nonadiabatic transition at the level-crossing of a Landau-Zener type as an elementary process, but the results are useful to consider the nonadiabatic transition of the potential-crossing system, in which the whole process must be treated dynamically. Closed expressions of the transition rate, some of which have been obtained previously, are derived in a unified way. Specifically, a formula is obtained that covers the limit of the strong phase-relaxation, bridging the high-temperature, weak-coupling limit and the low-temperature, strong-coupling limit.

Chapter 5 is devoted to the numerical results of the dynamical evolution of level-crossing system of a Landau-Zener type. The numerical calculations have made clear what is going on in the electronic system during the level crossing under the influence of the quantum dissipation through the time-dependent behavior of reduced density matrix. In the extreme

cases of the parameter values, the results of the analytical formulas are ascertained. In addition, a peculiar feature of the damping hyperoperator technique as a tool for such a calculation is revealed and critically examined.

The nonadiabatic transition processes of the potential-crossing system, and its application to realistic system is presented in chapter 6. It has been shown that the nonadiabatic transition goes on in two steps. First, the transition is induced dynamically during the lattice relaxation process as the phonon wave packet passes the crossing point. Then, the transition from the relaxed excited state follows statically by thermal excitation or quantum tunneling. The transition probability in the dynamical stage has been investigated quantitatively. As typical examples of the actual system, the shallow-to-deep transition dynamics of DX-center and the nonradiative transition process of F-center are calculated and discussed.

Concluding remarks are given in chapter 7. Finally in appendix, the derivation of the interaction mode, which is used to introduce the damping hyperoperator, and the derivation of the damping hyperoperator for the two-level system are noted.

Chapter 2

Model

2.1 Hamiltonian

Consider the energy levels of the two electronic states $|1\rangle$ and $|2\rangle$. The system initially exists in $|1\rangle$ makes a transition to $|2\rangle$ through a off-diagonal matrix element around the crossing. Throughout this study, *transition* is defined for diabatic basis set $|1\rangle$ and $|2\rangle$. Also $\hbar \equiv 1$ is adopted. The whole system is assumed as being subject to the perturbation by the elementary excitations in surrounding medium represented by phonons.

The prototype Hamiltonian to discuss transition dynamics is as follows:

$$H_T(t) = H_{\rm el}(t) + H_{\rm ph} + H_I\,, \tag{2.1}$$

where

$$H_{\rm el}(t) = \begin{pmatrix} \epsilon_1(t) & J \\ J & \epsilon_2(t) \end{pmatrix}, \tag{2.2}$$

$$H_{\rm ph} = \sum_k \omega_k {b_k}^\dagger b_k\,, \tag{2.3}$$

$$H_I = \sum_k \alpha_k \omega_k (b_k + {b_k}^\dagger) \begin{pmatrix} \frac{1}{2} & 0 \\ 0 & -\frac{1}{2} \end{pmatrix}. \tag{2.4}$$

$H_{\rm el}(t)$ is a Hamiltonian for the electronic system with a constant off-diagonal matrix element J. $\epsilon_1(t)$, $\epsilon_2(t)$ are the energy of the electronic states that approach and cross each other in accordance with the motion of a heavy degree of freedom or by the external modulation, and are assumed to have an explicit functionality of time. $H_{\rm ph}$ is a Hamiltonian for the phonon system, b_k (${b_k}^\dagger$) is annihilation (creation) operator for the k-th normal mode with energy ω_k. H_I is a Hamiltonian for the interaction between the electronic system and the phonon system, and α_k is the linear coupling constant with the k-th mode.

In this study, we choose $\epsilon_1(t)$ and $\epsilon_2(t)$ in two limiting but interesting cases and discuss the dynamics of the system.

Case 1: Let us consider the transition dynamics at a level crossing with quantum dissipation as an elementary process, by extending Zener's model. $\epsilon_1(t)$ and $\epsilon_2(t)$ are chosen such that $H_{\rm el}$ is the same as the Landau-Zener model,

$$\epsilon_1(t) = \frac{1}{2}vt, \quad \epsilon_2(t) = -\frac{1}{2}vt, \tag{2.5}$$

where v is the velocity of the change of the energy difference. The level-crossing scheme of original Landau-Zener model is shown in Figure 2.1. This model is referred as the standard model in previous chapter, and will be discussed analytically in Chapter 4, and numerically in Chapter 5.

As initial condition, it is assumed that at $t \to \infty$, the total system is represented by the density matrix ρ_i given by

$$\rho_i = |1\rangle\langle 1|\rho_1\,, \tag{2.6}$$

where ρ_1 represents the phonon equilibrium in the subspace $|1\rangle$, namely,

$$\rho_1 = \frac{\exp(-H_1/k_BT)}{\mathrm{Tr}\left[\exp(-H_1/k_BT)\right]} \tag{2.7}$$

with

$$H_1 = H_{\rm ph} + \frac{1}{2}\sum_k \alpha_k\omega_k(b_k + b_k{}^\dagger)\,. \tag{2.8}$$

The probability P that the electronic system exists in $|2\rangle$ at $t \to \infty$ is calculated. Note that the transition rate depends also on the sign of v unlike the original Landau-Zener model. The transition rate for $v > 0$ means the transition rate from the lower initial state to the another state, which becomes lower after the crossing. And that for $v < 0$ means the transition rate from the higher initial state to the another state, which becomes higher after the crossing. The transition rate will be modified by the existence of the energy dissipation so that the transition rate to the lower state gets larger probability.

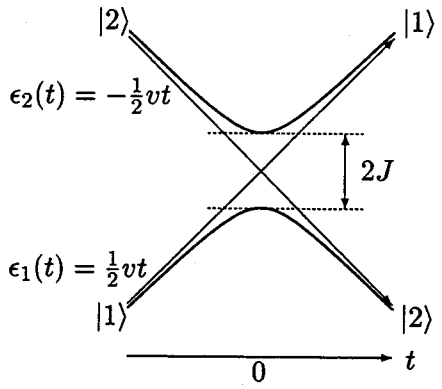

Figure 2.1: level-crossing scheme of the Landau-Zener.

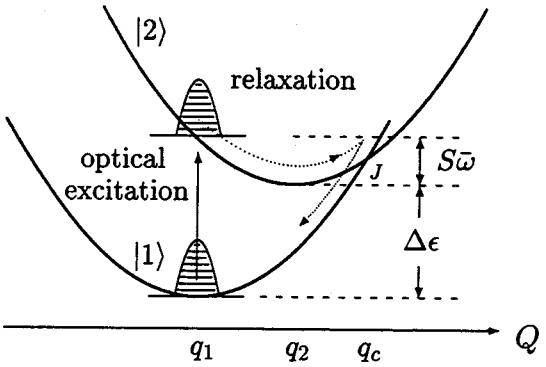

Figure 2.2: The potential crossing system. The potential energies as a function of the representative phonon mode Q cross each other at $Q = q_c$. Once the system is excited to $|1\rangle$ to $|2\rangle$, the nonradiative transition is induced dynamically during the relaxation process as the wave packet passes around the potential-crossing region.

Case 2: In order to investigate the whole transition dynamics as an autonomous system, we simply set $\epsilon_1(t)$ and $\epsilon_2(t)$ to constant,

$$\epsilon_1(t) = \epsilon_1\,, \quad \epsilon_2(t) = \epsilon_2\,, \quad \epsilon_2 - \epsilon_1 = \Delta\epsilon\,. \tag{2.9}$$

This model is a very useful model that represents a potential-crossing system (see Figure 2.2), and is essentially same as that of Leggett et al; only operators b_k and $b_k{}^\dagger$ are replaced with classical variables x_k in their model. They calculated the decay rate from the stationary state (relaxed state) by the quantum tunneling [24, 25], however, the dynamical transition process also needs to be considered when the system is initially in excited state.

Once the system is excited to higher state, the nonadiabatic transition will be induced dynamically during the lattice relaxation process around the potential-crossing region. The transition by the quantum tunneling will occur after the lattice relaxation process.

Suppose $|1\rangle$ corresponds to the ground state and $|2\rangle$ the excited state, and consider the case that the system is optically excited from $|1\rangle$ to $|2\rangle$. Under the Franck-Condon principle, the density matrix that represents the total system is initially given by

$$\rho_i = |2\rangle\langle 2|\rho_1 \,. \tag{2.10}$$

ρ_1 does not represent the equilibrium state of the electron-phonon system in the subspace $|2\rangle$, so the system starts to relax to the new equilibrium state in the subspace $|2\rangle$. During this process, the nonadiabatic transition to the ground state $|1\rangle$ will be induced when the phonon wave packet passes the crossing region of two potential curves. This process is well known as the nonradiative transition process in solids and is discussed in chapter 6. The probability P that the system undergoes nonradiative transition from $|1\rangle$ to $|2\rangle$ is calculated.

2.2 The electron-phonon system

Because of the Gaussian character of the linear electron-phonon interaction, the dynamics of the quantum dissipation can be completely specified by the spectral-density function $\phi(\omega)$ defined by

$$\begin{aligned} \phi(\omega) &= \frac{1}{2\pi}\int_{-\infty}^{\infty} \Big\langle W(t)W(0)\Big\rangle_0 e^{i\omega t}dt \\ &= \sum_k {\alpha_k}^2{\omega_k}^2\left[(n_k+1)\delta(\omega-\omega_k)+n_k\delta(\omega+\omega_k)\right] , \end{aligned} \tag{2.11}$$

where

$$W \equiv \sum_k \alpha_k\omega_k(b_k+{b_k}^\dagger)\,, \quad W(t) \equiv \exp(iH_{\rm ph}t)\,W\exp(-iH_{\rm ph}t)\,, \tag{2.12}$$

and $n_k \equiv \frac{1}{\exp(\omega_k/k_BT)-1}$. In the above equation, $\Big\langle\cdots\Big\rangle_0$ is the average over the density matrix $\rho_0 \equiv \exp(-H_{\rm ph}/k_BT)\Big/\mathrm{Tr}\left[\exp(-H_{\rm ph}/k_BT)\right]$.

The relaxation energy ΔE is given by

$$\Delta E = \int_{-\infty}^{\infty}\phi(\omega)\omega^{-1}d\omega\,, \tag{2.13}$$

which is half of the Stokes shift for the optical transition.

The amplitude of the energy fluctuation D is given by

$$D^2 = \int_{-\infty}^{\infty}\phi(\omega)d\omega\,. \tag{2.14}$$

We define the dimensionless coupling constant S by

$$S = \sum_k {\alpha_k}^2 \tag{2.15}$$

and the representative phonon energy $\bar{\omega}$ by

$$\Delta E = S\bar{\omega}\,. \tag{2.16}$$

The transition dynamics under the influence of quantum dissipation is insensitive to the detailed functional form of $\phi(\omega)$ but is characterized by the parameters $\bar{\omega}$, S, ΔE, D and k_BT . It should be noted that ΔE and D are related to each other through the Einstein relation,

$$D^2 \simeq 2k_BT^*\Delta E\,, \tag{2.17}$$

where, recovering $\hbar$, $T^* \equiv (\hbar\bar{\omega}/2k_B)\coth(\hbar\bar{\omega}/2k_BT)$ is the effective temperature. Therefore, the effect of the energy fluctuation becomes dominant while the energy dissipation can be neglected in the limit of weak coupling and high temperature,

$$\Delta E \to 0\,, \quad k_BT \to \infty \quad \text{with} \quad D \quad \text{finite}\,. \tag{2.18}$$

This is the case described well by the stochastic model [21]. On the other hand, in the limit of strong coupling and low temperature, the effect of the energy relaxation as well becomes important since in this limit,

$$\bar{\omega} \ll D \simeq \sqrt{S}\bar{\omega} \ll \Delta E\,. \tag{2.19}$$

The stochastic fluctuation of the energy difference generally leads to the phase relaxation. In the case that $D/\bar{\omega} \gg 1$, the relative-phase memory is completely lost within a short time of order of $\tau_{ph} \simeq D^{-1}(\ll \bar{\omega}^{-1})$. For $D/\bar{\omega} \leq 1$, the phase relaxation is incomplete. This is a feature of the linear coupling model and is connected with the presence of a sharp zero-phonon line in the optical-transition spectrum.

The generating function for the electron-phonon system is defined as

$$\begin{aligned} G(t) &\equiv \int_0^t ds \int_0^s ds' \Big\langle W(s)W(s') \Big\rangle_0 \\ &= \int_{-\infty}^{\infty} d\omega \phi(\omega) \left[(1 - e^{-i\omega t})\omega^{-2} - it\omega^{-1} \right] \\ &= +\frac{1}{2}D^2t^2 + \cdots . \end{aligned} \tag{2.20}$$

Note that the Fourier transformation of $G(t)$

$$I(E) = \frac{1}{2\pi}\int_{-\infty}^{\infty} dt\, e^{i(E-\varepsilon)t - G(t)} \tag{2.21}$$

gives the optical spectrum for the idealized system without off-diagonal interaction J. ε is the Franck-Condon energy for the idealized system.

The time constant $\tau_{\rm en}$ of the relaxation of the energy is given by $\tau_{\rm en} \simeq \gamma^{-1}$, where γ is the width of $\phi(\omega)$ at low temperature. In most cases, γ is roughly the same order of magnitude as $\bar{\omega}$ itself. The time constants $\tau_{\rm ph}$ and $\tau_{\rm en}$ should be compared with the time interval $\tau_{\rm tr}$ within which the system exists in the transition region. Since the off-diagonal coupling works for the energy difference of order of or less than J, $\tau_{\rm tr}$ is given by,

$$\tau_{\rm tr} \simeq J/|v| \tag{2.22}$$

in the case of the transition of Landau-Zener. The transition process is characterized by the degree of coherence, which is measured by the ratio of $\tau_{\rm ph}$ and $\tau_{\rm tr}$, as is shown in Chapter 4.

Chapter 3

Methodology

3.1 Analytical method

3.1.1 Formal perturbation expansion

The time evolution of the total system obeys the Liouville equation for density matrix,

$$i\frac{\partial \rho(t)}{\partial t} = [\, H_T(t)\,,\ \rho(t)\,], \tag{3.1}$$

which is, in practice, not solvable. The density matrix $\rho(t)$ at time t is formally given by

$$\rho(t) = \exp_+\left[-i\int_{-\infty}^{t} H_T(\tau)d\tau\right]\rho_i \exp_-\left[+i\int_{-\infty}^{t} H_T(\tau')d\tau'\right] \tag{3.2}$$

where $\exp_+(\exp_-)$ means the time-ordered exponential with increasing time toward left (right), defined by

$$\begin{aligned}
\exp_+\left[-i\int_{-\infty}^{t} H(\tau)d\tau\right] &\equiv 1 + (-i)\int_{-\infty}^{t} d\tau_1 H(\tau_1) \\
&\quad + (-i)^2\int_{-\infty}^{t} d\tau_1 \int_{-\infty}^{\tau_1} d\tau_2 H(\tau_1)H(\tau_2) \\
&\quad + (-i)^n\int_{-\infty}^{t} d\tau_1 \int_{-\infty}^{\tau_1} d\tau_2 \cdots \int_{-\infty}^{\tau_{n-1}} d\tau_n H(\tau_1)H(\tau_2)\cdots H(\tau_n) \\
&= \sum_{n=0}^{\infty}(-i)^n\int_{-\infty}^{t} d\tau_1 \int_{-\infty}^{\tau_1} d\tau_2 \cdots \int_{-\infty}^{\tau_{n-1}} d\tau_n H(\tau_1)H(\tau_2)\cdots H(\tau_n) \\
&= \sum_{n=0}^{\infty}(-i)^n\int_{-\infty}^{t} d\tau_1 \int_{\tau_1}^{t} d\tau_2 \cdots \int_{\tau_{n-1}}^{t} d\tau_n H(\tau_n)\cdots H(\tau_2)H(\tau_1)\,, \\
\exp_-\left[+i\int_{-\infty}^{t} H(\tau)d\tau\right] &\equiv \sum_{n=0}^{\infty}(+i)^n\int_{-\infty}^{t} d\tau_1 \int_{-\infty}^{\tau_1} d\tau_2 \cdots \int_{-\infty}^{\tau_{n-1}} d\tau_n H(\tau_n)\cdots H(\tau_2)H(\tau_1)\,.
\end{aligned}$$

The probability $p(t)$ that the system initially exists in $|1\rangle$ and make a transition to $|2\rangle$ in time t is given as

$$
\begin{aligned}
p(t) &= \mathrm{Tr}\langle 2|\rho(t)|2\rangle \\
&= \mathrm{Tr}\langle 2|\exp_+\left[-i\int_{-\infty}^{t} H_T(\tau)d\tau\right]\rho_i \exp_-\left[+i\int_{-\infty}^{t} H_T(\tau')d\tau'\right]|2\rangle \\
&= \mathrm{Tr}\langle 2|\exp_+\left[-i\int_{-\infty}^{t} H_T(\tau)d\tau\right]|1\rangle\rho_1\langle 1|\exp_-\left[+i\int_{-\infty}^{t} H_T(\tau')d\tau'\right]|2\rangle \\
&= \left\langle \left\{\exp_-\left[+i\int_{-\infty}^{t} H_T(\tau')d\tau'\right]\right\}_{1,2}\left\{\exp_+\left[-i\int_{-\infty}^{t} H_T(\tau)d\tau\right]\right\}_{2,1}\right\rangle_1 ,
\end{aligned}
\tag{3.3}
$$

in which $\{\cdots\}_{i,j}$ means that the (i,j) component should be taken and $\langle\cdots\rangle_1$ indicates the expectation value over the equilibrium phonon in the subspace $|1\rangle$,

$$
\langle\cdots\rangle_1 \equiv \mathrm{Tr}\{\rho_1\cdots\} \tag{3.4}
$$

The probability $p(t)$ can be expanded in a power series of J to infinite orders, namely,

$$
p(t) = -\sum_{n=1}^{\infty}(-J^2)^n L^{(n)}(t) \tag{3.5}
$$

In some extreme situations, we can calculate the perturbation terms $L^{(n)}$ for each n and sum over, then we can obtain useful formulas for the transition rate, which are discussed in the next chapter.

3.2 Numerical method

3.2.1 The interaction mode

First, we introduce *interaction mode* B by the unitary transformation of normal mode phonon b_k

$$
B = \sum_{k=1}^{N} U_{0,k}^* b_k , \quad B^\dagger = \sum_{k=1}^{N} U_{0,k} b_k{}^\dagger . \tag{3.6}
$$

The interaction mode was first proposed by Toyozawa and Inoue for the Jahn-Teller system [33]. In a little different form, it was also introduced by O'Brien [34]. The essential point of the interaction mode is that one can construct, out of a tremendous number of normal modes, a small number of modes that bear all of the relaxation energy within the relevant electronic subspace as components of the system. The rest of the modes span a basis set of the orthogonal complement of the interaction mode, which can be regarded as the reservoir.

The reservoir modes R_j are defined as

$$
R_j = \sum_{k=1}^{N} U_{j,k}^* b_k , \quad R_j{}^\dagger = \sum_{k=1}^{N} U_{j,k} b_k{}^\dagger , \quad j = 1,2,\cdots,N-1 . \tag{3.7}
$$

The condition that the interaction mode carries all of the relaxation energy requires

$$U_{0,k} = \alpha_k/\alpha\,, \tag{3.8}$$

with $\alpha^2 \equiv \sum_k {\alpha_k}^2 (\equiv S)$. The transformation coefficients $U_{j,k} (j = 1, 2, \cdots, N-1)$ are uniquely defined so that R_j lie in the orthogonal complement of B and are mutually orthogonal. The detailed procedure to determine the coefficients $U_{j,k}$ is shown in Appendix A.

The total Hamiltonian of the system is eventually rewritten to,

$$H_T(t) = H_{\rm sys}(t) + V_{\rm sys} + H_R + V_R\,, \tag{3.9}$$

$$H_{\rm sys}(t) = \begin{pmatrix} \epsilon_1(t) + \bar{\omega} {B_1}^\dagger B_1 & 0 \\ 0 & \epsilon_2(t) + \bar{\omega} {B_2}^\dagger B_2 \end{pmatrix}, \tag{3.10}$$

$$V_{\rm sys} = \begin{pmatrix} 0 & J \\ J & 0 \end{pmatrix}, \tag{3.11}$$

$$H_R = \sum_j \Omega_j {R_j}^\dagger R_j \begin{pmatrix} 1 & 0 \\ 0 & 1 \end{pmatrix}, \tag{3.12}$$

$$V_R = \begin{pmatrix} \sum_j \beta_j ({B_1}^\dagger R_j + B_1 {R_j}^\dagger) & 0 \\ 0 & \sum_j \beta_j ({B_2}^\dagger R_j + B_2 {R_j}^\dagger) \end{pmatrix}, \tag{3.13}$$

where

$$B_1 \equiv B + \frac{\alpha}{2}\,, \quad B_2 \equiv B - \frac{\alpha}{2}\,. \tag{3.14}$$

$\bar{\omega}$ is the energy of the interaction mode given by

$$\bar{\omega} = \sum_k \omega_k \left| U_{0,k} \right|^2, \tag{3.15}$$

and β_j is the coupling constant between the interaction mode and the reservoir modes,

$$\beta_j = \sum_k \omega_k U^*_{j,k} U_{0,k}\,. \tag{3.16}$$

It should be noted that the above definition correctly guarantees the relaxation of the interaction mode to the lowest state within the respective electronic subspace. It has been shown that the concept of the interaction mode is extended in a unique way to generic n-level systems coupled linearly with boson fields [35].

3.2.2 Damping hyperoperator method

The damping operator for the interaction mode coupled with the two-level system is introduced by extending the well-known procedure, which is shown in Appendix B. The

equation of motion for the total density matrix in the interaction representation is solved for a short time interval by the perturbation expansion to first order with respect to $V_{\rm sys}$ and to second order with respect to V_R. The variables for the reservoir modes are then eliminated by taking the trace over the subspace of the reserviour modes **R**. Under the assumption that the thermal equilibrium of **R** is undisturbed by the interaction and that the spectrum of **R** is wide enough to guarantee the Markovian approximation, we can obtain the reduced equation of motion for the density matrix of the system. In the Schrödinger picture, it reads

$$i\frac{\partial \rho_R(t)}{\partial t} = [\, H_{sys}(t) + V_{sys}\,,\ \rho_R(t)\,] + i\Gamma\cdot\rho_R\,, \tag{3.17}$$

where

$$\rho_R(t) = \mathrm{Tr}_R\,\rho(t) \tag{3.18}$$

means the reduced density matrix in which the information of the reserviour is eliminated by taking trace over **R**.

Γ is a hyperoperator defined for the 2x2 density matrix

$$\rho_R \equiv \begin{pmatrix} \rho_{1,1} & \rho_{1,2} \\ \rho_{2,1} & \rho_{2,2} \end{pmatrix} \tag{3.19}$$

as

$$\Gamma\cdot\rho_R = \begin{pmatrix} \Gamma_{1,1}\rho_{1,1} & \Gamma_{1,2}\rho_{1,2} \\ \Gamma_{2,1}\rho_{2,1} & \Gamma_{2,2}\rho_{2,2} \end{pmatrix} \tag{3.20}$$

with

$$\begin{aligned}\Gamma_{i,j}\rho_{i,j} \;=\; & \kappa(\bar{n}+1)\left(2B_i\rho_{i,j}B_j{}^\dagger - B_i{}^\dagger B_i\rho_{i,j} - \rho_{i,j}B_j{}^\dagger B_j\right) \\ & + \kappa\bar{n}\left(2B_i{}^\dagger\rho_{i,j}B_j - B_iB_i{}^\dagger\rho_{i,j} - \rho_{i,j}B_jB_j{}^\dagger\right)\,. \end{aligned} \tag{3.21}$$

In the above equation, κ is the effective coupling constant with the reservior modes and is taken as a free parameter, although the above equations are derived under rather restricted conditions on the spectrum of the reserviour modes. $\bar{n}$ means the thermal occupation number for the interaction mode phonon of energy $\bar{\omega}$, that is,

$$\bar{n} \equiv \frac{1}{\exp[\bar{\omega}/k_BT]-1}\,. \tag{3.22}$$

The energy relaxation time τ_{en} is given by

$$\tau_{en} \sim \kappa^{-1}\,. \tag{3.23}$$

Equation (3.17) is transformed into a set of simultaneous differential equations for the coefficients of the number state representation of the interaction mode, by expanding $\rho_{i,j}$ as

$$\rho_{i,j}(t) = \sum_{n,m=0}^{M} C_{i,j}(n,m;t)|n\rangle\langle m|\,. \tag{3.24}$$

and solved numerically. M, the highest phonon state needed for the calculation, depends on the electron-phonon coupling parameter S and temperature. In typical case of the strongly-coupled electron-phonon system, over 200 phonon states must be taken into account and the number of total basis states needed for the calculation exceeds 80,000.

Chapter 4

The Landau-Zener Problem I. Analytical Investigations

4.1 Formalism by generating function

In this chapter, we calculate the transition rate under the influence of quantum dissipation P , within the framework of Landau and Zener. The transition rate P is defined as

$$\begin{aligned} P &= p(\infty) \\ &= \left\langle \left\{ \exp_- \left[+i \int_{-\infty}^{\infty} H_T(\tau') d\tau' \right] \right\}_{1,2} \left\{ \exp_+ \left[-i \int_{-\infty}^{\infty} H_T(\tau) d\tau \right] \right\}_{2,1} \right\rangle_1 . \end{aligned} \tag{4.1}$$

And we define the transition rate for $v > 0$ as P_+ and that for $v < 0$ as P_-. P_+ is the transition rate from the lower inititial branch to the lower branch, P_- from the higher initial branch to the higher branch.

In order to calculate the transition rate, we first divide the time-ordered exponentials into the diagonal part H_0 and the off-diagonal part $V_{\rm sys}$ for the electronic system. By using Feynman's disentangling theorem

$$\begin{aligned} \exp_+ \left[-i \int_{-\infty}^{t} H_T(\tau) d\tau \right] &= \exp_+ \left[-i \int_{-\infty}^{t} (H_0(\tau) + V_{\rm sys})\, d\tau \right] \\ &= \exp_+ \left[-i \int_{-\infty}^{t} H_0(\tau) d\tau \right] \cdot \exp_+ \left[-i \int_{-\infty}^{t} \tilde{V}_{\rm sys}(\tau) d\tau \right] \\ \exp_- \left[+i \int_{-\infty}^{t} H_T(\tau) d\tau \right] &= \exp_- \left[+i \int_{-\infty}^{t} \tilde{V}_{\rm sys}(\tau) d\tau \right] \cdot \exp_- \left[+i \int_{-\infty}^{t} H_0(\tau) d\tau \right] \end{aligned}$$

where

$$\begin{aligned} H_0(\tau) &= \begin{pmatrix} \frac{1}{2} v\tau & 0 \\ 0 & -\frac{1}{2} v\tau \end{pmatrix} + H_{\rm ph} + H_I \\ &\equiv \begin{pmatrix} H_1(\tau) & 0 \\ 0 & H_2(\tau) \end{pmatrix}, \end{aligned} \tag{4.2}$$

$$\begin{aligned}\tilde{V}_{\rm sys}(\tau) &= \exp_-\left[+i\int_{-\infty}^{\tau}H_0(\tau')d\tau'\right]V_{\rm sys}\exp_+\left[-i\int_{-\infty}^{\tau}H_0(\tau')d\tau'\right]\\ &= J\left(\exp\left[+i\int_{-\infty}^{\tau}H_1(\tau')d\tau'\right]\cdot\exp\left[-i\int_{-\infty}^{\tau}H_2(\tau')d\tau'\right]|1\rangle\langle 2|\right.\\ &\quad\left.+\exp\left[+i\int_{-\infty}^{\tau}H_2(\tau')d\tau'\right]\cdot\exp\left[-i\int_{-\infty}^{\tau}H_1(\tau')d\tau'\right]|2\rangle\langle 1|\right)\,, \qquad (4.3)\end{aligned}$$

$(2,1)$ and $(1,2)$ component in Eq. (4.1) is rewritten as

$$\begin{aligned}&\left\{\exp_+\left[-i\int_{-\infty}^{\infty}H_T(\tau')d\tau'\right]\right\}_{2,1}\\ &\qquad= \langle 2|\exp_+\left[-i\int_{-\infty}^{\infty}H_0(\tau)d\tau\right]\cdot\exp_+\left[-i\int_{-\infty}^{\infty}\tilde{V}_{\rm sys}(\tau)d\tau\right]|1\rangle\\ &\qquad= \exp\left[-i\int_{-\infty}^{\infty}H_2(\tau)d\tau\right]\cdot\langle 2|\exp_+\left[-i\int_{-\infty}^{\infty}\tilde{V}_{\rm sys}(\tau)d\tau\right]|1\rangle\,, \qquad (4.4)\\ &\left\{\exp_-\left[+i\int_{-\infty}^{\infty}H_T(\tau')d\tau'\right]\right\}_{1,2}\\ &\qquad= \langle 1|\exp_+\left[+i\int_{-\infty}^{\infty}\tilde{V}_{\rm sys}(\tau)d\tau\right]|2\rangle\cdot\exp\left[+i\int_{-\infty}^{\infty}H_2(\tau)d\tau\right]\,. \qquad (4.5)\end{aligned}$$

The time ordered exponentials in Eq.(4.4) and Eq.(4.5) are expanded. The perturbation terms of even order for $\tilde{V}_{\rm sys}$ vanish when $(2,1)$ component is taken,

$$\begin{aligned}&\langle 2|\exp_+\left[-i\int_{-\infty}^{\infty}\tilde{V}_{sys}(\tau)d\tau\right]|1\rangle\\ &\quad= \sum_{m=1}^{\infty}(-i)^{2m-1}\int_{-\infty}^{\infty}d\tau_1\int_{\tau_1}^{\infty}d\tau_2\cdots\int_{\tau_{2m-2}}^{\infty}d\tau_{2m-1}\\ &\qquad\langle 2|\tilde{V}_{\rm sys}(\tau_{2m-1})|1\rangle\langle 1|\cdots\cdots|1\rangle\langle 1|\tilde{V}_{\rm sys}(\tau_2)|2\rangle\langle 2|\tilde{V}_{\rm sys}(\tau_1)|1\rangle \qquad (4.6)\\ &\quad= \sum_{m=1}^{\infty}(-iJ)^{2m-1}\int_{-\infty}^{\infty}d\tau_1\int_{\tau_1}^{\infty}d\tau_2\cdots\int_{\tau_{2m-2}}^{\infty}d\tau_{2m-1}\\ &\qquad\exp\left[+i\int_{-\infty}^{\tau_{2m-1}}H_2(\tau)d\tau\right]\cdot\exp\left[-i\int_{\tau_{2m-2}}^{\tau_{2m-1}}H_1(\tau)d\tau\right]\times\cdots\\ &\qquad\times\exp\left[-i\int_{\tau_1}^{\tau_2}H_2(\tau)d\tau\right]\exp\left[-i\int_{-\infty}^{\tau_1}H_1(\tau)d\tau\right]\,. \qquad (4.7)\end{aligned}$$

$(1,2)$ component can be calculated in the same way, that is,

$$\begin{aligned}&\langle 1|\exp_+\left[+i\int_{-\infty}^{\infty}\tilde{V}_{\rm sys}(\tau)d\tau\right]|2\rangle\\ &\quad= \sum_{m=1}^{\infty}(+iJ)^{2m-1}\int_{-\infty}^{\infty}d\tau_1'\int_{-\infty}^{\tau_1'}d\tau_2'\cdots\int_{-\infty}^{\tau_{2m-2}'}d\tau_{2m-1}'\\ &\qquad\exp\left[+i\int_{-\infty}^{\tau_{2m-1}'}H_1(\tau')d\tau'\right]\cdot\exp\left[-i\int_{\tau_{2m-2}'}^{\tau_{2m-1}'}H_2(\tau')d\tau'\right]\times\cdots\end{aligned}$$

$$\times \exp\left[-i\int_{\tau_1'}^{\tau_2'} H_1(\tau')d\tau'\right] \exp\left[-i\int_{-\infty}^{\tau_1'} H_2(\tau')d\tau'\right] . \tag{4.8}$$

From Eq. (4.7) and Eq. (4.8), we obtain

$$\begin{aligned} P &= -\sum_{n=1}^{\infty}\sum_{m=1}^{n}(-J^2)^n \int_{-\infty}^{\infty} d\tau_1 \int_{\tau_1}^{\infty} d\tau_2 \cdots \int_{\tau_{2m-2}}^{\infty} d\tau_{2m-1} \\ &\quad \cdot \int_{-\infty}^{\infty} d\tau_{2m} \int_{-\infty}^{\tau_{2m}} d\tau_{2m+1} \cdots \int_{-\infty}^{\tau_{2n-1}} d\tau_{2n}\, \mathcal{F}(\tau_1, \tau_2, \cdots, \tau_{2n}) . \end{aligned} \tag{4.9}$$

Note that ρ_1 and $H_1(\tau)$ commute. The integrand $\mathcal{F}(\tau_1, \tau_2, \cdots, \tau_{2n})$ in Eq. (4.9) is given as follows :

$$\begin{aligned} \mathcal{F}(\tau_1, \tau_2, \cdots, \tau_{2n}) &= \left\langle \exp\left[-i\int_{\tau_{2n}}^{\tau_1} H_1(\tau)d\tau\right] \cdot \exp\left[-i\int_{\tau_{2n-1}}^{\tau_{2n}} H_2(\tau)d\tau\right] \cdots \right. \\ &\quad \left. \cdots \exp\left[-i\int_{\tau_2}^{\tau_3} H_1(\tau)d\tau\right] \cdot \exp\left[-i\int_{\tau_1}^{\tau_2} H_2(\tau)d\tau\right] \right\rangle_1 . \end{aligned} \tag{4.10}$$

The diagrammatic representation of Eq. (4.10) is shown in Figure 4.1 as a double-path propagator for the density matrix. The upper side of the diagram represents the motion of the ket vector in Hilbert space, and the downer side represents that of the bra vector. The system makes a transition at each vertex $\{\tau_1, \tau_2, \cdots, \tau_{2n}\}$ from $|1\rangle$ ($\langle 1|$) to $|2\rangle$ ($\langle 2|$) or vice versa. The system is driven by H_1 (in the region by solid line) or by H_2 (in the region by dotted line), according to which electronic state the system is in.

In Figure 4.1, the system propagator for the system starts from the density matrix ρ_{11}. At time τ_1 it makes a transition to ρ_{21} and switches to ρ_{11} at time τ_2. At time interval between τ_8 and τ_3, the system propagates by ρ_{12}, and by ρ_{22} between τ_3 and τ_7, by ρ_{21} between τ_7 and τ_4, by ρ_{11} between τ_4 and τ_5, by ρ_{21} between τ_5 and τ_6. Finally, after time τ_6, the system propagates by ρ_{22}.

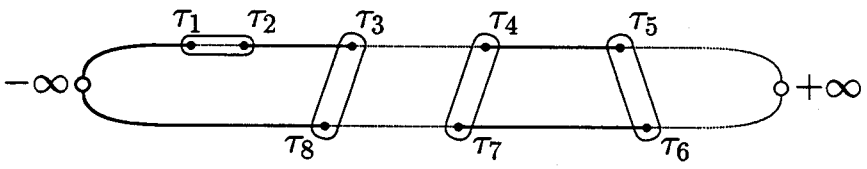

Figure 4.1: The double-path Feynmann diagram for $n = 4$, $m = 3$. In the limit of large amplitude fluctuation, time vertices encircled by the ellipses must be paired off (see next section).

We shift the origin of the phonons and the origin of the energy so that

$$b_k + \frac{1}{2}\alpha_k \longrightarrow b_k\,, \qquad b_k{}^\dagger + \frac{1}{2}\alpha_k \longrightarrow b_k{}^\dagger\,, \tag{4.11}$$

then

$$\begin{aligned} H_1(\tau) \;&\longrightarrow\; \frac{1}{2}v\tau + \sum_k \omega_k b_k{}^\dagger b_k \\ &\equiv\; \frac{1}{2}v\tau + H_{\rm ph}\,, \end{aligned} \tag{4.12}$$

$$\begin{aligned} H_2(\tau) \;&\longrightarrow\; -\frac{1}{2}v\tau + \sum_k \omega_k b_k{}^\dagger b_k - \sum_k \alpha_k\omega_k(b_k + b_k{}^\dagger) + \sum_k \alpha_k^2\omega_k \\ &\equiv\; -\frac{1}{2}v\tau + S\bar{\omega} + H_{\rm ph} - W\,. \end{aligned} \tag{4.13}$$

Equation (4.10) remains in the same form and can be divided into electronic part and phonon part, that is,

$$\mathcal{F}(\tau_1,\tau_2,\cdots,\tau_{2n}) = e^{i\mathcal{E}(\tau_1,\tau_2,\cdots,\tau_{2n})}\mathcal{P}(\tau_1,\tau_2,\cdots,\tau_{2n})\,, \tag{4.14}$$

where the electronic part $\mathcal{E}(\tau_1,\tau_2,\cdots,\tau_{2n})$ is written as

$$\begin{aligned} \mathcal{E}(\tau_1,\tau_2,\cdots,\tau_{2n}) \;&=\; -\frac{v}{4}(\tau_1^2 - \tau_{2n}^2) + \frac{v}{4}(\tau_{2n}^2 - \tau_{2n-1}^2) - \cdots + \frac{v}{4}(\tau_2^2 - \tau_1^2) \\ &\qquad -S\bar{\omega}(\tau_{2n} - \tau_{2n-1} + \cdots + \tau_2 - \tau_1) \\ &=\; \frac{v}{2}\sum_{j=1}^{2n}(-1)^j\tau_j^2 - S\bar{\omega}\sum_{j=1}^{2n}(-1)^j\tau_j\,. \end{aligned} \tag{4.15}$$

The phonon part $\mathcal{P}(\tau_1,\tau_2,\cdots,\tau_{2n})$ is rewritten to, after a rather complicated mathematics, that is,

$$\begin{aligned} \mathcal{P}(\tau_1,\tau_2,\cdots,\tau_{2n}) \;&=\; \Big\langle e^{-iH_{\rm ph}(\tau_1-\tau_{2n})}\cdot e^{-i(H_{\rm ph}-W)(\tau_{2n}-\tau_{2n-1})}\cdot e^{-iH_{\rm ph}(\tau_{2n-1}-\tau_{2n-2})}\cdot \\ &\qquad \cdots e^{-iH_{\rm ph}(\tau_3-\tau_2)}\cdot e^{-i(H_{\rm ph}-W)(\tau_2-\tau_1)}\Big\rangle_1 \qquad (4.16) \\ &=\; \exp\left[\sum_{i=2}^{2n}\sum_{j=1}^{i-1}(-1)^{i+j}G(\tau_i-\tau_j)\right], \qquad (4.17) \end{aligned}$$

where $G(\tau)$ is the generating function defined by Eq. (2.20).

Finally, we can write down the general perturbation terms of n-th order, and the formal expression for the transition rate P, at a Landau-Zener crossing with quantum dissipation, is described as follows :

$$P \;=\; -\sum_{n=1}^{\infty}(-J^2)^n L^{(n)}\,, \tag{4.18}$$

$$\begin{aligned} L^{(n)} \;&=\; \sum_{m=1}^{n}\int_{-\infty}^{\infty}d\tau_1\int_{\tau_1}^{\infty}d\tau_2\cdots\int_{\tau_{2m-2}}^{\infty}d\tau_{2m-1} \\ &\qquad \cdot\int_{-\infty}^{\infty}d\tau_{2m}\int_{-\infty}^{\tau_{2m}}d\tau_{2m+1}\cdots\int_{-\infty}^{\tau_{2n-1}}d\tau_{2n}\;\mathcal{F}(\tau_1,\tau_2,\cdots,\tau_{2n})\,, \end{aligned} \tag{4.19}$$

$$\mathcal{F}(\tau_1,\tau_2,\cdots,\tau_{2n}) = \exp\left[\frac{v}{2}i\sum_{j=1}^{2n}(-1)^j\tau_j^2 - iS\bar{\omega}\sum_{j=1}^{2n}(-1)^j\tau_j + \sum_{i=2}^{2n}\sum_{j=1}^{i-1}(-1)^{i+j}G(\tau_i-\tau_j)\right]. \tag{4.20}$$

4.2 Rapid passage limit

The first result in this study is that the lowest-order term of P coincides with that of the Landau-Zener formula irrespective of the phonon coupling, since

$$\begin{aligned} L^{(1)} &= \int_{-\infty}^{\infty}d\tau_1\int_{-\infty}^{\infty}d\tau_2\,\exp\left[i\frac{v}{2}({\tau_2}^2-{\tau_1}^2) - iS\bar{\omega}(\tau_2-\tau_1) - G(\tau_2-\tau_1)\right] \\ &= \int_{-\infty}^{\infty}d\mu\int_{-\infty}^{\infty}d\sigma\,\exp\left[iv\sigma\mu - iS\bar{\omega}\sigma - G(\sigma)\right] \\ &= \frac{2\pi}{|v|}. \end{aligned} \tag{4.21}$$

where new variables are introduced, $\mu = (\tau_1+\tau_2)/2$ and $\sigma = \tau_2 - \tau_1$. This means that in the rapid passage limit of $J^2/|v| \ll 1$, the transition rate is not affected by the quantum dissipation and given by the Landau-Zener formula,

$$\begin{aligned} P &\sim P_{LZ} \\ &= \frac{2\pi J^2}{|v|} + O(J^4). \end{aligned} \tag{4.22}$$

4.3 Large amplitude fluctuation limit

4.3.1 Pairing-off theorem

It is difficult to evaluate the multiple integrals for general terms, however, the meaning of formula becomes clear in the limit of large amplitude $D/\bar{\omega} \gg 1$, namely in the limit of strong coupling or high temperature. The following theorem is primary important for the analysis of the dynamical process in this limit.

Pairing-off theorem. Out of all the configurations of the time vertices that appear in the diagrams shown in Figure 4.1, only those make nonvanishing contributions to the integral in Eq. (4.19), in which $2n$ vertices make pairs with intrapair distance less than D^{-1} except for special cases in which an even number of vertices not less than four make groups with mutual distance less than $(\bar{\omega}D)^{1/2}$.

Proof. In order to prove the theorem, we divide the exponent of Eq. (4.20) into the real part $\mathcal{R}(\tau_1, \tau_2, \cdots, \tau_{2n})$ and the imaginary part $\mathcal{I}(\tau_1, \tau_2, \cdots, \tau_{2n})$. The real part

$$\mathcal{R}(\tau_1, \tau_2, \cdots, \tau_{2n}) = \mathrm{Re}\left[\sum_{i=2}^{2n}\sum_{j=1}^{i-1}(-1)^{i+j}G(\tau_i - \tau_j)\right] \tag{4.23}$$

originates from the fluctuation of the energy. We observe that $\mathcal{R}(\tau_1, \tau_2, \cdots, \tau_{2n})$ can be rewritten as

$$\mathcal{R}(\tau_1, \tau_2, \cdots, \tau_{2n}) = -\frac{1}{2}\int_{-\infty}^{\infty} d\omega\phi(\omega)\omega^{-2} \times \left|\sum_{j=1}^{2n}(-1)^j e^{i\omega\tau_j}\right|^2 . \tag{4.24}$$

Note that $\mathcal{R}(\tau_1, \tau_2, \cdots, \tau_{2n})$ is a nonpositive definite quantity. Since

$$\int_{-\infty}^{\infty} d\omega\phi(\omega)\omega^{-2} \simeq D^2/\bar{\omega}^2 \gg 1\,, \tag{4.25}$$

$\mathcal{R}(\tau_1, \tau_2, \cdots, \tau_{2n})$ becomes negative with a large absolute value unless the following condition is satisfied:

$$\left|\sum_{j=1}^{2n}(-1)^j e^{i\omega\tau_j}\right| < \bar{\omega}/D\,. \tag{4.26}$$

Since the integral with respect to ω runs over the interval of order γ, the above condition is satisfied in the limit $D/\bar{\omega} \to \infty$ only when $2n$ vertices are paired off, namely, a time vertex with even suffix coincides with a time vertex with odd suffix to be canceled out as shown in Figure 4.1. By expanding the expression $\sum_{j=1}^{2n}(-1)^j e^{i\omega\tau_j}$ in a power series around the paired-off configuration, the theorem is immediately proved.

The pairing-off property of the strongly coupled localized electron-phonon system has been described by Kusunoki [9] in a less clear way. Sumi correctly stated the pairing-off ansatz in his study of the nonradiative process in solids [10]. The pairing-off theorem plays an essential role in understanding the dual character of the Raman scattering and the luminescence in the second-order optical process of the strongly coupled electron-phonon system [36].

The above theorem provides a mathematical basis for the *noninteracting blip approximation*, which is widely used in the study of the dynamics of the spin-boson system. In its lowest order, the noninteracting blip approximation requires us to simply drop all the terms $G(\tau_i - \tau_j)$ that extend over different pairs [25]. By this approximation, the memory of the boson system about the previous history is instantly lost at each blip. In order to correctly describe the energy relaxation, which is important in the strong-coupling limit, the history must be taken into account as the interaction between blips.

The pairing-off theorem is a consequence of the ultrafast phase relaxation in the large-amplitude fluctuation limit. As can be seen from Figure 4.1, the density matrix propagates almost always in the diagonal form in this limit.

If one notices that

$$\sum_{i=2}^{2n}\sum_{j=1}^{i-1}(-1)^{i+j}(\tau_i-\tau_j) = -\sum_{j=1}^{2n}(-1)^j\tau_j\,,$$

the imaginary part $\mathcal{I}(\tau_1,\tau_2,\cdots,\tau_{2n})$ of the exponent of Eq. (4.20) can be rewritten as

$$\begin{aligned}\mathcal{I}(\tau_1,\tau_2,\cdots,\tau_{2n}) &= \frac{1}{2}v\sum_{j=1}^{2n}(-1)^j\tau_j^2 \\ &\quad -\int_{-\infty}^{\infty}d\omega\frac{\phi(\omega)}{\omega^2}\times\sum_{i=2}^{2n}\sum_{j=1}^{i-1}(-1)^{i+j}\sin\omega(\tau_i-\tau_j)\,. \end{aligned} \tag{4.27}$$

We classify the paired configuration into two groups: the vertical pairs and the horizontal pairs. The vertical pairs lies across the upper and the lower propagator like pairs (τ_3,τ_8), (τ_7,τ_4), and (τ_5,τ_6) in Figure 4.1. The horizontal pair lies within the upper or lower propagator like (τ_1,τ_2). Denote the pairs as $(\tau_{\lambda_1},\tau_{\lambda_2})\,,(\tau_{\lambda_3},\tau_{\lambda_4})\,,\cdots,(\tau_{\lambda_{2n-1}},\tau_{\lambda_{2n}})$ as they are ordered from left toward right, where we take λ_{2m-1}=odd and λ_{2m}=even. Introduce a set of new variables as

$$\mu_m = (\tau_{\lambda_{2m}}+\tau_{\lambda_{2m-1}})/2\,,\quad \sigma_m = \tau_{\lambda_{2m}}-\tau_{\lambda_{2m-1}}\,. \tag{4.28}$$

Then in the limit of $D/\bar{\omega}\gg 1$, the saddle-point method can be applied to the evaluation of the multiple time-ordered integrals by expanding $\mathcal{R}(\tau_1,\tau_2,\cdots,\tau_{2n})$ and $\mathcal{I}(\tau_1,\tau_2,\cdots,\tau_{2n})$ to the lowest order in σ_m. The real part can be readily approximated as

$$\mathcal{R}(\tau_1,\tau_2,\cdots,\tau_{2n}) \sim -\frac{1}{2}\int_{-\infty}^{\infty}d\omega\phi(\omega)\times\sum_{p=1}^{m}\sum_{q=1}^{m}\cos\omega(\mu_p-\mu_q)\cdot\sigma_p\sigma_q\,. \tag{4.29}$$

On the other hand, the imaginary part can be evaluated by an elementary but somewhat tedious counting-up of the diagram and by some exercise of trigonometry as

$$\mathcal{I}(\tau_1,\tau_2,\cdots,\tau_{2n}) \sim \sum_{p=1}^{n}E_p^{(q)}(\mu_{v_1},\mu_{v_2},\cdots,\mu_{v_q};\mu_p)\sigma_p\,, \tag{4.30}$$

where $E_p^{(q)}(\mu_{v_1},\mu_{v_2},\cdots,\mu_{v_q};\mu_p)$ is given by

$$\begin{aligned}E_p^{(q)}(\mu_{v_1},\mu_{v_2},\cdots,\mu_{v_q};\mu_p) &= v\mu_p+(-1)^{q+1}S\bar{\omega} \\ &\quad +2\sum_{j=1}^{q}(-1)^j\times\int_{-\infty}^{\infty}d\omega\frac{\phi(\omega)}{\omega}\cos\omega(\mu_p-\mu_j)\,. \end{aligned} \tag{4.31}$$

In the above equation, μ_{v_1}, μ_{v_2}, $\cdots$, μ_{v_q} are the times for the vertical pairs that lie to the left of μ_p in Figure 4.1. For the case that there is no vertical pair before μ_p, $E_p^{(q)}$ should read as $E_p^{(0)}\equiv v\mu_p-S\bar{\omega}$.

Although the derivation is somewhat complicated, the meaning of the above formula is obvious. The energy $E_p^{(q)}$ is nothing but the negative value of the Franck-Condon energy measured from $|1\rangle$ to $|2\rangle$ for the phonon wave packet, which has following history; it starts from the equilibrium distribution in the subspace $|1\rangle$, makes a vertical transition to the adiabatic potential surface of $|2\rangle$ at time μ_{v_1}, is driven by the Hamiltonian within the subspace $|2\rangle$ until the time μ_{v_2} at which it jumps again to the adiabatic potential surface of $|1\rangle$, and so on. For q even, the packet lies on the adiabatic potential surface in $|1\rangle$ and for q odd, in $|2\rangle$. Therefore, it can be said that the vertical pair correspond to the *transition* while the horizontal pair corresponds to the *polarization*. At each time the system make a transition, the equilibrium point of the phonon system shifts from left to right and vice versa. Such a situation may be visualized by the configuration coordinate diagram for the interaction mode, as shown in Figure 4.2.

So far, we have not considered the time duration $\tau_{\rm tr}$ within which the system exists in the transition region. The time $\tau_{\rm tr}$ is a measure of the time interval for which the multiple-integral of Eq. (4.19) converges. On the other hand, the pairing-off theorem tells us that the contribution from the integral over σ_p for each pair is restricted within the time interval $|\sigma_p| < \tau_{\rm ph}(\sim D^{-1})$ in the order of magnitude. The transition associated with each pair becomes a *real* transition only in the case that the phase relaxation time is far less than the transition time, namely, $\tau_{\rm ph} \ll \tau_{\rm tr}$.

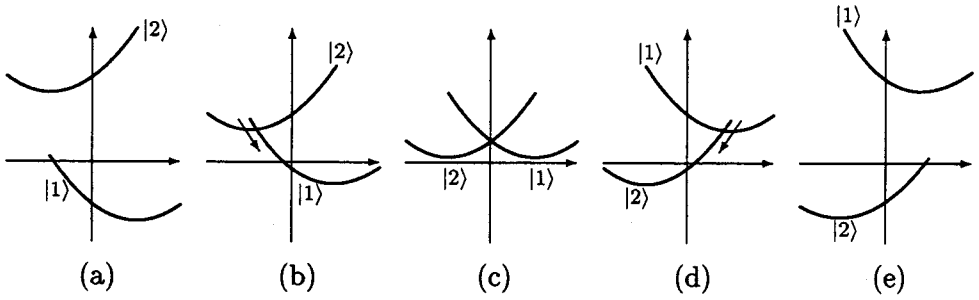

Figure 4.2: The schematic time evolution of the configuration coordinate diagram for the level crossing with energy dissipation. The time evolution is from (a) to (e) in the case $v > 0$ and from (e) to (a) in the case $v < 0$.

4.3.2 Coherent limit of fast passage

Here, we consider the case that the velocity $|v|$ is so large that the condition $\tau_{\rm ph} \gg \tau_{\rm tr}$ is satisfied. In this case, the real part $\mathcal{R}(\tau_1, \tau_2, \cdots, \tau_{2n})$ given in Eq. (4.29) can be approximated as

$$\mathcal{R}(\tau_1,\tau_2,\cdots,\tau_{2n}) = -\frac{1}{2}D^2\left(\sum_{p=1}^{n}\sum_{q=1}^{n}\sigma_p\sigma_q\right)$$
$$= -\frac{1}{2}D^2\left\{\sum_{j=1}^{2n}(-1)^j\tau_j\right\}^2, \tag{4.32}$$

since $|\mu_p - \mu_q| \ll \gamma^{-1}$ for all p and q. Likewise, the imaginary part can be approximated simply as

$$\mathcal{I}(\tau_1,\tau_2,\cdots,\tau_{2n}) = \frac{1}{2}v\sum_{j=1}^{2n}(-1)^j\tau_j^2. \tag{4.33}$$

Equation (4.32) means that the fluctuation of the energy behaves as a static Gaussian distribution of the energy for a very short time interval. In fact, the effect of $\mathcal{R}(\tau_1,\tau_2,\cdots,\tau_{2n})$ can be eliminated by applying the identity

$$\exp\left[-\frac{D^2X^2}{2}\right] = \frac{1}{\sqrt{2\pi}D}\int_{-\infty}^{\infty}dq\,\exp\left[-\frac{q^2}{2D^2} - iqX\right], \tag{4.34}$$

for $X \equiv \sum_{j=1}^{2n}(-1)^j\tau_j$. The integrand of Eq. (4.20) then becomes

$$\frac{1}{\sqrt{2\pi}D}\int_{-\infty}^{\infty}dq\,\exp\left[i\frac{v}{2}\sum_{j=1}^{2n}(-1)^j\left(\tau_j - \frac{q}{v}\right)^2 - \frac{q^2}{2D^2}\right]. \tag{4.35}$$

The change of integral variables from τ_j to $\tau_j' \equiv \tau_j - q/v$ does slightly change the integral domain by q/v, however, this effect can be neglected when the upper and the lower bound for τ_j integral are $[-\infty,\infty]$, or, in the case that the condition $D/|v| \ll 1/\bar{\omega}$ is satisfied because the dominant contribution to the integral of Eq. (4.35) comes from the region $|q| < D$. By interchanging the order of the integration over q and τ_j, we obtain the desired result.

The integrand of the perturbation terms are then rewritten as,

$$\mathcal{F}(\tau_1,\tau_2,\cdots,\tau_{2n}) = \exp\left[i\frac{v}{2}\sum_{j=1}^{2n}(-1)^j\tau_j^2\right], \tag{4.36}$$

this is, nothing but the perturbation expression of original Zener's model for the transition rate. The evaluation of all the perturbation terms results in the Landau-Zener formula,

$$L^{(n)} = \frac{1}{n!}\left(\frac{2\pi}{|v|}\right)^n, \tag{4.37}$$

$$P = P_{LZ} \equiv 1 - \exp\left[-2\pi J^2/|v|\right]. \tag{4.38}$$

The argument here is the essence of the proof of the applicabity of the Landau-Zener formula to the nonradiative hot transitions in the strongly coupled localized electron-phonon system with a potential crossing [11].

4.3.3 Incoherent limit of slow passage

Next, we turn to the limit of slow passage, $\tau_{\rm tr} \gg \tau_{\rm ph}$. In this case, the coherence is interrupted every moment in the relatively long time interval $\tau_{\rm tr}$ and the vertical pairs in Figure 4.1 can be interpreted as representing real transitions. The system makes multiple transitions between $|1\rangle$ and $|2\rangle$ while relaxing toward the equilibrium state within the respective electronic subspace. Therefore, the probability P would be depend on the relative length of $\tau_{\rm tr}$ and $\tau_{\rm en}$. Useful expressions for P can be obtained in the case that a little stronger condition

$$\tau_{\rm tr} > \tau_{\rm en} \tag{4.39}$$

is satisfied. In this case, $\mathcal{R}(\tau_1, \tau_2, \cdots, \tau_{2n})$ can be approximated as

$$\mathcal{R}(\tau_1, \tau_2, \cdots, \tau_{2n}) = -\frac{1}{2} D^2 \left(\sum_{p=1}^{n} \sigma_p^2 \right) , \tag{4.40}$$

since the cross terms vanish because of the dephasing,

$$\int_{-\infty}^{\infty} d\omega \phi(\omega) \omega^{-1} \cos \omega(\mu_p - \mu_q) \sim 0 , \tag{4.41}$$

for general configurations of μ_p and μ_q with $|\mu_p - \mu_q| \sim O(\tau_{\rm en})$. The variables of integration are changed from $(\tau_1, \tau_2, \cdots, \tau_{2n})$ to $(\mu_1, \mu_2, \cdots, \mu_n, \sigma_1, \sigma_2, \cdots, \sigma_n)$. We assign a set of signatures $(\xi_1, \xi_2, \cdots, \xi_n)$ to each diagram corresponding to a serial time ordering, where $\xi_m = +1$ if $\tau_{\lambda_{2m-1}} < \tau_{\lambda_{2m}}$ and $\xi_m = -1$ if $\tau_{\lambda_{2m}} < \tau_{\lambda_{2m-1}}$. For example, $(\xi_1, \xi_2, \xi_3, \xi_4) = (+1, -1, -1, +1)$ in the case of time ordering in Figure 4.1. Then, the following lemma can be proved by an elementary counting up of the diagram.

Lemma 1. In the total set of possible time ordering that appears in the $2n$-th order terms of the perturbation expansion, every set $(\xi_1, \xi_2, \cdots, \xi_n)$ with $\xi_p = \pm 1$ for $p = 1, 2, \cdots, n$ appear 2^{n-1} times.

Since the integral over σ_p converges for $|\sigma_p| < \tau_{\rm ph}$, the restriction on the integral domain for μ_p can be safely relaxed as $-\infty < \mu_1 \le \mu_1 \le \cdots \le \mu_n < \infty$. On the other hand, the integral domain of σ_p can be extended to $-\infty < \sigma_p < \infty$ for the vertical pairs and to $0 \le \sigma_p < \infty$ or $-\infty < \sigma_p \le 0$ for the horizontal pairs.

First, we calculate P for the case that the energy dissipation is negligible, $S\bar{\omega} \to 0$, while the condition $D/\bar{\omega} \gg 1$ is still satisfied. This corresponds to the high-temperature limit with small coupling. The imaginary part $\mathcal{I}(\tau_1, \tau_2, \cdots, \tau_{2n})$ can be written as

$$\mathcal{I}(\tau_1, \tau_2, \cdots, \tau_{2n}) = v \sum_{p=1}^{n} \mu_p \sigma_p , \tag{4.42}$$

and because of the above lemma, we find

$$
\begin{aligned}
L^{(n)} &= 2^{n-1}\int_{-\infty}^{\infty}d\mu_1\int_{\mu_1}^{\infty}d\mu_2\cdots\int_{\mu_{n-1}}^{\infty}d\mu_n\cdot\int_{-\infty}^{\infty}d\sigma_1\int_{-\infty}^{\infty}d\sigma_2\cdots\int_{-\infty}^{\infty}d\sigma_n \\
&\qquad\times\exp\left[i\sum_{p=1}^{n}\left(v\mu_p\sigma_p-\frac{1}{2}D^2\sigma_p^2\right)\right] \\
&= \frac{2^{n-1}}{n!}\left\{\int_{-\infty}^{\infty}d\mu\int_{-\infty}^{\infty}d\sigma\exp\left[iv\mu\sigma-\frac{1}{2}D^2\sigma^2\right]\right\}^n \\
&= \frac{1}{2}\frac{1}{n!}\left(\frac{4\pi}{|v|}\right)^n . \qquad (4.43)
\end{aligned}
$$

Inserting the above result into Eq. (4.18), we obtain,

$$
P = P_{SD} \equiv \frac{1}{2}\left(1-\exp\left[-4\pi J^2/|v|\right]\right) . \qquad (4.44)
$$

This formula has been derived by Kayanuma [21] with a slightly different argument for the stochastic model. It should be noted that

$$
P_{SD}\to 2\pi J^2/|v| \quad \text{for } J^2/|v|\to 0 , \qquad (4.45)
$$

as is consistent with the previous argument, and

$$
P_{SD}\to\frac{1}{2} \quad \text{for } J^2/|v|\to\infty . \qquad (4.46)
$$

This means that the strong decoherence reduces the whole transition process to diffusionlike so that the system exists with even probability in both states, after the slow passage.

Next, we consider the effect of the energy dissipation for general values of ΔE. According to the pairing-off theorem, we obtain

$$
\begin{aligned}
L^{(n)} &= \sum_c\int_{-\infty}^{\infty}d\mu_1\int_{\mu_1}^{\infty}d\mu_2\cdots\int_{\mu_{n-1}}^{\infty}d\mu_n\cdot\int_{-\infty}^{\infty}d\sigma_1\int_{-\infty}^{\infty}d\sigma_2\cdots\int_{-\infty}^{\infty}d\sigma_n \\
&\qquad\times\exp\left[i\sum_{p=1}^{n}E_p^{(q)}(\mu_{v_1},\mu_{v_2},\cdots,\mu_{v_q};\mu_p)\sigma_p-\frac{1}{2}D^2\sum_{p=1}^{n}\sigma_p^2\right] , \qquad (4.47)
\end{aligned}
$$

where the summation $\sum_c$ runs over all of the possible configurations of the vertical pairs. The integration over σ_p gives

$$
L^{(n)} = \sum_c\int_{-\infty}^{\infty}d\mu_1\int_{\mu_1}^{\infty}d\mu_2\cdots\int_{\mu_{n-1}}^{\infty}d\mu_n\prod_{p=1}^{n}K(\mu_{v_1},\mu_{v_2},\cdots,\mu_{v_q};\mu_p) , \qquad (4.48)
$$

where

$$
K(\mu_{v_1},\mu_{v_2},\cdots,\mu_{v_q};\mu_p) = \frac{\sqrt{2\pi}}{D}\exp\left[-\frac{\left\{E_p^{(q)}(\mu_{v_1},\mu_{v_2},\cdots,\mu_{v_q};\mu_p)\right\}^2}{2D^2}\right] . \qquad (4.49)
$$

Equation (4.48) indicates that the probability P is determined by the successive incoherent transitions of the wave packets of phonons, which are subject to sudden shift of the equilibrium position while undergoing the relaxed oscillation.

In the cases of slow-passage limit, we can approximate the Frank-Condon energy $E_p^{(q)}(\mu_{v_1}, \mu_{v_2}, \cdots, \mu_{v_q}; \mu_p)$ by its asymtonic value

$$E_p^{(q)} \equiv v\mu_p + (-1)^{q+1} S\bar{\omega} \tag{4.50}$$

for $|\mu_p - \mu_j| \gg \tau_{\rm en}$, since the variables μ_p are distributed sparsely in the integral domain of order of $\tau_{\rm tr}$. This means that the phonon system relaxes to the equilibrium cofiguration immediately after the transition so that each transition event occurs always from the bottoms of the adiabatic potentials of the respective electronic subspace. The equilibrium configuration at time μ_p depends on the number q of the vertical pairs before μ_p.

$K(\mu_{v_1}, \mu_{v_2}, \cdots, \mu_{v_q}; \mu_p)$ in Eq. (4.49) is then rewritten as

$$\begin{aligned} K(\mu_{v_1}, \mu_{v_2}, \cdots, \mu_{v_q}; \mu_p) &= \frac{\sqrt{2\pi}}{D} \exp\left[-\frac{(S\bar{\omega} - v\mu_p)^2}{2D^2}\right] \equiv F_-(\mu_p) \\ &\equiv 2\pi F(S\bar{\omega} - v\mu_p) \qquad \text{for} \quad q = \text{even}, \end{aligned} \tag{4.51}$$

or

$$\begin{aligned} K(\mu_{v_1}, \mu_{v_2}, \cdots, \mu_{v_q}; \mu_p) &= \frac{\sqrt{2\pi}}{D} \exp\left[-\frac{(S\bar{\omega} + v\mu_p)^2}{2D^2}\right] \equiv F_+(\mu_p) \\ &\equiv 2\pi F(S\bar{\omega} + v\mu_p) \qquad \text{for} \quad q = \text{odd}, \end{aligned} \tag{4.52}$$

where the quantity

$$F(E) \equiv \frac{1}{2\pi} \int_{-\infty}^{\infty} dt \exp\left[-iEt - \frac{D^2}{2}t^2\right] \tag{4.53}$$

means a line-shape function which is related to the optical absorption intensity of the system for virtual photon with energy zero. The integrand of Eq. (4.48) is given as a sum of all the possible combinations of the terms, like $F_-(\mu_1)F_-(\mu_2)F_+(\mu_3)\cdots F_-(\mu_n)$. Note that the first component is always $F_-(\mu_1)$. Again, an inspection leads to the following lemma.

Lemma 2. In the total set of possible diagrams that appear in the $2n$th order terms of the perturbation expansion, all the combinations of $F_{j_2}(\mu_2)F_{j_3}(\mu_3)\cdots F_{j_n}(\mu_n)$ with $j_p = \pm \quad (p = 2, 3, \cdots, n)$ appear once.

Then, $L^{(n)}$ is given by

$$L^{(n)} = \int_{-\infty}^{\infty} d\mu_1 \int_{\mu_1}^{\infty} d\mu_2 \cdots \int_{\mu_{n-1}}^{\infty} d\mu_n F_-(\mu_1) \times \prod_{m=2}^{n} \{F_+(\mu_m) + F_-(\mu_m)\} \,. \tag{4.54}$$

Since the integral is unchanged against the permutations of $(\mu_2, \mu_3, \cdots, \mu_n)$, we obtain

$$L^{(n)} = \frac{1}{(n-1)!} \int_{-\infty}^{\infty} d\mu_1 F_-(\mu_1) \cdot \left[\int_{\mu_1}^{\infty} d\mu_2 \{F_+(\mu_2) + F_-(\mu_2)\}\right]^{n-1} . \tag{4.55}$$

By inserting this into Eq. (4.18), we obtain

$$P = J^2 \int_{-\infty}^{\infty} d\mu_1 F_-(\mu_1) \cdot \exp\left[-J^2 \int_{\mu_1}^{\infty} d\mu_2 \{F_+(\mu_2) + F_-(\mu_2)\}\right] . \tag{4.56}$$

This is a central result of this section.

In the case of weak coupling and high temperature, we can put $F_+(\mu) = F_-(\mu) = 2\pi F(v\mu)$ with $F(v\mu) = (1/2\pi D)\exp[-v^2\mu^2/2D^2]$ and get

$$\begin{aligned} P &= 2\pi J^2 \int_{-\infty}^{\infty} d\mu_1 F(v\mu_1) \cdot \exp\left[-4\pi J^2 \int_{\mu_1}^{\infty} d\mu_2 F(v\mu_2)\right] \\ &= \frac{1}{2}\left(1 - \exp\left[-4\pi J^2/|v|\right]\right) , \end{aligned} \tag{4.57}$$

which recovers the formula (4.44). The identity

$$\exp\left[\int_a^b dt f(t)\right] = 1 + \int_a^b dt f(t) \exp\left[\int_t^b d\tau f(\tau)\right] . \tag{4.58}$$

has been used in deriving the above result.

In the limit of strong coupling at low temperature, we set $D \to \sqrt{S\bar{\omega}}$. It should be noted that $F_+(\mu)$ and $F_-(\mu)$ have nonvanishing values only at around $\mu = -S\bar{\omega}/v$ and $\mu = S\bar{\omega}/v$, respectively. The value of P strongly depends on the sign of v. We denote the value of P for $v > 0$ ($v < 0$) as P_+ (P_-) hereafter. In the case $v > 0$, $F_+(\mu)$ in the exponent of Eq. (4.56) can be neglected since the contribution from μ_1 integration is limited at around $\mu_1 \sim S\bar{\omega}/v$. Then, we obtain

$$\begin{aligned} P_+ &= J^2 \int_{-\infty}^{\infty} d\mu_1 F_-(\mu_1) \cdot \exp\left[-J^2 \int_{\mu_1}^{\infty} d\mu_2 F_-(\mu_2)\right] \\ &= 1 - \exp\left[-2\pi J^2/v\right] = P_{LZ} . \end{aligned} \tag{4.59}$$

On the other hand, in the case $v < 0$, both $F_+(\mu)$ and $F_-(\mu)$ must be considered. However, the nonvanishing domains of $F_+(\mu)$ and $F_-(\mu)$ are separated each other and the contribution of the integral over μ_1 comes from $\mu_1 \sim S\bar{\omega}/v \ll 0$, while the main contribution of the integral for $F_+(\mu)$ over μ_2 comes from $\mu_2 \sim -S\bar{\omega}/v \gg 0$. We can safely extend the lower limit of the integration for $F_+(\mu)$ over μ_2 to $-\infty$. Namely,

$$\begin{aligned} P_- &= J^2 \int_{-\infty}^{\infty} d\mu_1 F_-(\mu_1) \cdot \exp\left[-J^2 \int_{\mu_1}^{\infty} d\mu_2 F_-(\mu_2) - J^2 \int_{-\infty}^{\infty} d\mu_2 F_+(\mu_2)\right] \\ &= \left\{1 - \exp\left[-2\pi J^2/|v|\right]\right\} \cdot \exp[-2\pi J^2|v|] \\ &= P_{LZ}(1 - P_{LZ}) . \end{aligned} \tag{4.60}$$

Ao and Rammer [23] first pointed out that, at zero temperature, the transition rate becomes identical with the Landau-Zener formula in spite of the dissipation. This is correct provided that the speed of passage is slow enough and the crossing occurs from the lower-energy side.

For intermediate values of v, P_+ deviates to P_{LZ} to increase the apparent nonadiabaticity, as will be shown in the next chapter. It is a little surprising that P_+ becomes identical with P_{LZ} both in the limit of rapid passage as shown in Eq. (4.38) and in the slow passage as shown in Eq. (4.59). The reason is, however, quite different between the two cases. Since the original Landau-Zener formula is derived for the coherent process, it may be said that the formula (4.59) obtained for the incoherent limit is a result of coincidence [23]. In the case of $v < 0$, the sequential application of P_{LZ} leads to Eq. (4.60) as a whole transition rate. The level crossing effectively occurs twice in this case, first at $t = -S\bar{\omega}/|v|$ and next at $t = S\bar{\omega}/|v|$ as shown in Figure 4.2.

Note the fact that P_+ (P_-) can be obtained as the value of $\tilde{p}(t)$ at $t \to \infty$, which obeys the rate equation,

$$\frac{d\tilde{p}(t)}{dt} = J^2 F_-(t)\tilde{p}(t) - J^2 F_+(t)\{1 - \tilde{p}(t)\}\ , \quad \tilde{p}(0) = 0\,. \tag{4.61}$$

If one notes that F_+ and F_- are interchanged by the change of the sign of v, a useful relation is obtained from Eq. (4.56) as

$$\begin{aligned} P_+ + P_- &= J^2 \int_{-\infty}^{\infty} d\mu_1 \{F_+(\mu_1) + F_-(\mu_1)\} \exp\left[-J^2 \int_{\mu_1}^{\infty} d\mu_2 \{F_+(\mu_2) + F_-(\mu_2)\}\right] \\ &= 1 - \exp\left[-4\pi J^2/|v|\right] = 2P_{SD}\,. \end{aligned} \tag{4.62}$$

For sufficiently large $J^2/|v|$, this behaves as $P_+ + P_- = 1$, which means the transition rate is not affected by the initial state from which the system undergoes level-crossing. The transition rate can be determined just by the final state, namely, the transition rate to the lower branch is given by $P_{LZ} \sim 1$, and that to the higher branch by $1 - P_{LZ}$.

4.4 General cases

The general behavior for the transition rate is made clear by numerical calculations, in next chapter. The transition rate has a tendency to decrease under the existence of energy fluctuation. It can be said that the effect of phase relaxation increases nonadiabacity. In the limit of the energy fluctuation alone, it is possible to treat the environmental perturbation as a Gaussian stochastic fluctuation of the energy levels with the amplitude D and the decay constant of the correlation of order of γ. It has been shown that, as a function of the speed of the passage, there is an optimum value of v that maximizes the transition rate, and P tends to $P_{SD}(\sim 1/2)$ in the limit of slow passage [21].

On the other hand, the transition rate to the lower branch has a tendency to decrease, and that to the upper branch has a tendency to increase under the energy dissipation, so the transition rate depends on the sign of v. In general, the transition rate from the lower branch P_+ is bounded as $P_{SD} \leq P_+ \leq P_{LZ}$ for a fixed value of $J^2/|v|$.

4.5 Summary

The transition rate for the Landau-Zener problem with dissipation is analytically investigated by the formal perturbation expansion series with respect to the off-diagonal matrix element. Closed expressions of the transition rate are derived for various limiting situations in a unified way. The formulas derived are listed as follows:

1. Generally, (in the rapid passage limit $J^2/|v| \ll 1$),

$$P_+ = P_- = \frac{2\pi J^2}{|v|} + O(J^4) \sim P_{LZ}\,.$$

2. Coherence limit $\tau_{\rm tr} \ll \tau_{\rm ph}$,

$$P_+ = P_- = P_{LZ}\,.$$

3. Decoherence limit $\tau_{\rm ph} \ll \tau_{\rm tr}$ and $\tau_{\rm tr} > \tau_{\rm en}$,

$$P = 2\pi J^2 \int_{-\infty}^{\infty} d\mu_1 F(S\bar{\omega} - v\mu_1) \times \exp\left[-2\pi J^2 \int_{\mu_1}^{\infty} d\mu_2 \left\{F(S\bar{\omega} + v\mu_2) + F(S\bar{\omega} - v\mu_2)\right\}\right].$$

$$P_+ = P_- = P_{SD} \qquad \text{for } S \to 0 \text{ with } D = \text{finite}.$$

$$P_+ = P_{LZ}\,, \quad P_- = P_{LZ}(1 - P_{LZ}) \qquad \text{for } S \gg 1 \text{ and } T = 0.$$

where $\tau_{\rm ph} \equiv 1/D$, $\tau_{\rm tr} \equiv J/|v|$, $F(E)$ is a line-shape function for optical excitation for virtual photon with energy zero.

Chapter 5

The Landau-Zener Problem II. Numerical Results

In this chapter, we show the numerical results for the transition rate of Landau-Zener model with dissipation. The probability $p(t)$ that the system exists in $|2\rangle$ at time t under the condition it starts from $|1\rangle$ at a remote past is calculated. The notations $p_+(t)$ and $p_-(t)$ are used in order to specify the sign of v; $p_+(t)$ for $v > 0$ and $p_-(t)$ for $v < 0$. Also we define the transition rate P_+ and P_- as $p_+(t)$ and $p_-(t)$ at $t \to +\infty$, respectively. In the presentation of the results, we adopt the dimensionless parameters normalized by $\bar{\omega}$; $\tilde{J} \equiv J/\bar{\omega}$, $\tilde{v} \equiv v/\bar{\omega}^2$, $\tilde{\kappa} \equiv \kappa/\bar{\omega}$, $\tilde{T} \equiv k_B T/\bar{\omega}$, and $\tilde{D} \equiv D/\bar{\omega}$.

5.1 Strong-coupling limit at zero temperature

5.1.1 Time evolution of the transition rate

First we show the results in strong-coupling limit at zero temperature, namely, $S \gg 1$ and $T = 0$. In this limit , the criterion of large amplitude fluctuation $\tilde{D} = \sqrt{S(2\bar{n}+1)} \gg 1$ is satisfied in any parameter values of $\{\tilde{J}, \tilde{v}, \tilde{\kappa}, \tilde{T}\}$, even at zero temperature, so we can check the validity of formulas for the transition rate in the coherent limit and in the incoherent limit.

In Figure 5.1, examples of the calculated $p_+(t)$ are shown for fixed values of $S = 10.0$, $\tilde{J} = 0.5$, and $\tilde{\kappa} = 0.2$ at zero temperature with $\tilde{v}$ as a parameter. In Figure 5.2 is also shown $p_-(t)$ for the same parameter values as in Figure 5.1, but for the negative sign of v. The behaviors of $p_+(t)$ and $p_-(t)$ are very similar in the rapid passage case, $|\tilde{v}| = 25.0$ for example, and P_+ and P_-, defined as $P_+ \equiv \lim_{t\to\infty} p_+(t)$, $P_- \equiv \lim_{t\to\infty} p_-(t)$ agree with the Landau-Zener formula $P_+ = P_- = P_{LZ}$ fairly well. This is the case of the coherent transition given by Eq. (4.38). As $|\tilde{v}|$ becomes smaller, the difference between $p_+(t)$ and $p_-(t)$ becomes evident. The behavior of $p_-(t)$ clearly shows the back-transfer effect.

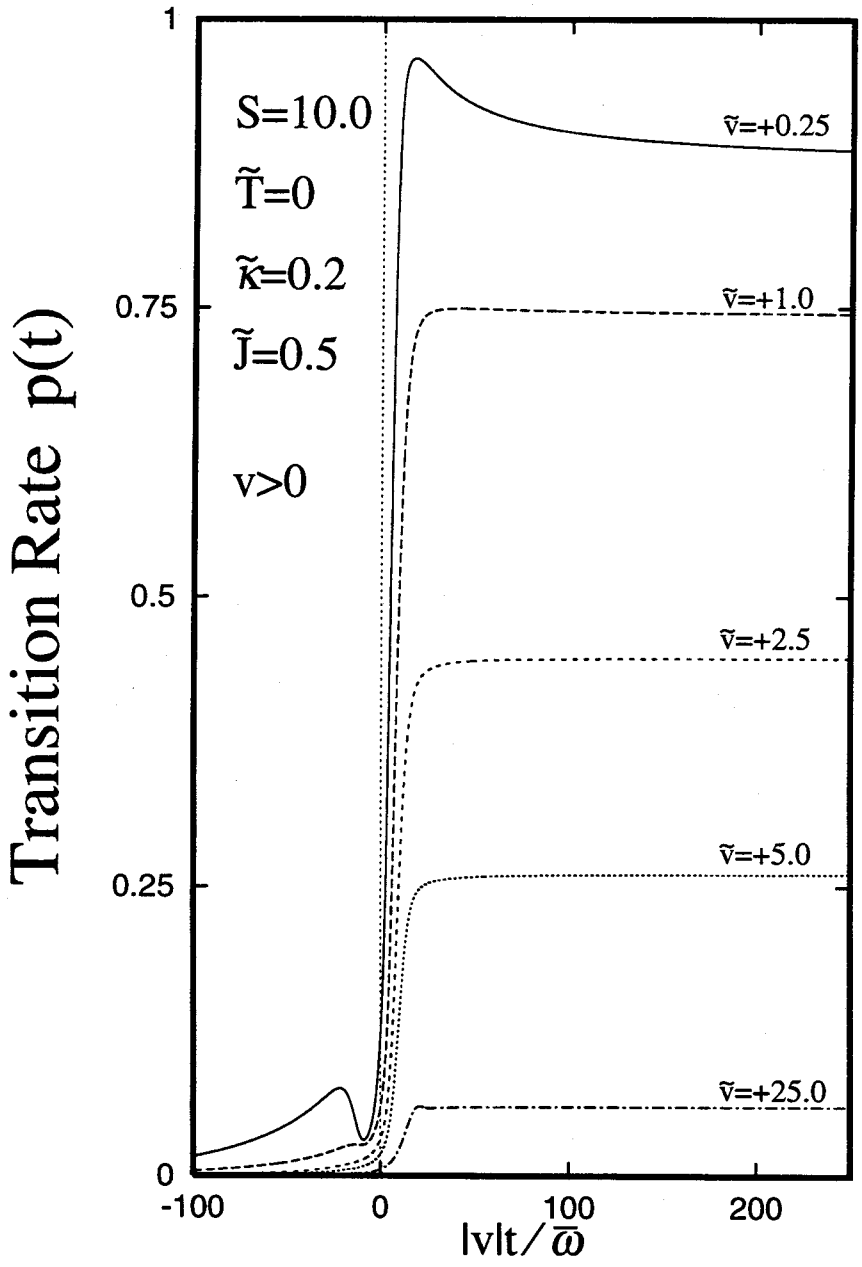

Figure 5.1: The time-dependent probability $p_+(t)$ in the zero temperature, strong-coupling case with $v > 0$ that system exists in $|2\rangle$ for the initial condition that it starts from $|1\rangle$ at remote past.

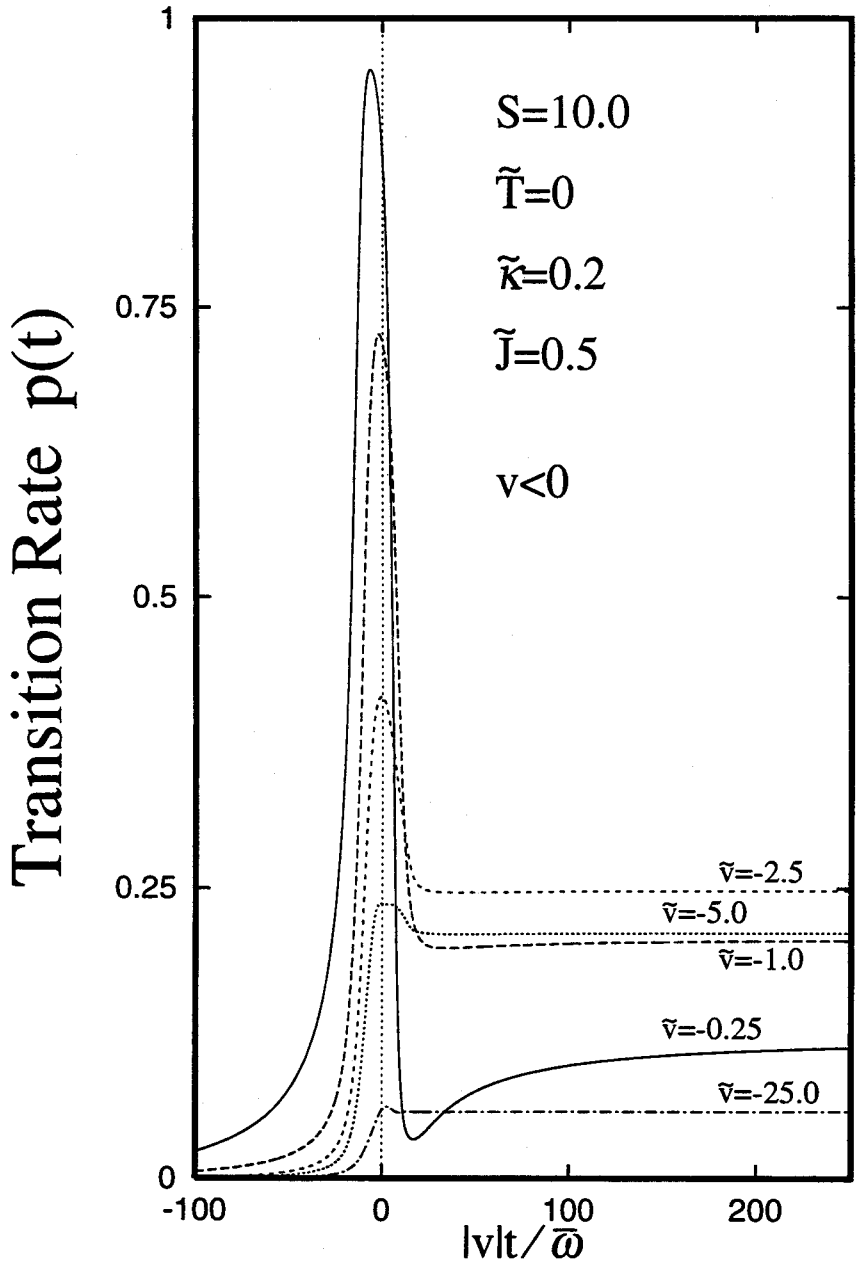

Figure 5.2: The time-dependent probability $p_{-}(t)$ in the zero temperature, strong-coupling case with $v < 0$ that system exists in $|2\rangle$ for the initial condition that it starts from $|1\rangle$ at remote past.

One of the remarkable results is that in the case of slow passage, the relation $p_+(t) + p_-(t) = 1(\sim 2P_{SD})$ holds for $t > 0$ for the same value of $|\tilde{v}|$, as can be seen from the comparison of the curves for $|\tilde{v}| = 0.25$. This means the branching ratio to the upper and the lower state after the crossing does not depend on the initial condition whether the system starts from the upper branch or the lower branch, as if *it forgets the history* from which it came.

5.1.2 Check for the formulas

In order to check the formulas obtained in previous capter, the results of P_+ (circle) and P_- (diamond) are plotted in Figure 5.3 against $1/|\tilde{v}|$ for a fixed value of the adiabaticity parameter $J^2/|v| = 0.2$ at zero temperature with $S = 10.0$ and $\tilde{\kappa} = 0.2$. The transition rate should be $P_+ = P_- = P_{LZ}$ at the rapid passage limit $1/|\tilde{v}| \to 0$, or $P_+ = P_{LZ}$, $P_- = P_{LZ}(1 - P_{LZ})$ at the slow passage limit $1/|\tilde{v}| \to \infty$. The values of P_{LZ} and $P_{LZ}(1 - P_{LZ})$ are also shown in the figure. In the limit of rapid passage, $1/|\tilde{v}| \to 0$, the process becomes coherent so $P_+ = P_- = P_{LZ}$ holds true as described earlier. As the speed of passage decreases, both P_+ and P_- deviates from P_{LZ} to lower values by the same amount. This increase of nonadiabaticity is due to the phase relaxation. As $|v|$ decreases further, P_+ takes a minimum value at an intermediate value of $1/|v|$ and then increases again to approach to P_{LZ} in the limit of slow passage, consistently with formula. On the other hand, P_- decreases dramatically from P_{LZ} to $P_{LZ}(1-P_{LZ})$ as $|v|$ is decreased. The small discrepancies between the calculated results and the prediction by formulas in the limit $1/|\tilde{v}| \to \infty$ are due to the peculiar character of the damping hyperoperator and will be investigated later. We also note a dip in P_- as a function of $1/|\tilde{v}|$ at around $1/|\tilde{v}| \sim 0.1$. This is interpreted as reflecting the dynamical motion of the wave packet in the configuration coordinate space of the interaction mode. The wave packet that has transfered to the potential curve $|2\rangle$ at the first crossing shown in Figure 4.2 undergoes a damping oscillation around the new equilibrium point. For $1/|\tilde{v}| \sim 0.1$, the crossing point of the two potential curves moves down in synchronization with this motion so that the transition rate form a dip at around $1/|\tilde{v}| \sim 0.1$ because of the nearly adiabatic back transfer.

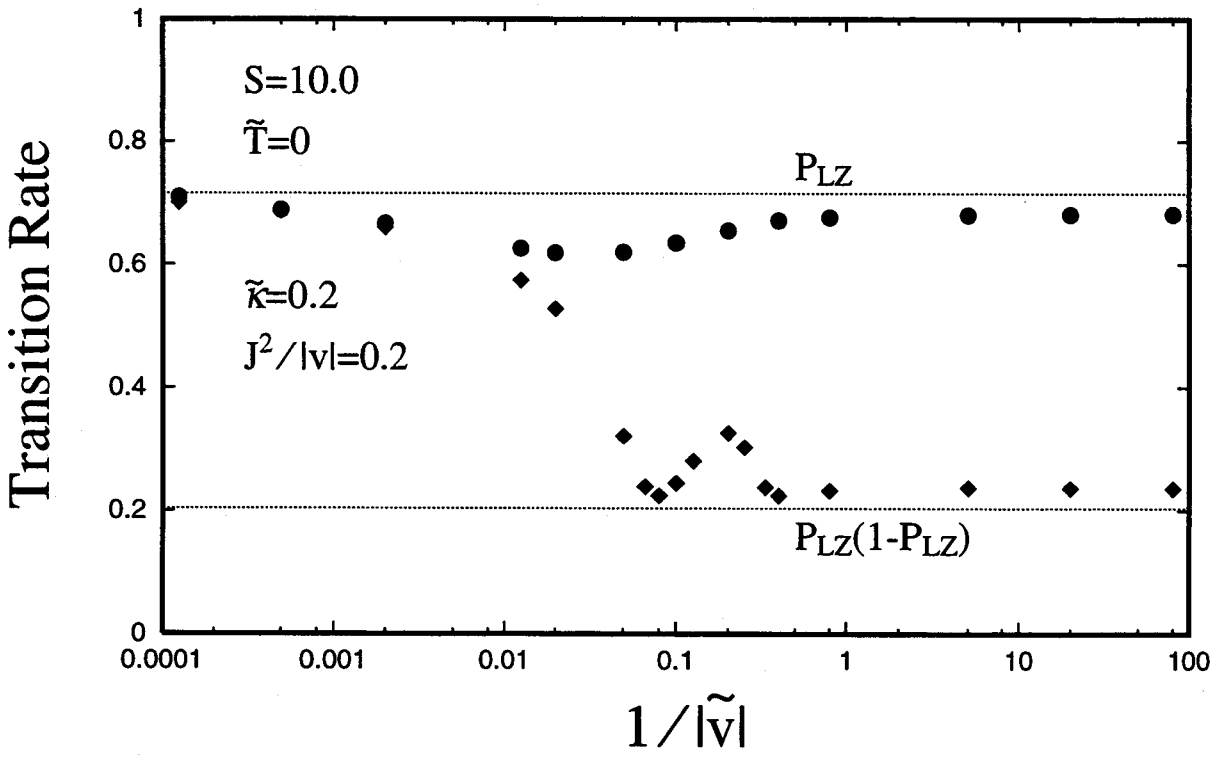

Figure 5.3: The transition rate P_+ (circle) and P_- (diamond) as a function of $1/|\tilde{v}|$ for a fixed value of $J^2/|v|$ in the zero-temperature, strong-coupling case. The predicted values by the formulas P_{LZ}, and $P_{LZ}(1-P_{LZ})$ are shown by the dotted lines.

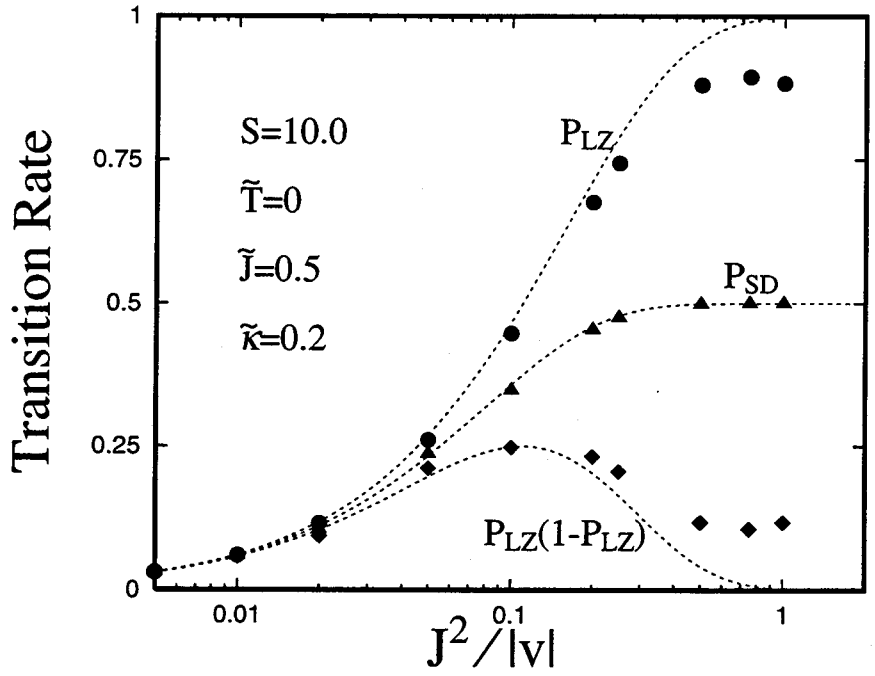

Figure 5.4: The transition rate P_+ (circle) and P_- (diamond) as a function of $J^2/|v|$ in the zero-temperature, strong-coupling case for fixed values of $\tilde{\kappa}$, $\tilde{J}$ and S. The values of $(P_+ + P_-)/2$ is also plotted by triangles. The prediction by the formulas P_{LZ}, $P_{LZ}(1-P_{LZ})$ are shown by the dashed lines.

In Figure 5.4, the transition rates P_+ and P_- are plotted for a fixed value of $\tilde{J} = 0.5$ against $J^2/|v|$ with $\tilde{T} = 0$, $S = 10$, and $\tilde{\kappa} = 0.2$. The value of $(P_+ + P_-)/2$ is also plotted by triangles. The values of P_{LZ}, $P_{LZ}(1 - P_{LZ})$, and P_{SD} are shown by dashed lines. For $J^2/|v|$ not greater than 0.25, P_+ and P_- agree with the formula P_{LZ} and $P_{LZ}(1 - P_{LZ})$ respectively, fairly well. The discrepancy which becomes salient for $J^2/|v| \geq 0.5$ is again attributed to the special character of the damping hyperoperator. It is remarkable that the formula $(P_+ + P_-)/2 = P_{SD}$ given in Eq. (4.62) works quite well all through the parameter region.

The dependence on S of P_+ and P_- at zero temperature is shown in Figure 5.5 for a fixed value of $\tilde{J} = 0.5$ in the case of slow passage, $|\tilde{v}| = 1.25$. It is remarkable that P_+ is essentially independent of S and is given by P_{LZ}. On the contrary, P_- is reduced strongly by the coupling with phonons even in the weak-coupling region.

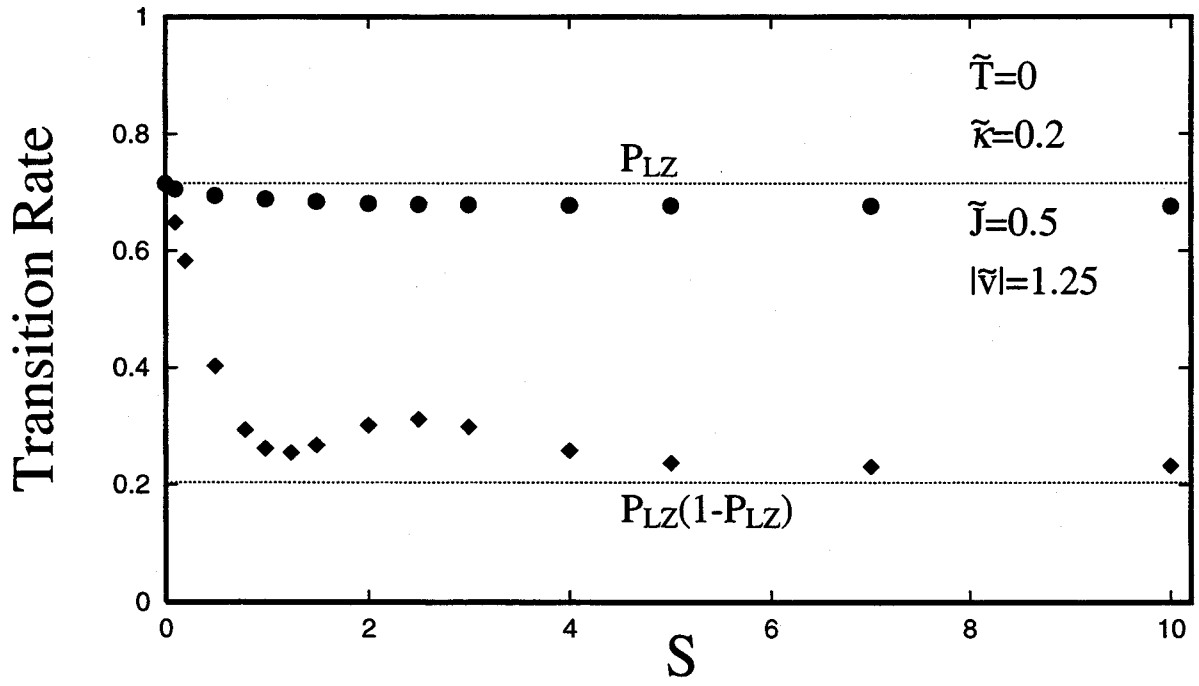

Figure 5.5: The transition rate P_+ (circle) and P_- (diamond) as a function of S in the zero-temperature, slow passage case for fixed values of $\tilde{J}$, $\tilde{v}$, and $\tilde{\kappa}$. The values of P_{LZ}, $P_{LZ}(1-P_{LZ})$ are shown by the dotted lines.

5.1.3 Roots of the discrepancy

Now, we discuss the origin of the discrepancy between the formulas given in the previous chapter and the numerical results. It is essentially the difference in the short-time behavior of the correlation function between the original model given by Eqs. (2.1)-(2.4) and the reduced model given by Eqs. (3.17)-(3.21). In order to see this, an analysis by the formal perturbation expansion series of the solution of Eq. (3.17) was performed parallel to that given in Chapter 4. The formal solution of Eq. (3.17) for the initial value $\tilde{\rho}_0$ is written as

$$\tilde{\rho}(t) = \mathrm{Exp}_+ \left[-i \int_{-\infty}^{t} d\tau \mathcal{L}(\tau) \right] \tilde{\rho}_0 \tag{5.1}$$

with

$$\mathcal{L}(t) = \mathcal{L}_0(t) + \mathcal{L}', \tag{5.2}$$

where the hyperoperator $\mathcal{L}_0(t)$ and $\mathcal{L}'$ are defined by

$$\mathcal{L}_0(t)\tilde{\rho} = [H_{\mathrm{sys}}(t),\ \tilde{\rho}] + i\Gamma\tilde{\rho}, \tag{5.3}$$

$$\mathcal{L}'\tilde{\rho} = [V_{\mathrm{sys}},\ \tilde{\rho}]. \tag{5.4}$$

and $\mathrm{Exp}_+[\cdots]$ now represents the time-ordered exponential for the hyperoperators. By an analogous procedure given in Chapter 4, $\tilde{\rho}(t)$ is expanded in a formal power series of $\mathcal{L}'$ as

$$\mathrm{Exp}_+\left[-i\int_{-\infty}^{t}d\tau\mathcal{L}(\tau)\right]\tilde{\rho}_0 = \mathrm{Exp}_+\left[-i\int_{-\infty}^{t}d\tau\mathcal{L}_0(\tau)\right] \times\sum_{n=0}^{\infty}(-i)^n\int_{-\infty}^{t}d\tau_n\int_{-\infty}^{\tau_n}d\tau_{n-1}\cdots\int_{-\infty}^{\tau_2}d\tau_1\mathcal{L}'(\tau_n)\mathcal{L}'(\tau_{n-1})\cdots\mathcal{L}'(\tau_1)\tilde{\rho}_0\,, \tag{5.5}$$

where $\mathcal{L}'(\tau)$ is the interaction representation of $\mathcal{L}'$. The expectation value of the above term is obtained after a somewhat complicated calculation by using the properties of the damping operator Γ. We arrive at the expression of the transition rate P,

$$P=-\sum_{n=1}^{\infty}(-J^2)^n\tilde{\mathcal{L}}^{(n)} \tag{5.6}$$

where $\tilde{\mathcal{L}}^{(n)}$ is given by the same form as given in Eq. (4.20) except that the function $G(t)$ is replaced by $\tilde{G}(t)$ given by

$$\tilde{G}(t)=-iS\bar{\omega}t+S(1-e^{-i\bar{\omega}t-\kappa|t|})\,, \tag{5.7}$$

at zero temperature. Note that $\tilde{G}(t)$ mimics the behavior of $G(t)$ fairly well, but, in the limit $t\to 0$, it behaves as

$$\tilde{G}(t)=S\kappa|t|+\frac{S}{2}(\bar{\omega}^2-\kappa^2)t^2\,, \tag{5.8}$$

for $S\gg 1$. This should be contrasted with the limiting value of $G(t)$

$$G(t)\sim\frac{S}{2}\bar{\omega}^2t^2\,. \tag{5.9}$$

Consequently, the line-shape function $\tilde{F}_{\pm}(\mu)$ becomes

$$\begin{aligned}\tilde{F}_{\pm}(\mu) &= \int_{-\infty}^{\infty}d\sigma\,\exp\left[-i(S\bar{\omega}\pm v\mu)\sigma-\tilde{G}(\sigma)\right]\\ &= \sqrt{\frac{2}{\pi}}\frac{S\kappa}{D^*}\int_{-\infty}^{\infty}dx\frac{1}{x^2+(S\kappa)^2}\cdot\exp\left[-\frac{(S\bar{\omega}\pm v\mu-x)^2}{2D^{*2}}\right]\end{aligned} \tag{5.10}$$

with $D^{*2}\equiv S(\bar{\omega}^2-\kappa^2)$, namely, the convolution of a Gaussian function with a Lorentzian function of width $S\kappa$. This is a consequence of the Markovian approximation assumed in the derivation of Eqs. (3.17)-(3.21). Since $\tilde{F}_{\pm}(\mu)$ has a Lorentzian tail for $|\mu\pm S\bar{\omega}/v|\geq D^*/|v|$ unlike $F_{\pm}(\mu)$, the transition region is not confined well around the crossing times $\mu\sim\pm S\bar{\omega}/|v|$. This off-resonant transition causes the deviation of P from the formulas.

In fact, the hump before the steplike increase and the gradual decrease after it, seen in Figure 5.1 for the case $\tilde{v}=0.25$, for example, corresponds to this effect. In order to ascertain this point, P_+ has been calculated as a function of $J^2/|v|$ for several parameter

values of $\tilde{\kappa}$. In Figure 5.6, the calculated results are shown with the value of formula in which $F_{\pm}(\mu)$ is replaced by $\tilde{F}_{\pm}(\mu)$. The agreement is almost perfect.

This analysis indicates that the simulation of the nonadiabatic processes by the damping operator technique is useful, but one must take care about the spurious effect peculiar to this method.

In Figure 5.7, numerical results of P_+ in the limit of large amplitude fluctuation are shown, by changing the set of parameters $(S, \tilde{T})$ for the fixed value of $\tilde{D}^2 \equiv S(2\bar{n}+1)$ $(= 10.0)$ from the low temperature, strong-coupling limit to the high temperature, weak-coupling limit. The prediction of the general formula with replacement $F_{\pm}(\mu) \to \tilde{F}_{\pm}(\mu)$ is shown by dotted lines. The agreement is good, which indicates the correctness of the analysis in Chapter 4. The deviation from $P_+ = P_{LZ}$ in the limit $\tilde{T} = 0$ is again due to the Lorentzian tail of the line-shape function. If the line-shape function $\tilde{F}_{\pm}(\mu)$ has only a Gaussian tail, P_+ should coincide with P_{LZ} in this limit. See how the functional form of the transition rate changes from P_{LZ} to P_{SD} as the temperature increases.

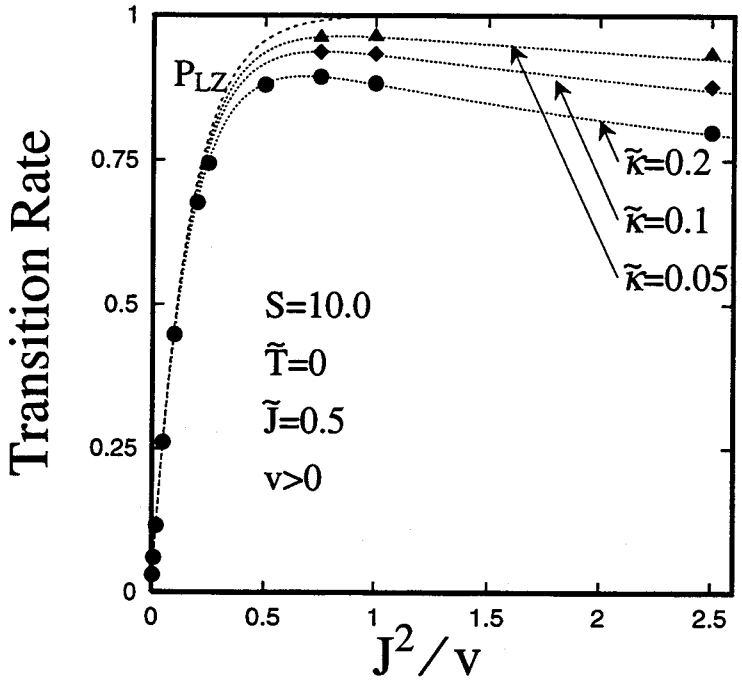

Figure 5.6: The $\tilde{\kappa}$ dependence of P_+ as a function of $J^2/|v|$. The prediction by the formula with replacement $F_{\pm}(\mu) \to \tilde{F}_{\pm}(\mu)$ is shown by dotted lines.

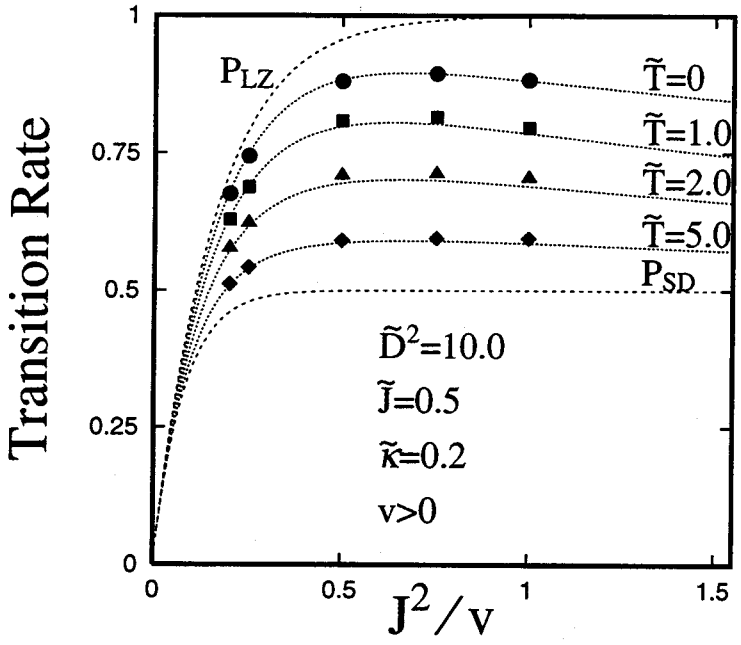

Figure 5.7: The transition rate P_+ as a function of $J^2/|v|$ for the case of strong decoherence. The parameter $\tilde{D}$ is fixed as $\tilde{D}^2 = 10$ and the temperature $\tilde{T}$ is varied from 0 to 5 with corresponding change of S. The prediction by the formula with replacement $F_\pm(\mu) \to \tilde{F}_\pm(\mu)$ is shown by dotted lines.

5.2 high temperature, weak coupling limit

In Figure 5.8, an example of numerical result for high temperature, weak coupling limit is shown for $p_+(t)$ and $p_-(t)$ with parameter values $\tilde{T} = 10.0$, $\tilde{D} = 1.0$, $\tilde{J} = 0.5$, $\tilde{\kappa} = 0.2$, and $|\tilde{v}| = 1.0$. In this case, the transition rate is almost independent of the sign of v but is strongly reduced from the value of P_{LZ}. In Figure 5.9, the dependence on the adiabaticity parameter $J^2/|v|$ of P_+ and P_- is shown for the two parameter values of $\tilde{D}$, with other parameters fixed as $\tilde{J} = 0.5$, $\tilde{\kappa} = 0.2$. The coupling constant S and the temperature $\tilde{T}$ are chosen so that the condition of the fluctuation dominance is satisfied; $S = 0.0499, \tilde{T} = 10.0$ for $\tilde{D} = 1.0$ and $S = 0.0249, \tilde{T} = 5.0$ for $\tilde{D} = 0.5$. This figure should be directly related with the results of the stochastic model [21]. As noted in Sec. 4.4, P is generally bounded as $P_{SD} \leq P \leq P_{LZ}$ except for small deviations, takes a maximum value at an intermediate value of $|v|$ because of the tradeoff between the influence of the phase relaxation, which increases the nonadiabaticity, and the slowness of the passage, which favors the adiabaticity. It is shown that P tends to P_{SD} in the limit $\tilde{D} \to \infty$.

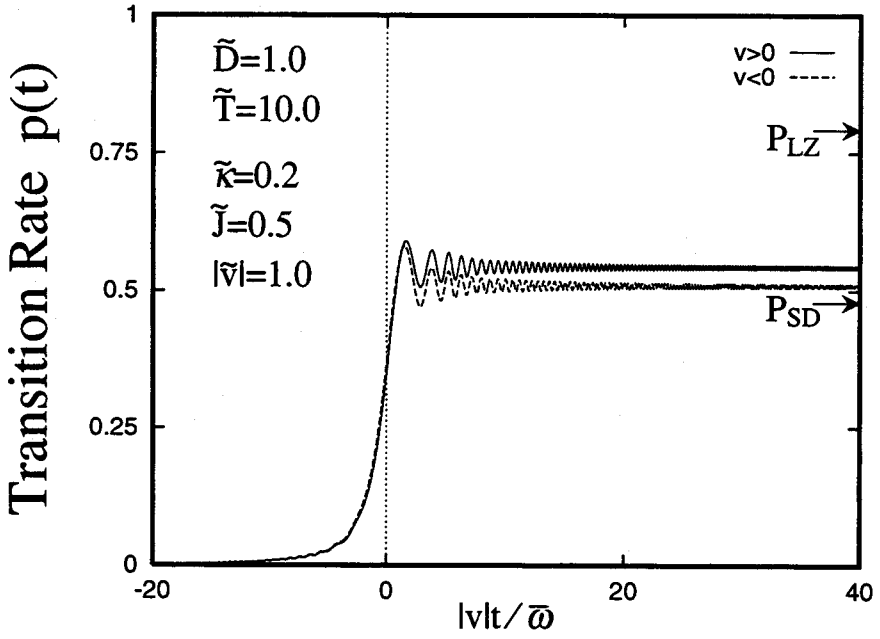

Figure 5.8: The time-dependent probability $p_+(t)$ (solid line) and $p_-(t)$ (dashed line) in the case of high temperature, weak coupling.

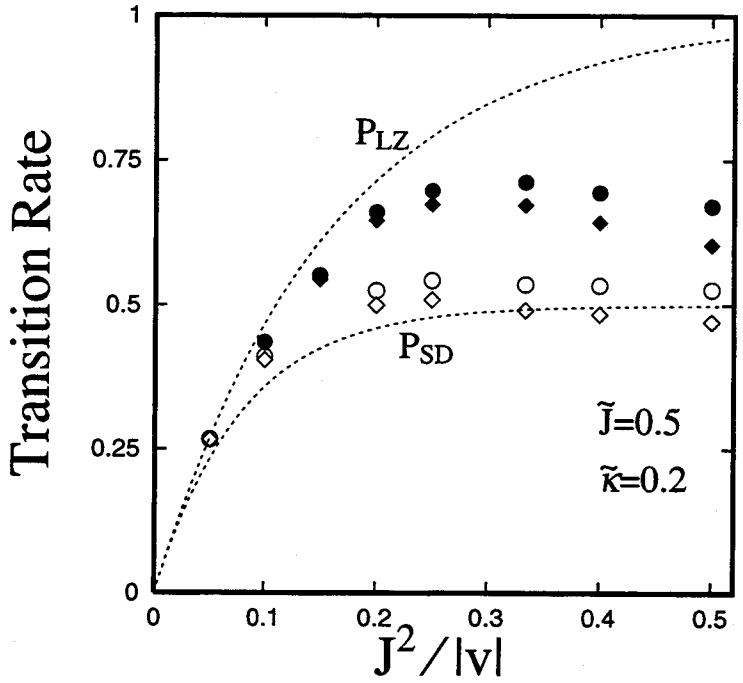

Figure 5.9: The transition rate P_+ (circle) and P_- (diamond) in the case of high temperature, weak coupling. The results for $\tilde{D} = 0.5$ and $\tilde{D} = 1.0$ are shown by the solid and open symbols, respectively.

5.3 Summary

Numerical calculations are performed for the transition rate for the Landau-Zener problem with dissipation, by utilizing the damping hyperoperator technique. The overall features of the time evolution of the level-crossing system are clarified. The analytical formulas obtained in previous chapter are ascertained, except for the deviation which are salient in the slow passage limit. The reason of the discrepancy is due to the Markoffian nature of the damping hyperoperator, which indicates that the simulation of the nonadiabatic processes by the damping operator technique is useful, but one must take care about the spurious effect.

Chapter 6

Application to the potential-crossing system

In this chapter, we discuss the dynamics of potential crossing system, shown in Figure 2.2. The time evolution of the transition rate that the system undergoes nonradiative transition from excited state $|2\rangle$ to ground state $|1\rangle$ after the electronic excitation at time $t = 0$ is calculated. The transition rate is given by, in this situation,

$$p(t) = \left\langle \{\exp[+iH_T t]\}_{2,1} \{\exp[-iH_T t]\}_{1,2} \right\rangle_{\mathrm{x}} , \tag{6.1}$$

where $\langle \cdots \rangle_{\mathrm{x}}$ means the expectation value over the phonon distribution in excited state ρ_{x}, namely,

$$\langle \cdots \rangle_{\mathrm{x}} = \mathrm{Tr}\{\rho_{\mathrm{x}} \cdots\} . \tag{6.2}$$

ρ_{x} is considered as

$$\rho_{\mathrm{x}} = \exp\left[-\left(H_1 - \sum_k \omega_k \delta_k (b_k + b_k{}^\dagger)\right)/k_B T\right] \Big/ \mathrm{Tr}\exp[-\{\cdots\}/k_B T] . \tag{6.3}$$

In the case of ideal white-pulse optical excitation, $\delta_k = 0$.

Numerical calculations are performed by using Eqs. (3.17)-(3.21). The initial state of reduced density matrix is then chosen to the coherent state for the interaction mode, as

$$\rho_R(0) = \exp\left[-\bar{\omega}(B_1{}^\dagger - \delta)(B_1 - \delta)/k_B T\right] \Big/ \mathrm{Tr}\exp[-\{\cdots\}/k_B T] . \tag{6.4}$$

Dimensionless parameters $\tilde{J} \equiv J/\bar{\omega}$, $\tilde{\kappa} \equiv \kappa/\bar{\omega}$, $\tilde{T} \equiv k_B T/\bar{\omega}$, and $\tilde{D} \equiv D/\bar{\omega}$ are used for numerical calculations.

It should be noted here that Eqs. (3.17)-(3.21) may not guarantee the system to relax to the thermal equilibrium of the total electron-phonon system. The hyperoperator makes the system relax to the thermal equiriblium state of phonons in each electron subspace, however,

the state is not the thermal equilibrium state of total electron-phonon system described by the Hamiltonian H_T with non-zero off-diagonal matrix element J. For significantly large J, this calculation method may not reproduce correct dynamics in long-time scale. Since we are interested in the dynamical behavior of the system in short-time scale, attention is focused on the short-time dynamics of the system after electronic excitation and the dynamics in the long-time scale is not discussed in this study.

6.1 Considerations for the weakly-coupled electron-phonon system

In the situation of weak electron-phonon coupling, $S \ll 1$, time evolution of the transition rate shows damping oscillation, which originates from the phase coherence between two levels. If no electron-phonon coupling exists in the system, the transition rate will show simply oscillating behavior, that is,

$$p(t) = \frac{4J^2}{\Delta\epsilon^2 + 4J^2} \sin^2 \frac{\sqrt{\Delta\epsilon^2 + 4J^2}}{2} t. \tag{6.5}$$

In Figure 6.1, the numerical results of the time evolution of the transition rate $p(t)$ in this limit at zero temperature are shown with different damping parameter $\tilde{\kappa}$. The time evolution of the system shows damping oscillation by the existence of phase relaxation.

Also we should notice in Figure 6.1 that, in some time intervals, the transition rate becomes larger than $\frac{4J^2}{\Delta\epsilon^2+4J^2} = 0.5$. This may be considered as the effect of the energy dissipation which slightly remains for small S.

In Figure 6.2, the time evolution of the transition rate $p(t)$ is shown with different temperature. With increasing temperature, $\tilde{D}$, the amplitude of the energy fluctuation given by $\tilde{D} \equiv \sqrt{(2\bar{n}+1)S}$ increases and the transition process changes from coherent transition to incoherent transition. At high temperature the transition dynamics shows incoherent behavior, then the oscillation of the transition rate, which is associated with phase coherence between the two states, vanishes rapidly and the transition rate evolutes almost exponentially.

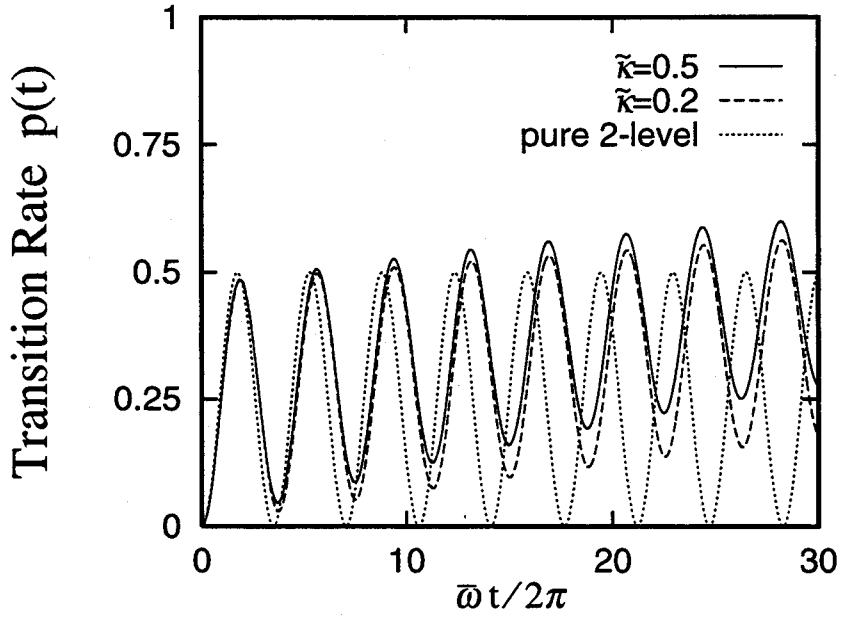

Figure 6.1: Dynamical evolution of the transition rate at white-pulse optical excitation for the parameters $\Delta\epsilon/\bar{\omega} = 0.2$, $\tilde{J} = 0.1$, $S = 0.25$, $\tilde{T} = 0$, and $\tilde{\kappa} = 0.5$ (solid line) or $\tilde{\kappa} = 0.2$ (dashed line), and for the pure two-level system (dotted line).

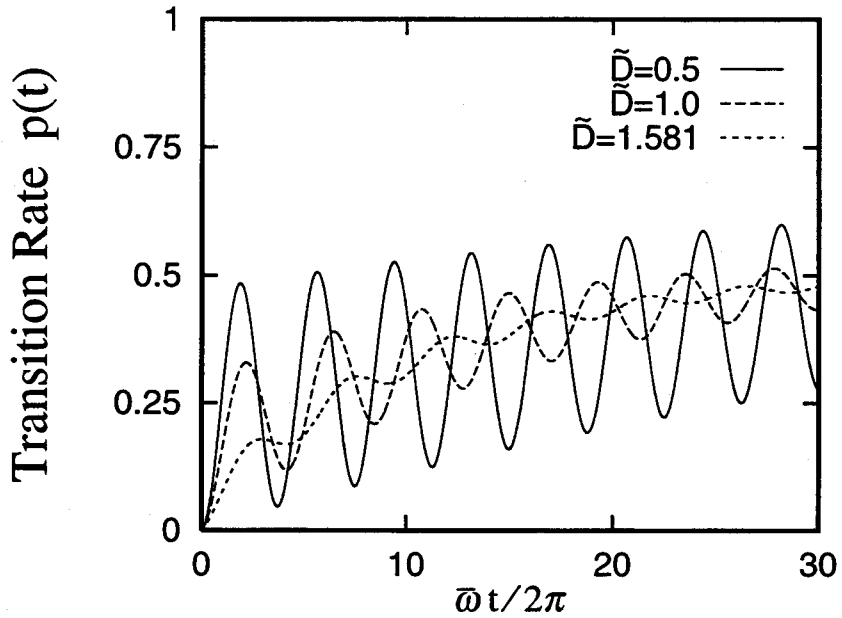

Figure 6.2: Dynamical evolution of the transition rate at white-pulse optical excitation for the parameters $\Delta\epsilon/\bar{\omega} = 0.2$, $\tilde{J} = 0.1$, $S = 0.25$, and $\tilde{\kappa} = 0.5$ with different temperatures.

6.2 Considerations for the strongly-coupled electron-phonon system

6.2.1 Two aspects of the transition process

In the situation of $S \gg 1$, transition process can be classified into two distinct processes, namely, dynamical *hot* transition and statical tunneling. Time evolution of transition rate $p(t)$ after white-pulse excitation clearly show these processes in Figure 6.3. The transition rate increases exponentially after stair-like increase. This result reflects the lattice relaxation process from the electronically excited state.

When the system is electronically excited, a wave packet of phonons begins to relax toward a new equilibrium configuration. The nonadiabatic transition is induced dynamically during the lattice relaxation process, if the wave packet passes around the potential crossing region (see Figure 2.2). The stair-like increase of the transition rate indicates this process clearly. After the wave packet relaxes to the new equilibrium, transition is induced only by the quantum tunneling. The exponential behavior of the transition rate indicates this process.

In the case that the damping constant for the relaxation of the energy $\tilde{\kappa}$ is small, the wave packet of phonons can pass the crossing region more than once. Then multiple dynamical transitions will be induced nonadiabatically. Result for $\tilde{\kappa} = 0.05$ in Figure 6.3 (solid line) clearly shows this multiple dynamical transitions. On the other hand, in the case for larger damping constant $\tilde{\kappa} = 0.25$, the wave packet relaxes to the new equilibrium so rapidly that the center of the wave packet can not pass the crossing region. In this case the contribution of the dynamical transition to the transition rate is small, but not zero because the tail of the wave packet can pass the crossing region.

One can calculate the motion of the wave packet damped by the hyperoperator, from the consideration of single-level system. The expectation value of dimensionless displacement defined by the operator $\hat{Q} = (B_2 + B_2{}^\dagger)/2$ is, for example, approximately given by

$$\langle Q(t) \rangle = \mathrm{Tr}\left\{\hat{Q} \cdot \rho_{22}\right\} = (\delta - \alpha) e^{-\kappa t} \cos \bar{\omega} t \tag{6.6}$$

In the case of the potential configuration in Figure 6.3, $\alpha = 5$ and $\delta = 0$. The crossing is at $Q_x = 3.0$.

The increase of the transition rate by dynamical transitions in each stair are, as for the first crossing event, given analytically by the Landau-Zener formula [11]. The analytical expression for the time-dependent transition rate defined by Eq. (6.1) is obtained by formal perturbation series expansion, that is,

$$p(t) = -\sum_{n=1}^{\infty} (-J^2)^n L^{(n)}(t)\,, \tag{6.7}$$

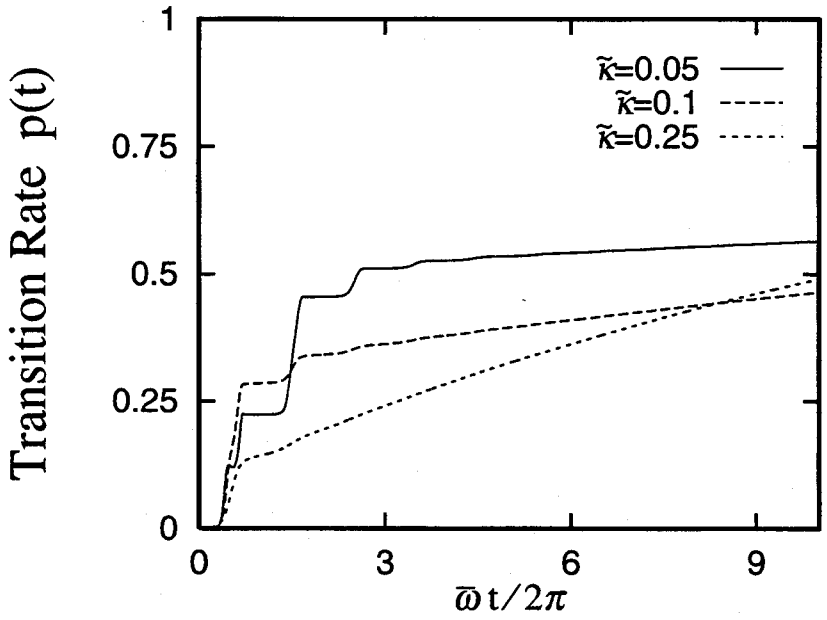

Figure 6.3: Time evolution of the transition rate for typical strongly-coupled electron-phonon systems at zero temperature after white-pulse optical excitation. The other parameters are, $S = 25$, $\Delta\epsilon/\bar{\omega} = 55.0$, and $\tilde{J} = 0.8$.

$$L^{(n)}(t) = \sum_{m=1}^{n} \int_0^t d\tau_1 \int_{\tau_1}^t d\tau_2 \cdots \int_{\tau_{2m-2}}^t d\tau_{2m-1} \int_0^t d\tau_{2m} \int_0^{\tau_{2m}} d\tau_{2m+1} \cdots \int_0^{\tau_{2n-1}} d\tau_{2n} \times \mathcal{F}(\tau_1, \tau_2, \cdots, \tau_{2n}), \tag{6.8}$$

$$\mathcal{F}(\tau_1, \tau_2, \cdots, \tau_{2n}) = \exp\left[i \sum_{j=1}^{2n} (-1)^j \left\{ (\Delta\epsilon - S\bar{\omega})\tau_j + 2\sum_k \alpha_k(\alpha_k - \delta_k) \sin\omega_k\tau_j \right\} + \sum_{i=2}^{2n} \sum_{j=1}^{i-1} (-1)^{i+j} G(\tau_i - \tau_j) \right]. \tag{6.9}$$

Since the real part of the exponent $\mathcal{R}(\tau_1, \tau_2, \cdots, \tau_{2n})$ is same as Eq. (4.24) and is a non-positive definite quantity in the limit of $S \gg 1$, we can evaluate the integral by the saddle point method. The contribution to the integral comes from a small region around the points where the imaginary part of the exponent $\mathcal{I}(\tau_1, \tau_2, \cdots, \tau_{2n})$ is *stationary* and the real part $\mathcal{R}(\tau_1, \tau_2, \cdots, \tau_{2n})$ is *maximum*, otherwise the integrand undergoes a destructive oscillation or the absolute value of the integrand itself damp drastically.

The condition to determine the saddle point reads, eventually,

$$\frac{\partial}{\partial\tau_j}\mathcal{I}(\tau_1, \tau_2, \cdots, \tau_{2n}) = (-1)^j E_j(\tau_j|\tau_1, \tau_2, \cdots, \tau_{j-1}) = 0, \text{for } j = 1, 2, \cdots, 2n.$$

$E_j(\tau_j|\tau_1, \tau_2, \cdots, \tau_{j-1})$ means physically the Franck-Condon energy from $|2\rangle$ to $|1\rangle$ at a time τ_j for the wave packet [11], which has the following history: it is excited on the potential curve of $|2\rangle$ at $t = 0$ and slides down along the potential curve like a classical particle, make a vertical transition to $|1\rangle$ at τ_1 and then moves along the potential curve $|1\rangle$, and again make a transition to $|2\rangle$ at τ_2 and so on, until the final transition at time τ_{j-1} .

Thus the main contribution of the integral comes at around the time region where the wave packet passes through the potential crossing. The integral is evaluated by expanding the exponent up to the second order with respect to $x_j \equiv \tau_j - t_1$ and we obtain

$$L^{(n)}(t) = \sum_{m=1}^{n} \int_{-t_1}^{t-t_1} d\tau_1 \cdots d\tau_{2n} \cdot \exp\left[i\frac{v}{2} \sum_{j=1}^{2n} (-1)^j x_j^2 - \frac{D^2}{2} \left\{ \sum_{j=1}^{2n} (-1)^j x_j \right\}^2 \right] \tag{6.10}$$

where $v(\sim S\bar{\omega}^2)$ is the velocity of change for Franck-Condon energy at the crossing. The right hand side of Eq. (6.10) can be eliminated from the discussion about the transition rate at the coherent passage in Sec. 4.3.2, if the condition $D/|v| \ll 1/\bar{\omega}$ is satisfied. Then we can obtain the Landau-Zener formula, after safely extending the boundary of the integration to $(-\infty, \infty)$ for $|v| \gg \bar{\omega}^2$ and for t well separated from the crossing time. The transition rate after the second and the third crossing are also described by the Landau-Zener formula, however, the discussion is more complicated.

The transition rate at the static stage is calculated as follows. We choose the lattice relaxed excited state as initial density matrix ρ_x at $t = 0$, and discuss the time evolution. By simply setting $\delta_k = \alpha_k$, the perturbation term of first order in Eq. (6.8) is written as

$$L^{(1)}(t) = \int_0^t d\tau_1 \int_0^t d\tau_2 e^{-i(S\bar{\omega}-\Delta\epsilon)(\tau_2-\tau_1)-G(\tau_2-\tau_1)} . \tag{6.11}$$

Note that the integrand is a function of $\tau_2 - \tau_1$. Introducing new variables $\mu = (\tau_1 + \tau_2)/2$ and $\sigma = \tau_2 - \tau_1$ and converting the integral domain, the derivative of Eq. (6.11) is written as follows;

$$\begin{aligned} \frac{d}{dt}L^{(1)}(t) &= \int_{-t}^{t} d\sigma e^{-i(S\bar{\omega}-\Delta\epsilon)\sigma-G(\sigma)} \\ &\sim 2\pi F(S\bar{\omega} - \Delta\epsilon) \qquad \text{for} \quad t \gg 1/D\,, \end{aligned} \tag{6.12}$$

where $F(E)$ is defined as Eq. (4.53), the line-shape function meaning the optical transition rate by virtual photon with energy zero. From Eq. (6.12), we obtain

$$\begin{aligned} \frac{d}{dt}p(t) &= 2\pi J^2 F(S\bar{\omega} - \Delta\epsilon) + O(J^4) \\ &\Rightarrow 2\pi J^2 F(S\bar{\omega} - \Delta\epsilon)(1 - p(0)) + O(J^4)\,, \end{aligned} \tag{6.13}$$

which shows an exponential decay. The decay rate from $|2\rangle$ to $|1\rangle$ per unit time is given by $2\pi J^2 F(S\bar{\omega} - \Delta\epsilon)$.

To be more precisely, the transition process from $|1\rangle$ to $|2\rangle$ should be taken into account as an inverse process. In this case Eq. (6.13) would be rewritten as,

$$\frac{d}{dt}p(t) \sim -2\pi J^2 F(S\bar{\omega} + \Delta\epsilon)p(t) + 2\pi J^2 F(S\bar{\omega} - \Delta\epsilon)(1 - p(t)) + O(J^4)\,. \tag{6.14}$$

The first term of right hand side of Eq. (6.14) indicates the transition process from $|1\rangle$ to $|2\rangle$, the second term indicates the transition process from $|2\rangle$ to $|1\rangle$.

We should notice that, the transition rate $F(S\bar{\omega} + \Delta\epsilon)$ and $F(S\bar{\omega} - \Delta\epsilon)$ are rewritten as

$$F(S\bar{\omega} - \Delta\epsilon) = \frac{1}{\sqrt{4\pi S k_B T^*}} e^{-\frac{E_x}{k_B T^*}}, \tag{6.15}$$

$$F(S\bar{\omega} + \Delta\epsilon) = \frac{1}{\sqrt{4\pi S k_B T^*}} e^{-\frac{E_x + \Delta\epsilon}{k_B T^*}}, \tag{6.16}$$

where E_x is the height of the potential barrier measured from $|2\rangle$ to $|1\rangle$, $E_x + \Delta\epsilon$ is that from $|1\rangle$ to $|2\rangle$.

The transition rate at static stage calculated by damping hyperoperator is, however, becomes too large and not consistent to Eq. (6.14). As is discussed in Sec. 5.1.3, in the system that are driven by the damping hyperoperator, the line-shape function $F(E)$ becomes no more a Gaussian function that reproduce the actual dynamics, it becomes a Gaussian function with Lorentzian tail. This causes overestimation of off-resonant transfer and leads to the not-realistic transition rate at the static stage.

Finally, the transition rate at the dynamical stage P_D can be evaluated from the asymptotic behavior at the static stage. The transition rate at the static stage is approximated as

$$p(t) \sim p(\infty) + (P_D - p(\infty))e^{-Wt}, \tag{6.17}$$

where $p(\infty)$ can set to 1 in usual situations. We define the transition rate at the dynamical stage P_D by this equation, and use this quantity to discuss quantitative behavior of dynamical transition.

6.2.2 Quantitative analysis of the dynamical nonradiative transition

In this section, we discuss the transition probability at the dynamical stage quantitatively. First, numerical results for the dynamical evolution of transition rate at zero temperature are plotted with $\tilde{J}$ as a parameter. The other parameters were chosen to $S = 25$, $\delta = -1$, $\Delta\epsilon/\bar{\omega} = 55.0$, and $\tilde{\kappa} = 0.05$ for Figure 6.5, $\tilde{\kappa} = 0.1$ for Figure 6.6. With increasing the off-diagonal matrix element $\tilde{J}$, transition dynamics changes from diabatic to adiabatic. For small J, the wave packet stays mainly in $|2\rangle$, makes a transition to $|1\rangle$ at each crossing event. This is diabatic case, shown in the figures for the parameter value $\tilde{J} = 0.8$. For large J, the wave packet moves mainly between $|2\rangle$ and the upper branch of $|1\rangle$, makes a transition to the lower branch at each crossing event. This is adiabatic case shown in the figures for the parameter value $\tilde{J} = 4.0$, where the dynamical evolution of the transition rate shows effective back-transfer.

It is convenient to define the times when the potential crossing event occurs, as t_1, $t_{1,1}$, t_2, which is described in detail in Figure 6.4. The first crossing event occurs at $t = t_1$, then a part of the wave packet makes a transition to $|1\rangle$ and swing back and passes the crossing point at $t = t_{1,1}$, or, the wave packet which has stayed in $|2\rangle$ after the crossing event at $t = t_1$ swing back and passes the crossing point at $t = t_2$. The main contribution of the transition rate comes, in diabatic case, from the crossing event at t_1 and t_2, and at t_1 and $t_{1,1}$ in adiabatic case. Also we define the transition rate after the crossing event at t_1 as P_{t_1}, at $t_{1,1}$ as $P_{t_{1,1}}$, and at t_2 as P_{t_2}.

In Figure 6.7, the transition rate P_{t_1}, $P_{t_{1,1}}$, P_{t_2}, and P_D, which were estimated from the data for the dynamical evolution of the transition rate, are plotted against $\tilde{J}$ for parameters $S = 25, \delta = -1, \Delta\epsilon/\bar{\omega} = 55.0$, and $\tilde{\kappa} = 0.05$. The predicted values from the Landau-Zener formula are also shown by dashed line as for the transition rate at the first crossing event, P_{t_1}. For small $\tilde{J}$ less than 2.0, P_{t_1} is given approximately by the Landau-Zener formula, which is also shown in the figure.

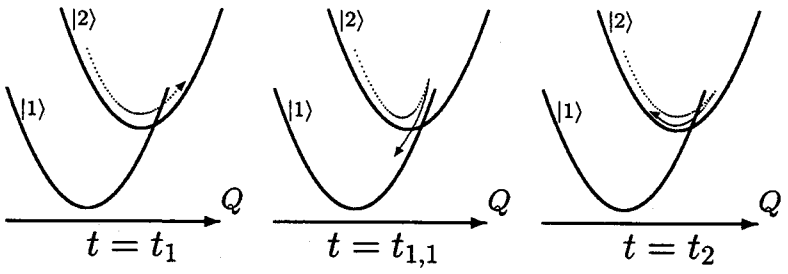

Figure 6.4: The crossing events of the wave packet that will occur after the electronic excitation in $0 < t < 2\pi/\bar{\omega}$.

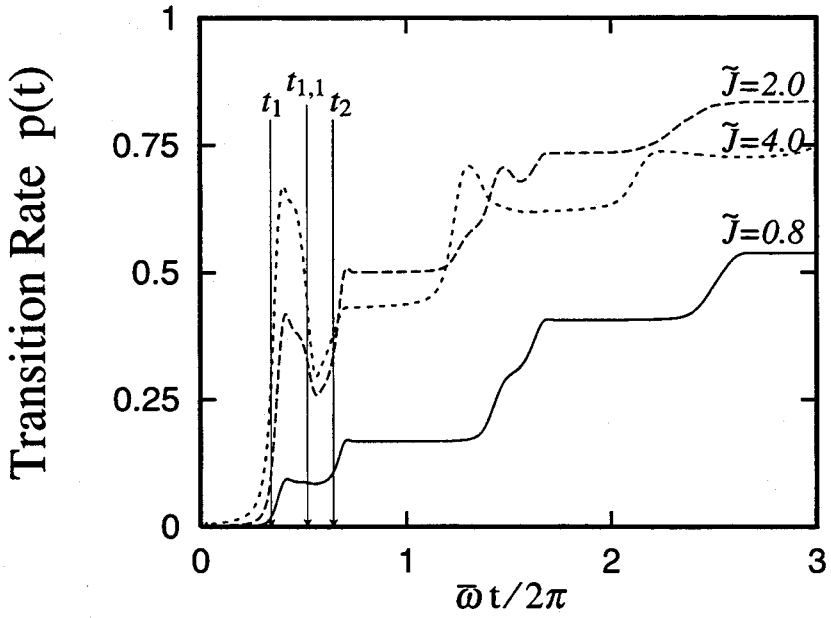

Figure 6.5: The dynamical behavior of the transition rate at the crossing. The parameters are, $S = 25$, $\delta = -1$, $\Delta\epsilon/\bar{\omega} = 55.0$, $\tilde{\kappa} = 0.05$. $\tilde{J}$ is shown in the figure. With increasing $\tilde{J}$, there occurs effective back transfer at $t = t_{1,1}$.

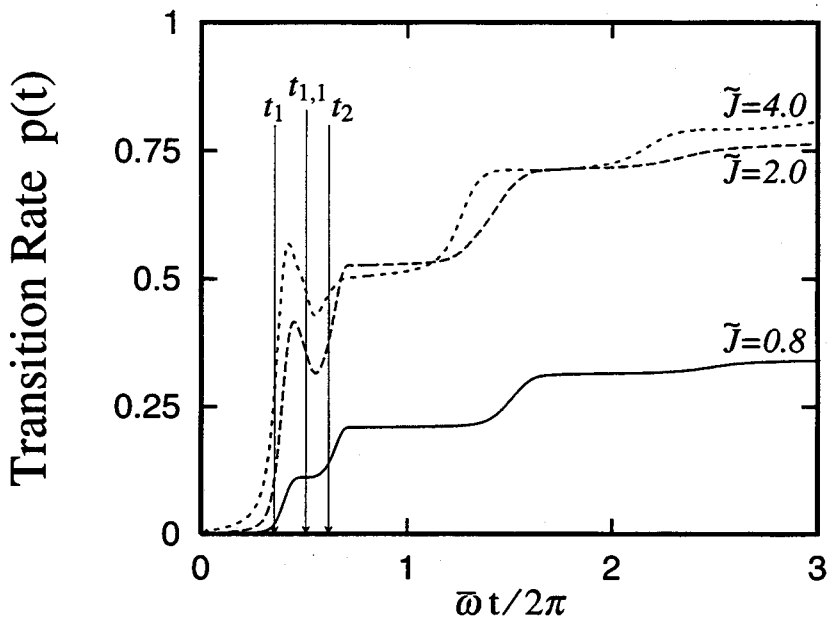

Figure 6.6: The dynamical behavior of the transition rate at the crossing. The parameters are, $S = 25$, $\delta = -1$, $\Delta\epsilon/\bar{\omega} = 55.0$, $\tilde{\kappa} = 0.1$. $\tilde{J}$ is shown in the figure. With increasing $\tilde{J}$, there occurs back transfer at $t = t_{1,1}$. However, the effect of the back transfer is weakened by the damping, as compared with the cases of $\tilde{\kappa} = 0.05$.

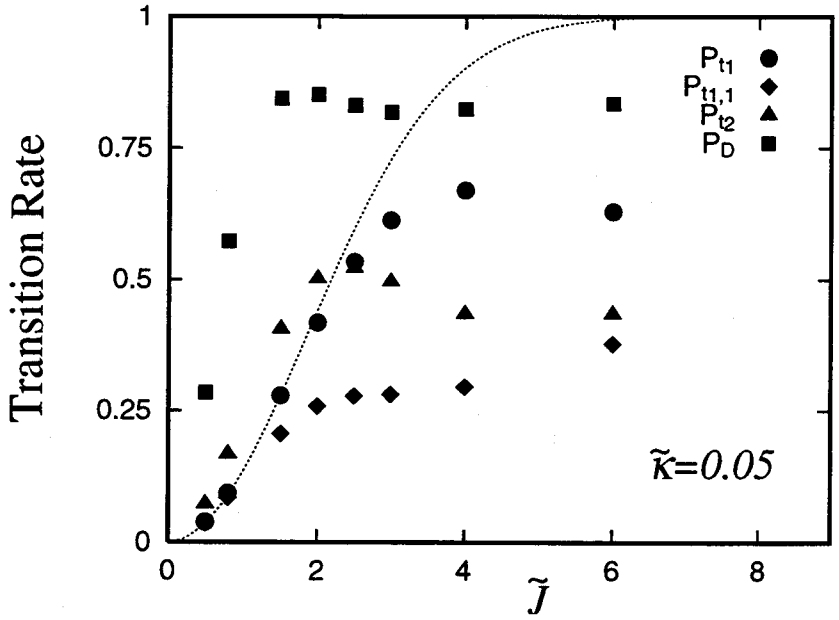

Figure 6.7: The transition rate P_{t_1} (circle), $P_{t_{1,1}}$ (diamond), P_{t_2} (triangle), and P_D (box) as a function of $\tilde{J}$. The predicted value for P_{t_1} by the Landau-Zener formula is also shown by dashed lines. The other parameters are, $S = 25$, $\delta = -1$, $\Delta\epsilon/\bar{\omega} = 55.0$, and $\tilde{\kappa} = 0.05$.

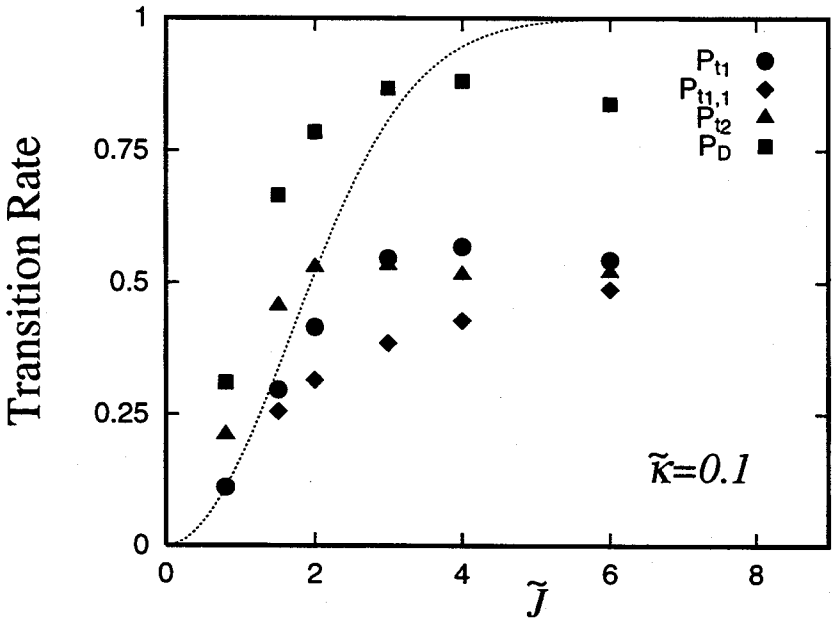

Figure 6.8: The transition rate P_{t_1} (circle), $P_{t_{1,1}}$ (diamond), P_{t_2} (triangle), and P_D (box) as a function of $\tilde{J}$. The predicted value for P_{t_1} by the Landau-Zener formula is also shown by dashed lines. The other parameters are, $S = 25$, $\delta = -1$, $\Delta\epsilon/\bar{\omega} = 55.0$, and $\tilde{\kappa} = 0.1$.

The deviation of P_{t_1} from the Landau-Zener formula, which is salient in a region $\tilde{J} > 2.0$ would be due to the crossover between the crossing event at $t = t_1$ and at $t = t_{1,1}$. In the case that the crossing events at t_1 and at $t_{1,1}$ are not well separated, the crossing event at $t_{1,1}$ starts before the crossing event at t_1 has been completed, then the transition rate P_{t_1} considered to be underestimated. (In a sense, there is a difficulty in defining P_{t_1} and $P_{t_{1,1}}$, here, P_{t_1} has been defined as the maximum value of the first hump, and $P_{t_{1,1}}$ as the minimum of the next dip for time-dependent transition rate.)

For small $\tilde{J}$, the change of the transition rate after the crossing event at $t_{1,1}$ is negligibly small and $P_{t_{1,1}}$ coincides P_{t_1}, which is shown by the result for $\tilde{J} = 0.8$. As $\tilde{J}$ increases, the effect of back transfer becomes significant and the transition rate $P_{t_{1,1}}$ decreases, gets smaller than P_{t_1}. After the crossing event at t_2, the transition rate increases again and recovers to the value P_{t_2}. The difference between P_{t_2} and $P_{t_{1,1}}$ is, however, decreases as $\tilde{J}$ increases. The data for $\tilde{J} = 6.0$ show almost adiabatic transfer, while the data for $\tilde{J} = 0.8$ show almost diabatic transfer.

In Figure 6.8 shows another calculated results of the transition rates P_{t_1}, $P_{t_{1,1}}$, P_{t_2}, and P_D against $\tilde{J}$, the parameters used are same as that used in Figure 6.8, except for a larger damping parameter $\tilde{\kappa} = 0.1$. Note that the transition rate P_{t_2} is slightly larger than $\frac{1}{2}$. If we evaluate the transition rate at each crossing event by Landau-Zener formula, with no effect of damping considered, then the transition rate P_{t_2} is simply estimated by $P_{t_2} = 2P_{LZ}(1 - P_{LZ})$, which can not take larger value than $\frac{1}{2}$. So, this can be considered as the effect of dissipation.

The transition rate P_{t_1}, $P_{t_{1,1}}$, P_{t_2}, and P_D are shown in Figure 6.9 with change of the position δ, as a function of the initial energy of the wave packet E_i measured from the bottom of the potential of $|2\rangle$. The other parameters are, $S = 25, \Delta\epsilon/\bar{\omega} = 55.0, \tilde{J} = 2.0$, and $\tilde{\kappa} = 0.05$. For the initial energy E_i smaller than $12.25\bar{\omega}$ ($\delta > 3.5$), the center of the phonon wave packet in the excited state can not pass the crossing point no more. In this case P_{t_1} and $P_{t_{1,1}}$ are not well-defined probability for the crossing, only P_{t_2} can be defined as a transition rate at $t = 2\pi/\bar{\omega}$ after the first damping oscillation of the wave packet. Note that the transition rate P_{t_2} as a function of $E_i/\bar{\omega}$ has a maximum value at $E_i = 12.25\,\bar{\omega}$. This fact means the transition rate P_{t_2} takes its maximum value, which is larger than $1/2$, in the situation that the wave packet of phonons swing back just around the crossing point of the potentials.

Another calculated results of the transition rates P_{t_1},$P_{t_{1,1}}$, P_{t_2}, and P_D, as a function of the initial energy of the wave packet E_i are shown in Figure 6.10, the parameters used are same as that used in Figure 6.9, except for a larger damping parameter $\tilde{\kappa} = 0.1$. In this figure, P_D is clearly shown to take larger values than $\frac{1}{2}$, due to the effect of dissipation at the crossing.

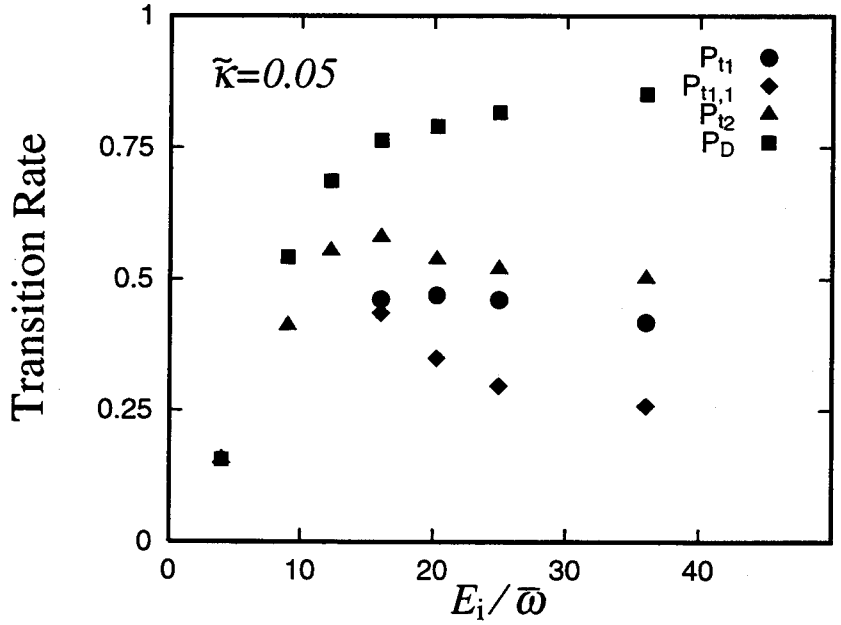

Figure 6.9: The transition rate P_{t_1} (circle), $P_{t_{1,1}}$ (diamond), P_{t_2} (triangle), and P_D (box) as a function of the initial energy E_i measured from the minimum of the potential, at $S = 25$, $\Delta\epsilon/\bar{\omega} = 55.0$, $\tilde{J} = 2.0$, and $\tilde{\kappa} = 0.05$.

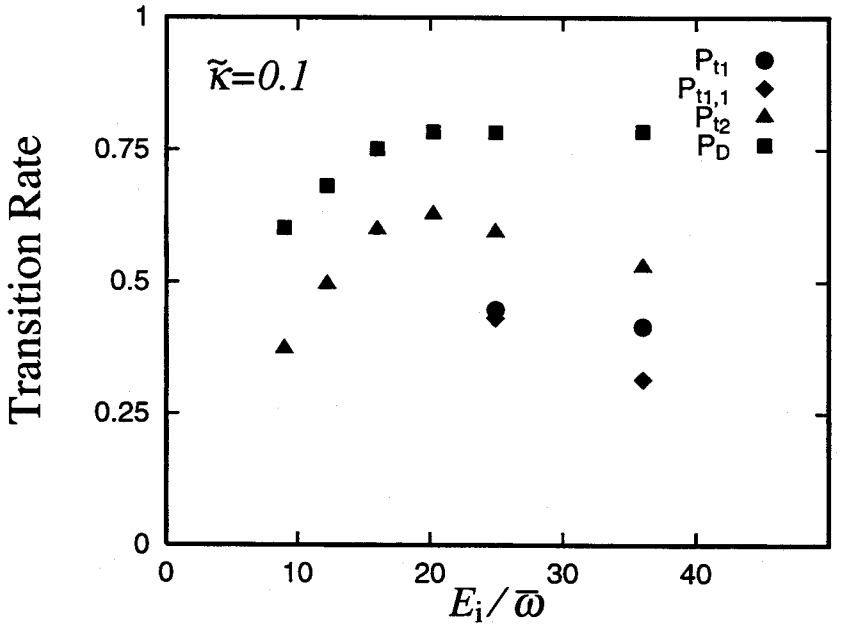

Figure 6.10: The transition rate P_{t_1} (circle), $P_{t_{1,1}}$ (diamond), P_{t_2} (triangle), and P_D (box) as a function of the initial energy E_i measured from the minimum of the potential, at $S = 25$, $\Delta\epsilon/\bar{\omega} = 55.0$, $\tilde{J} = 2.0$, and $\tilde{\kappa} = 0.1$.

6.3 Application to real systems

6.3.1 DX-Center

DX-center is one of the well-known defect in doped $Al_xGa_{1-x}As$ semiconductor alloy system, which shows the persistent photoconductivity (PPC) and the large lattice relaxation energy after optical excitation. It appears with the increase of the AlAs mole fraction x over the critical value x = 0.22. The origin and the structure of the DX-center had been a riddle (X of DX-center historically meant "unknown" [37]) until the DX-center was discovered in doped GaAs with the application of the hydrostatic pressure [38] and it was turned out that the DX-center is nothing but the substitutional donor. From the *ab-initio* calculation [39, 40], it has been shown that the DX-center is a negatively charged center and has a bistability between the shallow donor state ($d^0 + e$) and the deep DX state (DX^-), for the displacement of donor atom toward [111] direction. When the system is excited optically, a conversion from the DX state to the donor state is induced, that causes PPC. However, PPC vanishes at high temperature because a conversion from the donor state to the DX state is induced by thermal excitation (see Figure 6.11). The efficiency of the conversion and the stability of the shallow donor state against the relaxation to the deep DX state are controlled by the nonradiative transition.

The transition dynamics of the DX-center is understood by considering the nonradiative process induced by an off-diagonal interaction around the crossing region of two potential curves. Here, we apply the theory to the system of DX-center and clarify the transition dynamics.

There was a controversy on the origin of the large optical excitation energy which indicates large lattice relaxation energy. Several researchers could not believe that the donor atom can displace so large and they persisted in the small lattice relaxation (SLR) model.

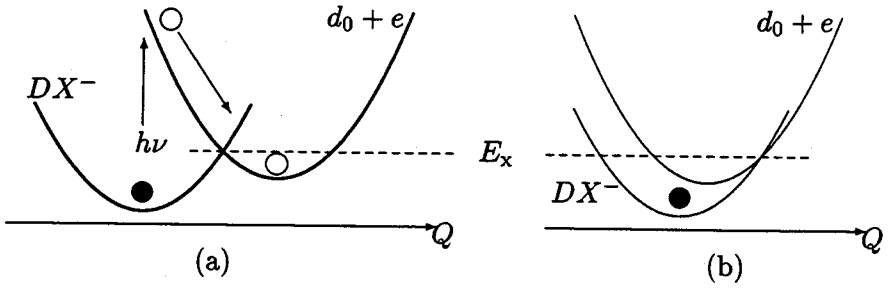

Figure 6.11: The potential configuration for the DX-center. Two possible configurations had been considered; (a) LLR model, (b) SLR model.

The large lattice relaxation (LLR) model and the SLR model give the same experimental data [41] for the activation energy for electron emmision from the DX state E_{DLTS} and electron capture to the DX state E_{CAP} and thermal ionization E_{TH}, except for the optical excitation energy E_{OPT} (see Figure 6.11 of the potential configuration). Now, the LLR model is fully accepted, and the system of DX-center is revealed to be a typical example of the system that the large atomic displacement is induced by electronic excitation.

The difference on the transition dynamics based on the SLR and the LLR model is, however, very distinct. From the discussion of previous section, calculated transition rate shows damping oscillation for the SLR case (see Sec. 6.1), or stair-like increase for the LLR case (see Sec. 6.2.1). These can be clearly distinguished if an elegant experimental method is developed to investigate the time evolution of the transition rate.

Figure 6.12 shows the calculated result [43] in LLR configuration for the time evolution of the probability that the system undergoes nonradiative transition to the DX state, after optical (white-pulse) excitation from the DX state to the donor state. The parameters were chosen so as to fit the adiabatic potential curve calculated by *ab-initio* total energy calculation [40]. The adiabatic potentials which should be compared with our model are that for the on-center neutral state and that for the strongly displaced negatively charged state. The potential curves were approximated by the harmonic potentials with the curvatures estimated at the equilibrium position. The difference in the curvature of the potentials is also neglected. Eventually, $\bar{\omega}$ is adjusted so as to reproduce the experimental optical ionization energy 1.3eV [42]. Thus we set $\bar{\omega} \sim 12.7\text{meV}$, $\Delta\epsilon = 0.03\text{eV}$, $S = 100$. Although these approximation is rather crude, it is sufficient to discuss the dynamics semi-quantitatively. The magnitude of J was estimated by the energy at the crossing point E_{x} and the experimental capture barrier energy E_{CAP}. From the fact that the off-diagonal interaction opens the energy gap of order J around crossing region, namely, $E_{\text{x}} - E_{CAP} \sim J$, we set $J \sim 0.02\text{eV}$ for $E_{CAP} = 0.28\text{eV}$. $\kappa = 0.1\bar{\omega}$ is chosen as an reasonable value.

The transition process is classified into the dynamical transition and the statical transition, as is discussed in Sec. 6.2.1. Experimentally, the existence of PPC means that the nonradiative transition probability in static stage is quite small at moderate temperatures. Therefore, it can be concluded that the nonradiative transition in the actual cases of DX-centers is determined by the transition probability in the dynamical stage. The transition probability in this process governs the quantum yield of the optical conversion from the DX to the shallow donor state and can be estimated experimentally.

The temperature dependence of the transition probability in the static stage can be also calculated in the same way. The probability shows exponential decay, however, the decay rate calculated by the damping hyperoperator method tends to be too large and the calculated result is not reflect the actual system of DX-center.

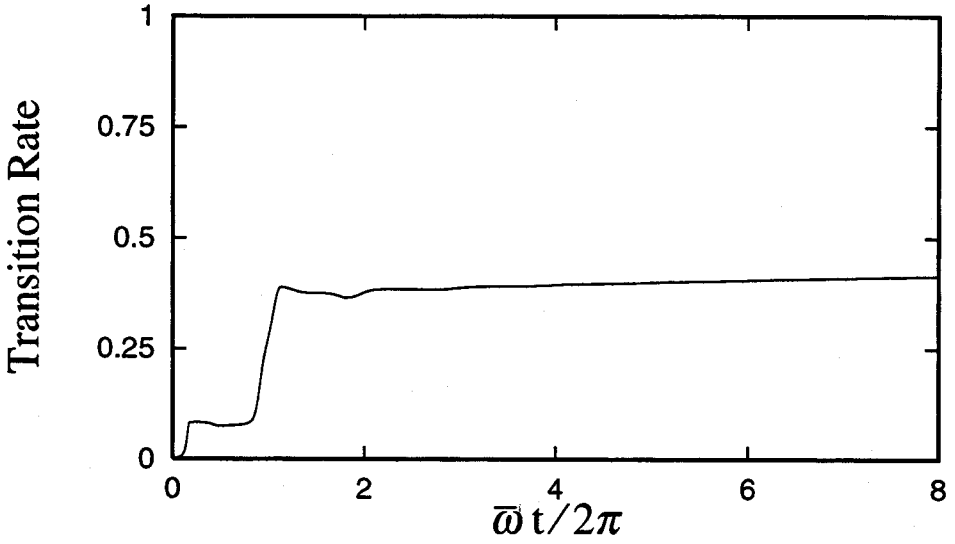

Figure 6.12: The time-dependent nonradiative transition rate to DX^- state from $d_0 + e$ state after the optical excitation to $d_0 + e$, at zero temperature.

6.3.2 F-Center

F-center is one of the color centers in ionic crystals. An electron is trapped by the electronic field generated by the anion vacancy and makes a hydrogen-like energy levels. At the excitation by visible light, the system of F-center shows intense optical absorption corresponding to $1s \rightarrow 2p$ transition, and its absorption spectrum shows broad band structure due to the strong electron-phonon coupling. In spite of the intense absorption spectrum, however, some of the F-centers do not show luminescence. For example, the luminescence was observed in K halides, but not observed in Li halides. This occurrence or non-occurrence of luminescence has been considered to be directly related to the nonradiative processes with multi-phonon emission.

The possibility of the dynamical nonradiative transition has been suggested [6] since the nonradiative transition rate from the relaxed excited state was shown to be negligibly small at low temperatures. Dexter, Klick and Russel proposed a mechanism for the dynamical nonradiative process associated with the potential configuration of two electronic states, the ground state and the excited state, that if the energy of a wave packet generated optically in excited state is higher than that of the crossing point of the potentials, transition to the ground state can occur during the lattice relaxation process when the wave packet passes through the potential crossing region. This is called the DKR mechanism for the luminescence quenching. Bartram and Stoneham [7] analyzed the experimental data of various F-centers to check the validity of the DKR mechanism and showed that the occurrence or non-occurrence of luminescence can be, in actual systems, qualitatively determined by the position of the potential crossing point and the excited state in the potential configuration

space.

According to Bartram and Stoneham, the criterion for the occurrence of luminescence is given by the condition,

$$\Lambda \equiv \frac{S\bar{\omega}}{\Delta\epsilon + S\bar{\omega}} < \frac{1}{4}, \tag{6.18}$$

where Λ is the ratio of lattice relaxation energy to optical absorption energy.

Here, we do a quantitative check for the validity of the DKR mechanism by numerical calculations, by changing the position of the excited state δ in the configuration coordinate. In actual system of F-centers, the electron-phonon coupling constant S is large quantity $S \gg 1$ and off-diagonal interaction is of order of $\bar{\omega}$, so parameters are chosen to $S = 40, \tilde{J} = 2.0$ as reasonable value. The position of the potential crossing is chosen to so that the potential energy at the crossing measured from the bottom of the potential is half of that of optically excited state at the ideal white-pulse excitation (see Figure 6.13(b) for details). In this configuration, Λ is calculated to 0.2929.

First, time-dependent transition rate is shown for $\tilde{\kappa} = 0.05$ with changing the position of the excited state in Figure 6.13. The transition dynamics is classified into dynamical transition process and statical transition process. The transition rate from the initial state which is labeled as E shows only the statical tunneling process, because initial state is already in the relaxed excited state. However, the transition rate in the static stage is too large due to the reasons mentioned in Sec. 6.2.1 and does not reflect the actual system. The time evolutions of the transition rate should be flat in the static stage.

Note that the result of the transition rate from the initial state labeled as C, which means the phonon wave packet starts the damping oscillation initially with the same energy as the crossing point, gives the probability of nonradiative transition rate of nearly a third.

The quantum efficiency of the luminescence after optical excitation of energy ε will be then proportional to η_F, defined as

$$\eta_F(\varepsilon) \propto (1 - P_D) I(\varepsilon) \tag{6.19}$$

where $I(\varepsilon)$ is the optical absorption function for photon energy ε, given by

$$I(\varepsilon) = \frac{1}{\sqrt{2\pi}D} e^{-\frac{(\varepsilon - \Delta\epsilon - S\bar{\omega})^2}{2D^2}} \tag{6.20}$$

In Figure 6.14, quantum efficiency for radiative transition $1 - P_D$ is plotted as a function of optical excitation energy. The optical absorption spectrum, $I(\varepsilon)$ is also plotted for the reference. The result shows good tendency, as compared with the experimental data for the F-center in KI crystal [44].

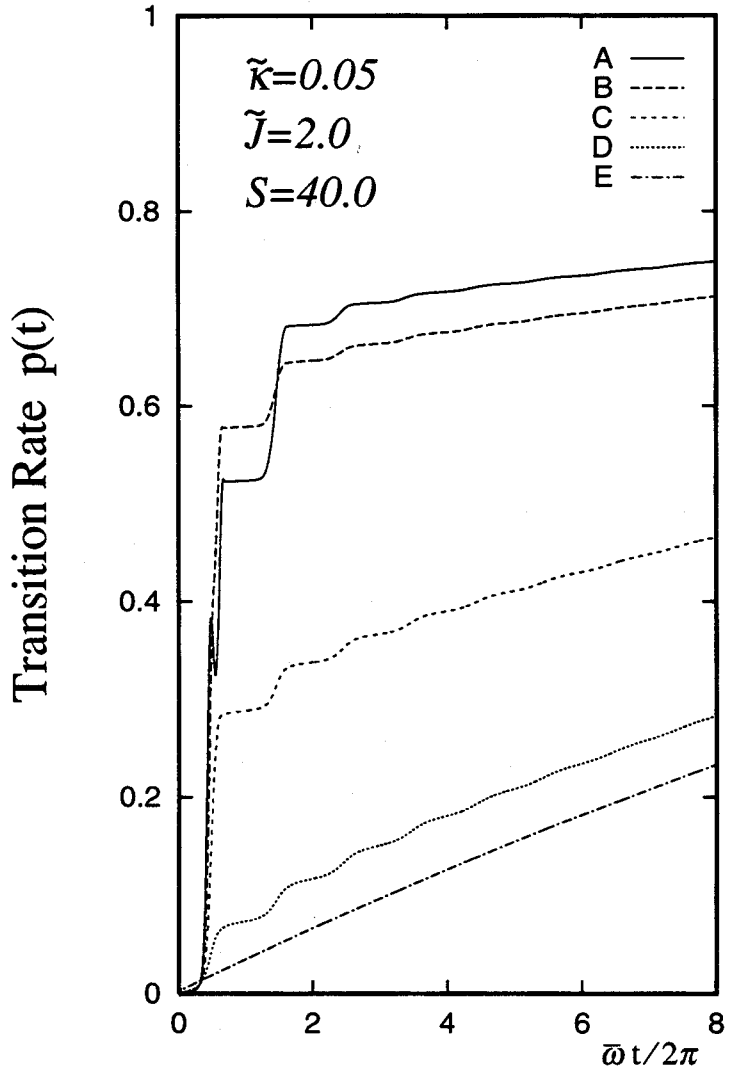

Figure 6.13: (a)The time-dependent transition rate for the nonradiative process at zero temperature. The parameters are chosen so as to reflect the actual cases of F-center, and labels A,B,$\cdots$ in the figure correspond to the initial configuration of the excited state, which are described in (b).

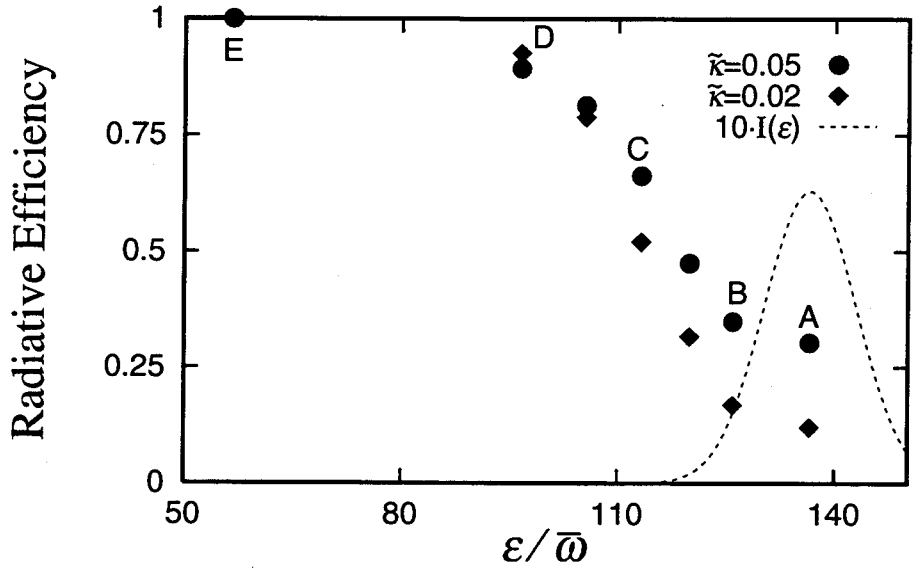

Figure 6.14: The quantum efficiency for radiative transition of typical F-center, as a function of optical excitation energy. The optical absorption spectrum is also shown for reference. Numerical calculations were performed for the parameters, $S = 40$, $\Delta\epsilon/\bar{\omega} = 96.569$, $\tilde{J} = 2.0$, and $\tilde{\kappa} = 0.05$ or 0.02 at zero temperature.

6.4 Summary

Numerical calculations were performed to clarify the transition dynamics of the potential crossing system after the electronic excitation. In the weakly-coupled electron-phonon system, time-evolution of the transition probability shows oscillating behavior, which is originated from the phase coherence between two levels. In the strongly-coupled electron-phonon system, the transition dynamics of the system is classified in two aspects, namely, dynamical hot transition and statical tunneling. The dynamical evolution of the transition rate of the system shows at first stair-like behavior, reflecting the motion of the phonon wave packet in excited state which passes through the crossing region during the lattice relaxation process. After the lattice relaxation process, the dynamical evolution of the transition rate of the system shows exponential behavior, reflecting the quantum tunneling process from the relaxed excited state. The tunneling rate at the static stage becomes, however, too large due to the characteristics of the numerical method using damping hyperoperator.

The dynamical transition rate at each crossing event is investigated quantitatively. In general cases, the transition rate at the first crossing is given by Landau-Zener formula. In the case that the phonon wave packet passes relatively slowly around the potential crossing, the transition rate deviates from the Landau-Zener formula. In special cases the transition rate after the first damping oscillation becomes larger than 1/2 due to the effect of dissipation.

Also, the theory was applied for the transition dynamics of the DX-center, and the nonradiative transition of F-center.

Chapter 7

Concluding Remarks

In this work, transition dynamics at a level crossing with dissipation has been clarified theoretically, both by analytical consideration and by numerical calculation. Calculations based upon the Landau-Zener model and for autonomous potential crossing system have been performed.

From the analytical consideration for the Landau-Zener model with dissipative environment, it has been shown that two extreme situations occur with respect to the ratio of the transition time $\tau_{\rm tr}$ and the phase relaxation time $\tau_{\rm ph}$, namely, the essential coherent case with $\tau_{\rm tr} \ll \tau_{\rm ph}$ and the incoherent case with $\tau_{\rm tr} \gg \tau_{\rm ph}$. The latter case is further classified into two, in accordance with the magnitude of the energy relaxation, namely, the strong-coupling limit at zero temperature and the weak-coupling high-temperature limit. A closed expression of the transition rate that covers the incoherent limit has been obtained. These results have been ascertained by numerical simulation for the time-dependent transition rate, by applying the damping operator technique to the interaction mode.

From the calculations of autonomous potential crossing system, it has been shown that the dynamics of nonadiabatic transition of the system after the electronic excitation is classified in two aspects, namely, dynamical hot transition induced by the motion of the wave packet through the potential crossing region, and statical quantum tunneling, which shows exponential decay of the transition rate. The transition dynamics of the system in the dynamical stage has been studied quantitatively with relation to the motion of the wave packet. The transition dynamics of the actual system, F-center and DX-center, has been discussed. In cases that electronic energy in excited state is higher than that at the potential crossing point and the wave packet can pass around the potential crossing several times or more, successive nonradiative hot transition is induced and the transition rate can be dramatically enhanced. This multiple transition may play a crucial role in the nonradiative process of F-center.

It may be said that the Landau-Zener formula has a kind of *stability* against the dissipative perturbation. It is unaltered in the limit of the rapid passage, or the slow modulation

limit, as shown in Eq.(4.22) and Eq.(4.38). It is also valid to describe the transition rate in the limit of slow passage at low temperature, namely, the rapid modulation limit, as shown in Eq.(4.59). This stability is most clearly exhibited in Figure 5.4. It is also applicable to the nonadiabatic transition rate at the potential crossing. The reason why the Landau-Zener formula is valid for the dynamical hot transition rate for the potential-curve crossing system is, that the wave packet of phonon passes the crossing region so rapidly that the modulation is in the slow limit as described in the derivation of Eq.(4.38). In the case that the wave packet passes slowly and swing back just around the potential crossing region, the transition rate deviates from the Landau-Zener formula, as is shown in Sec. 6.2.2 by numerical calculation.

The special character of the damping hyperoperator, which is common in the hyperoperator with the form shown in Eq.(3.21), has been revealed. Numerical calculations with this type of damping hyperoperator tends to overestimate the off-resonant transition. This spurious effect leads to the overestimation of transition rate from relaxed excited state, or smaller transition rate to the lower branch in the slow passage limit. In order to discuss whole transition dynamics quantitatively and explain various experimental data, we need to improve the calculation method, which is left for the future work. Or we may need to develop an other numerical calculation method which is efficient and applicable to real dynamical system. This would be the final goal.

Appendix A

The interaction mode

In localized centers of crystals, the excess electron generally couples with many modes of phonons with different frequencies. If this coupling is strong enough, it may give rise to a large relaxation of the electronic energy, or even a lowering of local symmetry by the Jahn-Teller effect. The interaction mode, proposed first by Toyozawa and Inoue [33] and quantum-mechanically by O'Brien [34], is useful to discuss the dynamical properties in such systems. The interaction mode is defined uniquely by linear combination of the normal mode phonons, as a mode which carries all the relaxation energy. Moreover, the interaction mode can be regarded as being coupled with the reservoir of the rest modes. The system relaxes toward the thermal equilibrium via phonon emission or absorption through a bilinear term between the interaction mode and the reservior modes, that is well suited for the theoretical treatment by the damping-hyperoperator formalism. Also, the concept of the interaction mode can be extended to multilevel electron-phonon system [35].

We start with the Hamiltonian

$$\mathcal{H} = \mathcal{H}_1|1\rangle\langle 1| + \mathcal{H}_2|2\rangle\langle 2|\,, \tag{A.1}$$

$$\mathcal{H}_1 = \epsilon_1 + \sum_k \omega_k b_k^\dagger b_k\,, \tag{A.2}$$

$$\mathcal{H}_2 = \epsilon_2 + \sum_k \omega_k b_k^\dagger b_k - \sum_k \alpha_k \omega_k (b_k + b_k^\dagger) \tag{A.3}$$

$\mathcal{H}$ is equivalent to the Hamiltonian H_{el} in Eq. (2.2) without J, after the shift of the origin for the phonons and the energy. The interaction mode B and the reservoir modes R_j can be obtained by unitary transformation of the normal modes, defined by

$$B = \sum_{k=1}^{N} U_{0,k}^* b_k \quad , \qquad B^\dagger = \sum_{k=1}^{N} U_{0,k} b_k^\dagger\,, \tag{A.4}$$

$$R_j = \sum_{k=1}^{N} U_{j,k}^* b_k \quad , \qquad R_j^\dagger = \sum_{k=1}^{N} U_{j,k} b_k^\dagger\,, \quad j = 1, 2, \cdots, N-1\,,, \tag{A.5}$$

and the inverse transformation to the normal modes b_k is given by

$$b_k = U_{0,k}B + \sum_{j=1}^{N-1} U_{j,k}R_j\,, \quad b_k^\dagger = U_{0,k}^* B^\dagger + \sum_{j=1}^{N-1} U_{j,k}^* R_j^\dagger\,. \tag{A.6}$$

$\mathcal{H}_1$ and $\mathcal{H}_2$ are calculated by inserting Eq. (A.6) into Eqs. (A.1) - (A.3). If we pick up the terms including only B or $B^\dagger$, they are

$$\mathcal{H}_1 = \sum_{k=1}^{N} \left| U_{0,k} \right|^2 \omega_k B^\dagger B + \cdots\,, \tag{A.7}$$

$$\begin{aligned}\mathcal{H}_2 &= \sum_{k=1}^{N} \left| U_{0,k} \right|^2 \omega_k B^\dagger B - \sum_{k=1}^{N} \alpha_k \omega_k (U_{0,k}B + U_{0,k}^* B^\dagger) + \cdots\,, \\ &= -\Delta E + \left(\sum_{k=1}^{N} \left| U_{0,k} \right|^2 \omega_k \right) \left(B^\dagger - \alpha^* \right) (B - \alpha) + \cdots\,,\end{aligned} \tag{A.8}$$

where ΔE is a relaxation energy in the subspace of B, given by

$$\Delta E = \left| \sum_{k=1}^{N} \alpha_k \omega_k U_{0,k} \right|^2 \Big/ \sum_{k=1}^{N} \left| U_{0,k} \right|^2 \omega_k\,, \tag{A.9}$$

and

$$\alpha = \sum_{k=1}^{N} \alpha_k \omega_k U_{0,k} \Big/ \sum_{k=1}^{N} \left| U_{0,k} \right|^2 \omega_k\,. \tag{A.10}$$

We choose the coefficients $U_{0,k}$ so that the relaxation energy ΔE is maximized in this direction. From the condition

$$\frac{\partial \Delta E}{\partial U_{0,k}^*} = \left(\alpha_k \omega_k \cdot \alpha - \alpha \sum_{k'=1}^{N} \alpha_{k'} \omega_{k'} U_{0,k'}^* \cdot \omega_k U_{0,k} \right) \Big/ \sum_{k=1}^{N} \left| U_{0,k} \right|^2 \omega_k (=0)\,, \tag{A.11}$$

and the unitary condition $\sum_k U_{0,k}^* U_{0,k} = 1$, we can obtain

$$U_{0,k} = \alpha_k \Big/ \sqrt{\sum_{k=1}^{N} \alpha_k^2} = \alpha_k/\alpha\,, \tag{A.12}$$

$$\Delta E = \sum_{k=1}^{N} \alpha_k^2 \omega_k \equiv S\bar{\omega}\,, \tag{A.13}$$

$$\bar{\omega} = \sum_{k=1}^{N} \alpha_k^2 \omega_k / \alpha^2\,, \quad \alpha^2 \equiv S\,, \tag{A.14}$$

The coefficients $U_{j,k}$ for the reservoir modes are chosen so that the cross term such as $R_j^\dagger R_{j'}$ vanishes in $\sum_k \omega_k b_k^\dagger b_k$. Since this is equivalent to diagonalize $\sum_k \omega_k b_k^\dagger b_k$ in the subspace orthogonal to the interaction mode B, the problem comes down to the problem to

re-choose the principle axes $\mathbf{e}_j$ for the ellipsoid $\sum_k \omega_k x_k^2 = 1$ in N-dimensional hyperplane, under the constraints

$$\sum_k e^*_{0,k} \cdot e_{j,k} = 0\,, \quad \text{where} \quad e_{0,k} = U_{0,k}\,. \tag{A.15}$$

The coefficients $U_{j,k}$ can be determined, as the values of x_k at which the function $F(\{x_k\}) = \sum_k \omega_k x^*_k x_k$ is extremized, under the constraints

$$\sum_{k=1}^{N} |x_k|^2 = 1\,, \quad \sum_{k=1}^{N} x_k U^*_{0,k} = 0\,. \tag{A.16}$$

Since

$$\frac{\partial}{\partial x^*_k}\left\{\sum_{k'=1}^{N} \omega_{k'} x^*{}_{k'} x_{k'} - \lambda \sum_{k'=1}^{N} x^*{}_{k'} x_{k'} - \mu \sum_{k'=1}^{N} x^*{}_{k'} U_{0,k'}\right\} = 0 \tag{A.17}$$

where λ and μ are used as Lagrange multipliers, we obtain

$$\omega_k x_k - \lambda x_k - \mu U_{0,k} = 0\,, \tag{A.18}$$

then

$$x_k = \frac{\mu}{\omega_k - \lambda} U_{0,k}\,. \tag{A.19}$$

From Eq. (A.16) and Eq. (A.18), we can obtain

$$\lambda = \sum_{k=1}^{N} \omega_k x^*_k x_k\,, \tag{A.20}$$

and from Eq. (A.16) and Eq. (A.19), we can obtain

$$\sum_{k=1}^{N} \frac{\mu}{\omega_k - \lambda} \Big| U_{0,k} \Big|^2 = 0\,. \tag{A.21}$$

Equation (A.21) has $N-1$ number of solutions for λ. We define Ω_j as the solution of Eq. (A.21), which lies in the region $\omega_j < \Omega_j < \omega_{j+1}$ for $j = 1, 2, \cdots, N-1$. Then the coefficients $U_{j,k}$ are

$$U_{j,k} = \frac{\mu}{\omega_k - \Omega_j} U_{0,k}\,, \tag{A.22}$$

where μ is determined by the condition $\sum_k U^*_{j,k} U_{j,k} = 1$. Eventually, we obtain

$$U_{j,k} = \frac{U_{0,k}}{\omega_k - \Omega_j} \Bigg/ \sqrt{\sum_{k=1}^{N} \frac{|U_{0,k}|^2}{(\omega_k - \Omega_j)^2}}\,. \tag{A.23}$$

After the whole transformation, $\mathcal{H}_1$ and $\mathcal{H}_2$ in Eq. (A.2) and Eq. (A.3) are rewritten down to

$$\mathcal{H}_1 = \epsilon_1 + \bar{\omega} B^\dagger B + \sum_{j=1}^{N-1} \Omega_j R_j^\dagger R_j + \sum_{j=1}^{N-1} \beta_j (B^\dagger R_j + B R_j^\dagger), \tag{A.24}$$

$$\begin{aligned} \mathcal{H}_2 = {} & \epsilon_2 - \Delta E + \bar{\omega}(B^\dagger - \alpha)(B - \alpha) + \sum_{j=1}^{N-1} \Omega_j R_j^\dagger R_j \\ & + \sum_{j=1}^{N-1} \beta_j \left\{ (B^\dagger - \alpha) R_j + (B - \alpha) R_j^\dagger \right\}, \end{aligned} \tag{A.25}$$

where β_j, the linear coupling constant between the interaction mode and the j-th reservoir mode, is written as

$$\beta_j = \sum_{k=1}^{N} \omega_k U_{j,k}^* U_{0,k} \,. \tag{A.26}$$

Appendix B

Damping hyperoperator

The damping operator for the interaction mode coupled with the two-level system can be derived by extending the well-known procedure [29]. The equation of motion for the system driven by the Hamiltonian (3.9)-(3.13) is

$$\begin{aligned} i\frac{\partial \rho}{\partial t} &= i[\, H_T\,, \quad \rho(t)\,] \\ &= [\, H_{\rm sys}(t) + V_{\rm sys} + H_R + V_R\,, \quad \rho(t)\,], \end{aligned} \tag{B.1}$$

where $\rho(t)$ is a density matrix for the system. The expectation value of an arbitrary operator $\hat{A}$ can be calculated as

$$\langle \hat{A}(t) \rangle = {\rm Tr}[\hat{A} \cdot \rho(t)]\,. \tag{B.2}$$

In actual cases, $\hat{A}$ is a function of the interaction mode B, $B^\dagger$ only. The information of the reservoir can be then eliminated by taking trace over the reservoir, that is,

$$\begin{aligned} \langle \hat{A}(t) \rangle &= {\rm Tr}_S \left[\hat{A} \cdot {\rm Tr}_R[\rho(t)] \right] \\ &= {\rm Tr}_S \left[\hat{A} \cdot \rho_R(t) \right], \end{aligned} \tag{B.3}$$

where ρ_R is called reduced density matrix. Now we go back to Eq. (B.1). In interaction representation, it reads

$$i\frac{\partial \chi}{\partial t} = [\, V_{\rm sys}(t) + V_R(t)\,, \quad \chi(t)\,] \tag{B.4}$$

where

$$\rho(t) = \exp_+ \left[-i \int^t d\tau (H_{\rm sys}(\tau) + H_R) \right] \chi(t) \exp_- \left[+i \int^t d\tau (H_{\rm sys}(\tau) + H_R) \right], \tag{B.5}$$

$$V_{\rm sys}(t) = \exp_- \left[+i \int^t d\tau H_{\rm sys}(\tau) \right] V_{\rm sys} \exp_+ \left[-i \int^t d\tau H_{\rm sys}(\tau) \right], \tag{B.6}$$

$$V_R(t) = \exp_-\left[+i\int^t d\tau(H_{\rm sys}(\tau)+H_R)\right] V_R \exp_+\left[-i\int^t d\tau(H_{\rm sys}(\tau)+H_R)\right]$$
$$= \begin{pmatrix} G^\dagger(t)B_1 + G(t)B_1^\dagger & 0 \\ 0 & G^\dagger(t)B_2 + G(t)B_2^\dagger \end{pmatrix}, \tag{B.7}$$

$$G(t) = \sum_j \beta_j e^{i(\bar{\omega}-\Omega_j)t} R_j\,, \quad G^\dagger(t) = \sum_j \beta_j e^{-i(\bar{\omega}-\Omega_j)t} R_j^\dagger\,. \tag{B.8}$$

Equation (B.4) is solved formally, as

$$\chi(t) - \chi(0) = -i\int_0^t d\tau[\,V_{\rm sys}(\tau)\,,\,\chi(\tau)\,] - i\int_0^t d\tau[\,V_R(\tau)\,,\,\chi(\tau)\,]\,. \tag{B.9}$$

and put this in the right hand side of Eq. (B.4), we obtain

$$i\frac{\partial\chi}{\partial t} = [\,V_{\rm sys}(t)\,,\,\chi(t)\,] + [\,V_R(t)\,,\,\chi(t)\,]$$
$$= [\,V_{\rm sys}(t)\,,\,\chi(t)\,] + [\,V_R(t)\,,\,\chi(0)\,] - i\int_0^t d\tau[\,V_R(t)\,,\,[\,V_{\rm sys}(\tau)\,,\,\chi(\tau)\,]]$$
$$-i\int_0^t d\tau[\,V_R(t)\,,\,[\,V_R(\tau)\,,\,\chi(\tau)\,]]\,. \tag{B.10}$$

The perturbation terms of first order with respect to $V_{\rm sys}$ and second order with respect to V_R are taken into account. Since the perturbation terms of first order with respect to V_R vanish when trace is taken over the reservoir subspace, from Eq. (B.10), we obtain

$$i\frac{\partial\chi_R}{\partial t} = [\,V_{\rm sys}(t)\,,\,\chi_R(t)\,] - i\int_0^t d\tau\cdot{\rm Tr}_R[\,V_R(t)\,,\,[\,V_R(\tau)\,,\,\chi(\tau)\,]]\,, \tag{B.11}$$

where

$$\chi_R(t) \equiv {\rm Tr}_R\chi(t) \tag{B.12}$$

is a reduced density matrix in the interaction representation. The relation between χ_R and ρ_R is obtained from Eq. (B.5), that is,

$$\rho_R(t) = {\rm Tr}_R\rho(t) = \exp_+\left[-i\int_0^t d\tau H_{\rm sys}(\tau)\right]\chi_R(t)\exp_-\left[+i\int_0^t d\tau H_{\rm sys}(\tau)\right]. \tag{B.13}$$

Because the system of the reservior is initially in thermal equilibrium,

$$\rho(0) = \chi(0) = \rho_R(0)\cdot f_0(\mathbf{R})\,, \quad f_0(\mathbf{R}) \propto e^{-H_R/k_BT}\,. \tag{B.14}$$

and, if the coupling between the system and the reservoir is weak enough, we can assume that the thermal equilibrium of the reservoir $\mathbf{R}$ is not disturbed by this coupling. This is called the weak-coupling approximation. It is assumed that

$$\chi(t) = \chi_R(t)f_0(\mathbf{R}) \quad \text{for all } t\,. \tag{B.15}$$

χ_R is expanded for the electron subspace, as

$$\chi_R(t) = \begin{pmatrix} \chi_{1,1}(t) & \chi_{1,2}(t) \\ \chi_{2,1}(t) & \chi_{2,2}(t) \end{pmatrix} \tag{B.16}$$

$\chi_{i,j}$ includes the information for the interaction mode only. The integrand in Eq.(B.11) can then be calculated, for example,

$$\begin{aligned} &\Big\{\mathrm{Tr}_R[\,V_R(t)V_R(\tau)\chi(\tau)\,]\Big\}_{1,1} \\ &\quad = \mathrm{Tr}_R\left[\Big(G(t)B_1^\dagger + G^\dagger(t)B_1\Big)\Big(G(\tau)B_1^\dagger + G^\dagger(\tau)B_1\Big)\chi_{1,1}(\tau)f_0(\mathbf{R})\right] \\ &\quad = \Big\langle G(t)G^\dagger(\tau)\Big\rangle B_1^\dagger B_1 + \Big\langle G^\dagger(t)G(\tau)\Big\rangle B_1 B_1^\dagger\,. \end{aligned} \tag{B.17}$$

where $\{\cdots\}_{1,1}$ means that the $(1,1)$ component is taken for electron subspace, and $\langle\cdots\rangle$ means the thermal average is taken for the reservoir. $\langle G(t)G^\dagger(\tau)\rangle$ and $\langle G^\dagger(t)G(\tau)\rangle$ is given by

$$\begin{aligned} \Big\langle G^\dagger(t)G(\tau)\Big\rangle &= \sum_j \beta_j^2 e^{i(\Omega_j-\bar{\omega})(t-\tau)}\langle R_j^\dagger R_j\rangle \\ &= \sum_j \beta_j^2 n_j e^{i(\Omega_j-\bar{\omega})(t-\tau)} \equiv \mathcal{K}_+(t-\tau)\,, \end{aligned} \tag{B.18}$$

$$\Big\langle G(t)G^\dagger(\tau)\Big\rangle = \sum_j \beta_j^2 (n_j+1) e^{i(\Omega_j-\bar{\omega})(\tau-t)} \equiv \mathcal{K}_-(\tau-t)\,, \tag{B.19}$$

where $n_j = \frac{1}{e^{-\Omega_j/k_BT}-1}$, and $\mathcal{K}_+$ ($\mathcal{K}_-$) means physically the absorption (emission) of the interaction mode phonon from (to) the reservoir.

If the spectrum of the reservoir, defined by

$$\beta^2(\omega) = \sum_j \beta_j^2 \delta(\omega-\Omega_j) \tag{B.20}$$

is wide enough to guarantee the Markovian approximation, $\mathcal{K}_+$ and $\mathcal{K}_-$ are approximated as

$$\begin{aligned} \mathcal{K}_+(t-\tau) &= \int_{-\infty}^{\infty} d\omega\, \beta^2(\omega) n(\omega) e^{i(\omega-\bar{\omega})(t-\tau)} \\ &\sim 2\pi\bar{n}\beta^2(\omega)\,\delta(t-\tau)\,, \end{aligned} \tag{B.21}$$

$$\begin{aligned} \mathcal{K}_-(\tau-t) &= \int_{-\infty}^{\infty} d\omega\, \beta^2(\omega)\,(n(\omega)+1)\, e^{i(\omega-\bar{\omega})(t-\tau)} \\ &\sim 2\pi(\bar{n}+1)\beta^2(\bar{\omega})\,\delta(\tau-t)\,. \end{aligned} \tag{B.22}$$

After the evaluation of all the terms that appear in the integrand in Eq.(B.11) under this approximation, the damping hyperoperator can be obtained, which has the form

$$-\int_0^t d\tau \cdot \mathrm{Tr}_R[\,V_R(t)\,,\,[\,V_R(\tau)\,,\,\chi(\tau)\,]] = \Gamma\cdot\chi_R(t)\,, \tag{B.23}$$

$$\Gamma \cdot \chi_R = \begin{pmatrix} \Gamma_{1,1}\chi_{1,1} & \Gamma_{1,2}\chi_{1,2} \\ \Gamma_{2,1}\chi_{2,1} & \Gamma_{2,2}\chi_{2,2} \end{pmatrix}, \tag{B.24}$$

$$\begin{aligned} \Gamma_{i,j}\chi_{i,j} &= \kappa(\bar{n}+1)\left(2B_i\chi_{i,j}B_j^\dagger - B_i^\dagger B_i\chi_{i,j} - \chi_{i,j}B_j^\dagger B_j\right) \\ &\quad + \kappa\bar{n}\left(2B_i^\dagger\chi_{i,j}B_j - B_iB_i^\dagger\chi_{i,j} - \chi_{i,j}B_jB_j^\dagger\right), \end{aligned} \tag{B.25}$$

with damping constant $\kappa \sim \pi\beta^2(\bar{\omega})$. Back to the Schrödinger picture, we finally obtain Eqs. (3.17)-(3.21).

References

[1] A.P.M. Baede, in *Advances in Chemical Physics*, edited by I. Prigogine and S.A. Rice (Wiley, London, 1975), Vol. 30, p. 463.

[2] L.D. Landau, Phys. Z. Sowjetunion **1**, 88 (1932); C. Zener, Proc. R. Soc. London, Ser. A **137**, 696 (1932).

[3] See, for instance, C. Zhu and H. Nakamura, J. Chem. Phys. **101**, 10630(1994) and references therein.

[4] M.J. Rosker, T.S. Rose and A.H. Zewail, Chem. Phys. Lett. **146**, 175(1988); T.S. Rose, M.J. Rosker, and A.H. Zewail, J. Chem. Phys. **91**, 7415(1989).

[5] S.P. Mikheyev and A. Smirnov, Sov. J. Nucl. Phys. **42**, 913(1985); L. Wolfenstein, Phys. Rev. D **17**, 2369(1978); Y. Fukuda, *et al.*, Phys. Lett. B **335**, 237(1994); S. Kasuga *et al.*, Phys. Lett. B **374**, 238(1996).

[6] D.L. Dexter, C.C. Klick, and C.A. Russel, Phys. Rev. **110**, 603(1955); R. Englman and B. Barnett, J. Lumin. **3**, 37(1970); R.H. Bartram and A.M. Stoneham, Rep. Prog. Phys. **44**, 1251(1981).

[7] R.H. Bartram and A.M. Stoneham, Solid State Commun. **17**, 1593(1975).

[8] C.H. Henry and D.V. Lang, Phys. Rev. B **15**, 989(1975).

[9] M. Kusunoki, Phys. Rev. B **20**, 2512(1979).

[10] H. Sumi, J. Phys. Soc. Jpn. **49**, 1701(1980).

[11] Y. Kayanuma, J. Phys. Soc. Jpn. **51**, 3526(1982).

[12] R. Souda, M. Aono, C. Oshima, S. Otani, and Y. Ishizawa, Surf. Sci. **150**, L59(1985); M. Tsukada, S. Tsuneyuki, and N. Shima, Surf. Sci. **164** L811(1985); S. Tsuneyuki and M. Tsukada, Phys. Rev. B **34**, 5758(1986).

[13] C. Tully, Phys. Rev. B **16**, 4323(1977); W. Brenig, J. Phys. Soc. Jpn. **51**, 1914(1982); H. Ueba, Phys. Rev. B **31**, 3915(1985); S. Tsuneyuki and M. Tsukada, *ibid.* **34**, 5758(1986); S. Sawada and M. Metiu, J. Chem. Phys. **84**, 6293(1986).

[14] A. Nitzan and J. Jortner, J. Chem. Phys. **58**, 2412(1973); H. Frauenfelder and P. Wolynes, *Science* **229**, 337(1985); A. Garg, J.N. Onuchic, and V. Ambegaokar, J. Chem. Phys. **83**, 4491(1985); M. Sparpaglione and S. Mukamel, J. Phys. Chem. **91**, 3938(1987).

[15] D. Glas and U. Mosel, Nucl. Phys. A **264**, 268(1976); W. Nörenberg, Phys. Lett. **104B**, 107(1981); B. Milek and R. Reif, *ibid.* **157B**, 134(1985).

[16] A. A. Abragam, *The Principle of Nuclear Magnetism* (Oxford University Press, Oxford, 1975).

[17] M.M. Roy, Phys. Rev. Lett. **32**, 814(1974); S. Nakanishi, T. Endo, T. Muramoto, and T. Hashi, Opt. Commun. **38**, 419(1981).

[18] Y. Kayanuma, Phys. Rev. Lett **58**, 1934(1987); C. Camparo and R.R. Frueholtz, Phys. Rev. A **30**, 803(1984).

[19] S. Miyashita, J. Phys. Soc. Jpn. **64**, 3207(1995).

[20] M. Tsukada, J. Phys. Soc. Jpn. **51**, 2927(1982).

[21] Y. Kayanuma, J. Phys. Soc. Jpn. **53**, 108(1984); J. Phys. Soc. Jpn. **53**, 118(1984).

[22] Y. Gefen, E. Ben-Jacob, and A.O. Caldeira, Phys. Rev. B **36**, 2770(1987).

[23] P. Ao and J. Rammer, Phys. Rev. Lett. **62**, 3004(1989); Phys. Rev. B **43**, 5397(1991).

[24] A.O. Caldeira and A.J. Leggett, Rhys. Rev. Lett. **46**, 211(1981); S. Chakravarty and A.J. Leggett, Rhys. Rev. Lett. **52**, 5(1984).

[25] See, A.J. Leggett, S. Chakravarty, A.T. Dorsey, M.P.A. Fisher, A. Garg, and W. Zwerger, Rev. Mod. Phys. **59**, 1(1987).

[26] J.C. Tully, J. Chem. Phys. **93**, 1061(1990).

[27] T. Ikegami, T. Kondow, and S. Iwata, J. Chem. Phys. **99**, 358(1993).

[28] Y. Tanimura and P.G. Wolynes, Phys. Rev. A **43**, 4131(1991); Y. Tanimura and Y. Maruyama, J. Chem. Phys. **107**, 1779(1997).

[29] See, for example, W.H. Loisell, *Quantum Statistical Properties of Radiation* (Wiley, New York, 1989).

[30] T. Takagahara, E. Hanamura, and R. Kubo, J. Phys. Soc. Jpn. **44**, 728(1978).

[31] M. Murao, C. Uchiyama, and F. Shibata, Physica A **209**, 444(1994).

[32] B.M. Garraway and P.L. Knight, Phys. Rev. A **49**, 1266(1994).

[33] Y. Toyozawa and M. Inoue, J. Phys. Soc. Jpn. **21**, 1663(1966).

[34] M.C.M. O'Brien, J. Phys. C **5**, 2045(1971).

[35] Y. Kayanuma and H. Nakayama, J. Phys. Soc. Jpn. **67**, 3718(1998).

[36] Y. Kayanuma, J. Phys. Soc. Jpn. **57**, 292(1988); Phys. Rev. B **43**, 6326(1991).

[37] D.V. Lang, R.A. Logan, and M. Jaros, Phys. Rev. B **19**, 1015(1979).

[38] M. Mizuta, M. Tachikawa, H. Kukimoto, and S. Minomura, Jpn. J. Appl. Phys. **24**, L143(1985).

[39] D.J. Chadi and K.J. Chang, Phys. Rev. B **39**, 10063(1989); S.B. Zhang and D.J. Chadi, Phys. Rev. B **42**, 7174(1990); M. Saito, A. Oshiyama, and O. Sugino, Phys. Rev. B **45**, 13745(1992).

[40] J. Dabrowski and M. Scheffler, Mat. Sci. Forum Vol. **83-87**, 735(1992).

[41] E. Calleja, A. Gomez, and E. Munõz, App. Phys. Lett. **52**, 383(1988); N.Chand, T.Henderson, J. Klem, W.T. Masselink, R. Fisher, Y-C. Chang, H. Morkoç, Phys. Rev. B **30**, 4481(1984); P.M. Mooney, N.S. Caswell, and S.L. Wright, J. Appl. Phys. **62**, 4786(1987).

[42] P.M. Mooney, G.A. Northrop, T.N. Morgan, and H.G. Grimmeiss, Phys. Rev. B **37**, 8298(1988).

[43] H. Nakayama, Y. Katayama-Yoshida, and Y. Kayanuma, in *Shallow-Level Centers in Semiconductors*, edited by C.A.J. Ammerlaan and B. Pajot (World Scientific, 1997) p. 191.

[44] S. Wakita, Y. Suzuki, and M. Hirai, J. Phys. Soc. Jpn. **50**, 2781(1981).